Frequency synchronization for carrier allocation in uplink OFDMA systems

Babar Aziz

▶ To cite this version:

HAL Id: tel-00767906

https://theses.hal.science/tel-00767906

Submitted on 20 Dec 2012

îledeFrance

digiteo
Recherche en sciences & technologies de l'information

Ph.D. THESIS

presented to

University of Cergy-Pontoise
École Doctorale Sciences et Ingénierie

to obtain the title of

Doctor of Science of the University of Cergy-Pontoise
Specialty: Sciences and Technologies of Information and Communication

Defended by

Babar AZIZ

Frequency synchronization for carrier allocation in uplink OFDMA systems

prepared at
Équipes Traitement de l'Information et Systèmes (ETIS) - UMR 8051
ENSEA - Université de Cergy-Pontoise - CNRS

defense date: December 15, 2011

Jury:

Examinator:	Prof.	Marie-Laure Boucheret	INP - ENSEEIHT
Reviewers:	Prof.	Jacques Palicot	IETR- SUPELEC
Reviewers:	Prof.	Jean-Marc Brossier	GIPSA Lab - INPG
Examinator:	Dr.	Sylvain Traverso	Thales Group
Directress:	Prof.	Inbar Fijalkow	ETIS/ENSEA-UCP-CNRS
Co-Directress:	M.	Myriam Ariaudo	ETIS/ENSEA-UCP-CNRS

ETIS

CNRS

ENSEA
Ecole Nationale
Supérieure
de l'Electronique
et de ses Applications

UNIVERSITÉ
de Cergy-Pontoise

Abstract

Since OFDMA is extremely sensitive to frequency offsets, one of the most prominent issues in the design and implementation of OFDMA based systems is the need for a very fine frequency synchronization. The task of frequency synchronization becomes even more challenging in the uplink OFDMA based systems where one transmission symbol is generated by the contribution of different users. Our goals in this thesis include the study and analysis of problems resulting from frequency mismatches and to provide solutions to combat these problems. We first look at the interference resulting from carrier frequency offsets (CFOs) coming from the user terminal oscillator mismatch with the carrier frequency. A new analytical expression of the inter-carrier interference (ICI) that takes into account the effect of CFO on the cyclic prefix is proposed. This model proves to be non linear with respect to the CFO. We demonstrate that one must take into account the cyclic prefix while analyzing interference resulting from CFO. Then we focus our attention on establishing a trade-off between channel frequency diversity and robustness against CFO because there exists a contradiction between the two. We propose a trade-off in the form of a *Threshold blocksize*, to allow a good compromise between the channel diversity and robustness for CFO for the case when no channel state information (CSI) is available. For system where CSI is available, we propose an optimal block carrier allocation scheme through which both robustness to CFO and channel frequency diversity can be achieved using small blocksize for small CFO values. We also propose a *Critical CFO* value, above which the performance of the optimal block carrier allocation loses interest. We propose solutions for two important problems encountered in an uplink OFDMA system. First, based on polynomial approximation we propose an efficient method for joint estimation of channel impulse responses and carrier frequency errors at the receiver. Our proposed joint estimation method is simpler than the existing methods without any performance degradation. Next we propose a CFO compensation method based on successive interference cancellation. The proposed interference cancellation method reduces the implementation complexity one faces in case of large DFT matrices

Résumé

La mise en oeuvre de systèmes basés sur l'OFDMA nécessite une synchronisation de la fréquence très fine car l'OFDMA est extrêmement sensible aux décalages en fréquence porteuse (CFO). La tâche de synchronisation de fréquence devient encore plus difficile dans les systèmes avec accès multiple, OFDMA, en liaison montante. Nos objectifs comprennent l'étude et l'analyse des problèmes résultant des décalages en fréquence et la proposition de solutions pour lutter contre ces problèmes. Nous examinons d'abord les interférences résultant de décalages de fréquence porteuse présents dans l'oscillateur du terminal utilisateur. Nous démontrons que l'on doit prendre en compte le préfixe cyclique tout en analysant les interférences résultant du CFO. Ensuite, nous montrons qu'il existe une contradiction entre la diversité de fréquence de canal et la robustesse au CFO. Nous proposons un compromis sous la forme d'une taille de bloc de seuil, afin de permettre un bon compromis entre la diversité des canaux et la robustesse aux CFOs pour le cas où aucune connaissances du canal n'est disponible. Quand le canal est connu, nous proposons une allocation optimale par bloc grâce à laquelle la robustesse aux CFO et à la diversité de fréquence de canal peut être réalisée en utilisant une petite taille de bloc petit pour des CFO de petite valeur. Nous proposons également une valeur CFO critique, en dessous de laquelle l'allocation optimal par bloc est intéressant. Ensuite, nous proposons des solutions pour deux problèmes importants rencontrés dans un système OFDMA en liaison montante. Premièrement, nous proposons une méthode efficace pour l'estimation conjointe des réponses impulsionnelles des canaux et fréquences porteuses basée sur l'approximation polynomiale. Notre méthode d'estimation conjointe est plus simple que les méthodes existantes, sans aucune dégradation de performance. Ensuite, nous proposons une méthode de compensation des CFO basée sur l'annulation des interférences successives (SIC). La méthode d'annulation proposée réduit la complexité de mise en oeuvre quand le nombre de porteuses est important.

Contents

List of Figures

List of Figures

Glossary

3GPP	The Third Generation Partnership Project.
AMC	Adaptive Modulation and Coding
ADSL	Asymmetric Digital Subscriber Line.
CSI	Channel State Information.
CFO	Carrier Frequency Offset.
CIR	Channel Impulse Response.
CDMA	Code Division Multiple Access.
DAB	Digital Audio Broadcasting.
DFT	Discrete Fourier Transform.
DMT	Discrete Multitone.
DSL	Digital Subscriber Line.
DVB-T	Digital Video Broadcasting- Terrestrial.
FDMA	Frequency Division Multiple Access.
GSM	Global System for Mobile Communications.
IA	Interference Avoidance.
ICI	Inter-Carrier Interference.
IDFT	Inverse Discrete Fourier Transform.
ISI	Inter-Symbol Interference.
LTE	Long Term Evolution.
Mbps	Mega Bit per second.
MIMO	Multiple-Input and Multiple-Output.
MUI	Multiuser-Interference (multiuser-ICI).
ML	Maximum Likelihood.
MMSE	Minimum Mean Square Error.
MSE	Mean Square Error.
OFDM	Orthogonal Frequency Division Modulation.
OFDMA	Orthogonal Frequency Division Multiple Access.

PAPR	Peak-to-Average Power Ratio.
RF	Radio Frequency.
SINR	Signal to Interference plus Noise Ratio.
SNR	Signal to Noise Ratio.
TDMA	Time Division Multiple Access.
SDMA	Space Division Multiple Access.
SIC	Successive Interference Cancellation.
WiMAX	Worldwide Interoperability for Microwave Access.
WLAN	Wireless Local Area Network.

Chapter 1

Introduction - Context and Background

THE last few decades of the twentieth century are marked by the transition of communication world from the wired to wireless connection. Since the early 80's, after the Global System for Mobile communication (GSM) was developed, wireless communication have succeeded in replacing the fixed telephone lines. The fact that people can communicate at any place and at any time, despite being in motion, has given mobile communication a cutting edge over the wired communication in conquering the global market. However, initially the services provided by the mobile operators were mostly voice and transmission of short text-based messages, due to the limitation of low-speed wireless connection. In recent years, the demand for broadband access has increased substantially and the twenty-first century begins with the convergence of the trends, introduced at the end of the last century, namely higher data rate, more multimedia services and greater mobility [1, 2, 3, 4]. Due to the abundance of more and more intelligent and portable computing devices, many new wireless standards are developed to enhance the data rate in the wireless systems. In few years, cellular networks have evolved from analog first generation to digital multi-service third generation. If the move from the 1st Generation (1G) to the 2nd Generation (2G) mobile systems is characterized by the conversion from analog to digital, then the shift from 2G to 3rd Generation (3G) is from circuit-switch to packet-switch for bandwidth-on-demand packet-data services with the support of minimum data-rate of up to 2 Mbps for indoor/small-cell-outdoor environments and 384 kbps for wide-area coverage [3]. Such a broadband capacity aims at replacing the land-line DSL service and providing high quality of service for the next generation multimedia applications (real-time audio and high-definition video, high speed data, mobile TV etc.) ubiquitously, i.e. at any time and any place. In the second generation, Frequency Division Multiple Access (FDMA) and Time Division Multiple Access (TDMA) have been the leading access methods, while in the third generation, Code Division Multiple Access (CDMA) was the basis of all

standards and gained significant popularity as an access technique. The demand for high-data rate multimedia wireless communication is expected to continue in the future as the fourth generation (4G) of mobile communication systems has to offer hundreds of Mbps of data rate both in the downlink and uplink direction. In order to meet the augmenting demands, the communication systems need to be highly flexible and adaptive. Therefore, the next generation is expected to be dominated by Orthogonal Frequency Division Multiple Access (OFDMA) because its simplicity and flexibility, in conjunction with advanced radio features, promises very high data rates and multi-service support. As a result many current and evolving wireless standards such as Worldwide Interoperability for Microwave Access (WiMAX), based on IEEE 802.16 standard, and 3GPP Long Term Evolution (LTE) are adopting a multicarrier transmission technology based on OFDMA for their air interface.

Despite the worldwide popularity of OFDMA because of the great and mouth-watering advantages it offers, OFDMA faces certain challenges among which one basic issue is the strict requirement on frequency synchronization. Especially in the uplink transmission, frequency synchronization represents one of the most difficult tasks and plays a major role in the physical layer design. Consequently, need arises to study and analyze the frequency synchronization issues in uplink OFDMA-based systems and to introduce methods to combat the consequences of frequency synchronization errors. These studies of uplink OFDMA-based systems with frequency mismatches, analyses of the resulting impairments and methods to combat the menace of frequency desynchronization are the subject of this thesis.

In this chapter, we start first by presenting a review of the OFDM transmission technique since it is the fundamental building block of OFDMA. Then the context of the thesis is discussed. At the end, the contribution of thesis along with outline of next chapters is presented.

1.1 Orthogonal Frequency Division Modulation - An overview

One of the most challenging hurdles in wireless communication systems is the hostile wireless channel. There are different propagation phenomena which make mobile communications unreliable, among which the multipath fading is the toughest one to cope with [5, 6, 7, 8, 9]. Multipath fading occurs when a transmitted signal takes different paths to propagate from a transmitter, for instance a mobile user, to a receiver, for example a base station. A part of the signal may reach directly at the destination, but other portions will bounce off walls, cars, trees, human bodies or any other objects that get in their path and will arrive at the receiver with different

delays, phases and attenuations. These signals after propagating through different paths add up incoherently at the receiver, which causes fading and severe distortion of the received signal [5, 8]. The need of efficient communication through these frequency selective channels gave birth to what is known as Orthogonal Frequency Division Multiplexing (OFDM).

If the channel's delay spread, which is a measure of span of delays in a channel, is much smaller than the symbol period of the transmitted signal, then the received signal suffers "flat fading" [7]. The term "flat" points to the fact that all frequencies of the transmitted signal experience the same level of channel attenuation and, therefore, the transmitted spectrum is preserved at the receiver. On the other hand, a channel is frequency selective if the frequency response of the channel changes significantly within the band of the transmitted signal [7]. In other words, if the transmitted signal's symbol period is much shorter than the channel's delay spread, we have frequency-selective fading. In this case, the channel gain is not only fluctuating in time, but also is different for different frequency components of the transmitted signal. Digitally modulated signals going through a frequency-selective channel will be distorted, resulting in inter-symbol interference (ISI) [7]. With increase in the data-rate, the probability that a wireless system experiences frequency-selective fading increases. To mitigate the ISI, a complex equalizer [8] is usually needed to make the frequency response of the channel flat within the bandwidth of interest; or the symbol duration must be long enough so that the ISI affected portion of a symbol can be negligible. From the frequency-domain viewpoint, the later approach means to transmit a narrow-band signal within whose bandwidth the channel can be well considered to be flat fading. This fact gives the idea that one can transmit several low-rate data streams, each at a different carrier frequency through the channel in parallel, each data stream is ISI-free and only a simple one-tap equalizer is needed to compensate the flat fading. This transmission scheme is called Frequency Division Multiplexing (FDM). In classical FDM transmitter, the high-speed data stream is first divided into N_p parallel streams, which are running only at $1/N_p$ times the rate of original data stream. These streams are then modulated onto N_p non-overlapping frequency subcarriers. However, this multicarrier transmission scheme may suffer inter-carrier interference (ICI), i.e., the signals of neighboring carriers may interfere with each other. To avoid the ICI, additional space known as guard bands are employed in FDM to separate the subcarriers. The insertion of the guard bands results in a waste of the spectrum.

OFDM follows the very similar multicarrier modulation strategy and it can be viewed as an enhanced version of FDM. The main idea behind OFDM is to convert a frequency selective channel into a collection of flat-frequency subchannels, see Figure 1.1, using Discrete Fourier Transform (DFT). This goal is achieved by dividing
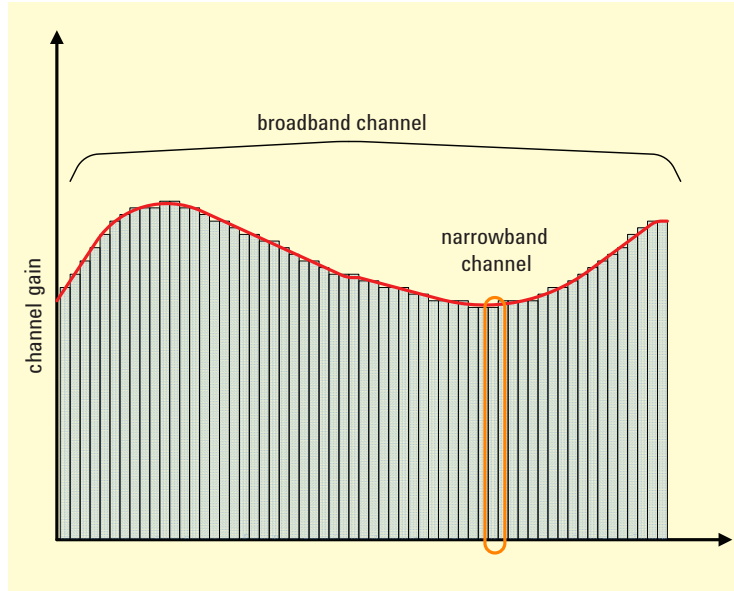
Figure 1.1: OFDM transmission converts a frequency selective channel into a collection of flat-frequency subchannels

the input high-rate data stream into a number of parallel sub-streams of reduced data rates (thus increased symbol duration) and each sub-stream is then transmitted on a separate orthogonal subcarrier. The increased symbol duration improves the robustness of OFDM to channel delay spread. Unlike the guard bands in FDM, OFDM employs the orthogonality principle among sub-carriers to eliminate the ICI, see Figure 1.2.

A time-frequency view of an OFDM signal is shown in Figure 1.3. We can see that even though the subcarrier signals are overlapping in time and frequency domains, there is no mutual interference when sampling is done at specific points. By using orthogonal subcarriers, OFDM-based systems gets more spectrally efficiency compared to the conventional multicarrier systems [10]. Figure 1.4 shows the bandwidth saved with OFDM compared to a conventional multicarrier scheme like FDM with the same subcarrier bandwidth. A guard interval is inserted in an OFDM symbol to protect against interference between OFDM symbols due to multipath channel. The granularities in the time and frequency domain are the OFDM symbol period T and the subcarrier spacing Δf, respectively, as shown in Figure 1.2. The choices of these parameters depend on several factors, e.g. channel conditions, and varies from standard to standard. For example, in a typical WLAN application where mobility is not an issue, the channel delay spread and frequency errors are important factors in the design of OFDM parameters. However, in mobile WiMAX systems, the
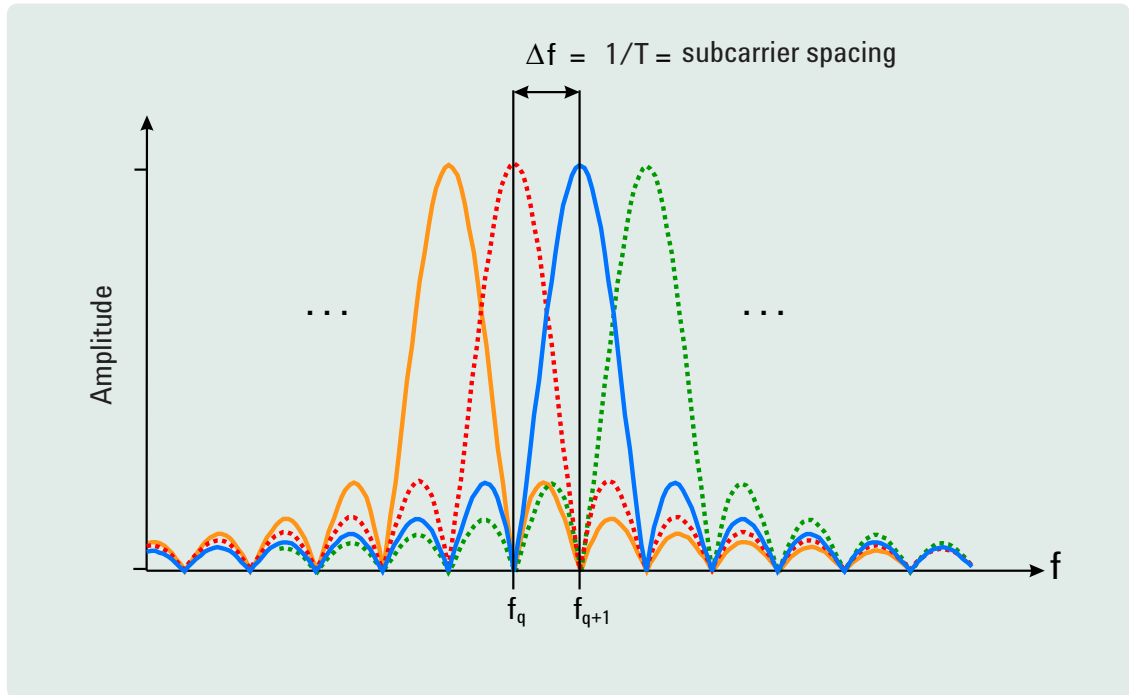
Figure 1.2: An OFDM system with orthogonal subcarriers. Each subcarrier has a null value at other subcarriers' center frequency.
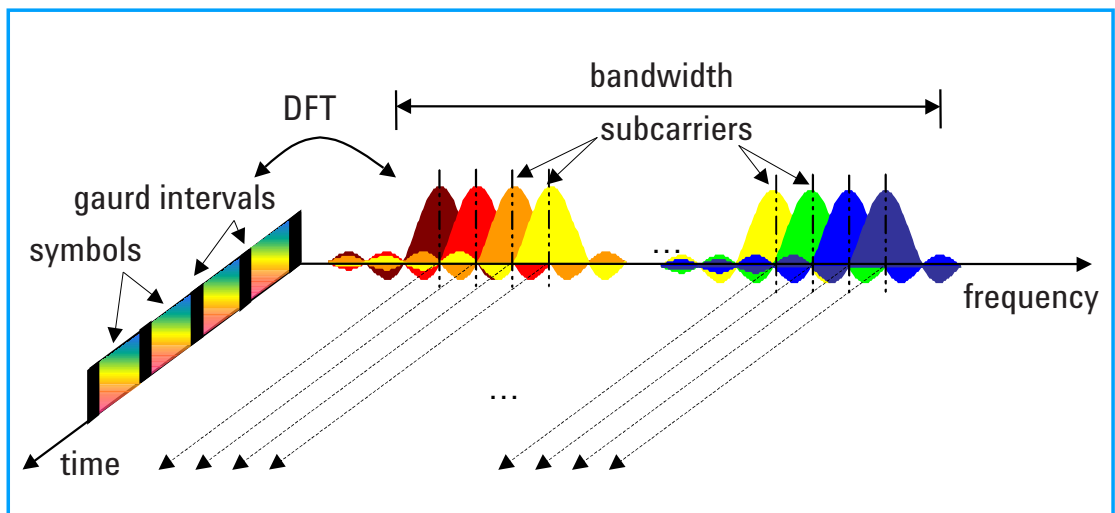
Figure 1.3: Time-frequency representation of OFDM signal
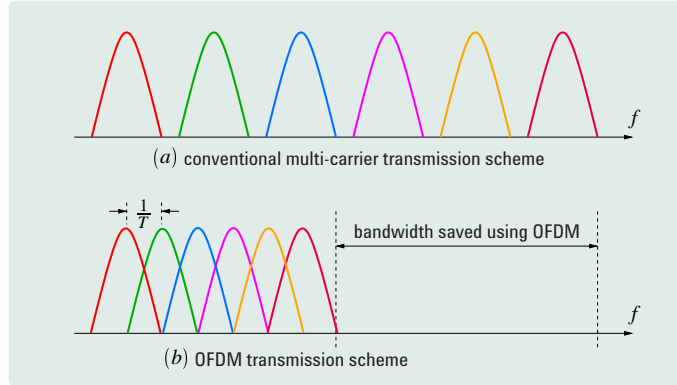
Figure 1.4: Spectral efficiency in OFDM due to orthogonal subcarriers (a) conventional multicarrier transmission (b) OFDM transmission scheme.

Doppler spread has to be considered also. For Wifi, the subcarrier spacing is about 300 kHz and in mobile WiMAX its value is about 11 kHz while the guard interval duration is around 800 nanoseconds for Wifi and is typically around 10 microseconds for WiMAX.

The OFDM transmission technique offers several rewards compared to the single-carrier modulation. As we have explained earlier, the key reasons to use OFDM are its spectrum efficiency and the ability to deal with frequency-selective fading channel with a reasonable implementation complexity. In a single-carrier system, the implementation complexity is dominated by the channel equalization, which is necessary when the channel delay spread is larger than about ten percent of the symbol duration. Moreover, compared to conventional single-carrier systems, OFDM offers increased robustness against multipath distortions as channel equalization can easily be performed in the frequency domain through a bank of one-tap multipliers [11]. For example, in IEEE 802.11a WLAN application, the usage of OFDM technique reduces the system complexity to 1/10 compared to the equivalent single-carrier system [12]. In single-carrier system, the equalization hardware is often built into the system and is unalterable. If the delay spread exceeds the value for which the equalizer is designed to work with, the system performance degrades abruptly. Due to error propagation in equalizer, the raw bit error probability increases so quickly that introducing lower rate coding or a lower constellation size does not significantly improve the situation. For OFDM, however, there are no such nonlinear effects as error propagation, and lower rate coding and/or lower constellation sizes can be employed to provide fall-back rates that are significantly more robust against large delay spread. This feature is desirable, as it enhances the coverage area and avoids the situation where users in deep fades (e.g. having very large delay spread) cannot get any connection at all [12]. Since the data stream is transmitted over the wireless

channel using parallel subcarriers, the quality of reception on individual subcarrier is not very important, compared to the single-carrier system. If one of the subcarriers is in error due to deep fade or narrowband interference, the whole data stream can still be recovered with sufficient channel error coding and interleaving. This is an inherent advantage of the spread spectrum communication. Furthermore, OFDM provides larger flexibility by allowing independent selection of the modulation parameters over each subcarrier [13]. This adaptive modulation and coding (AMC) offered by OFDM has been used in discrete multitone (DMT) system used in the ADSL modems. The knowledge of the frequency domain variations of the channel are used effectively with AMC to obtain higher data rates and lesser transmit power.

The basic principle of OFDM was presented by R. W. Chang [14] in the mid-60s. Shortly after Chang's paper, Saltzberg [15] analyzed the performance of OFDM and made an important conclusion that the strategy of designing an efficient parallel system should concentrate more on reducing crosstalk between adjacent channels than on perfecting the individual channels themselves, since the distortions due to crosstalk tend to dominate. In the 1960s, a large array of sinusoidal generators was used to implement the OFDM transmitter, while the receiver used to consist of a large bank of coherent demodulators with very high frequency accuracy [16, 14, 15]. Such direct implementation was unreasonably complex and expensive, making the OFDM technology unattractive for commercial applications. As a result, it was initially deployed only for military communications. In 1971, Weinstein and Ebert [17] first proposed to apply discrete Fourier transform (DFT) and inverse discrete Fourier transform (IDFT) to perform baseband modulation and demodulation in OFDM systems. Their contribution lies in the elimination of the banks of sub-carrier oscillators and the introduction of the efficient processing. This innovation makes OFDM technology more practical.

Over the last two decades, OFDM has been used in a wide variety of applications, both wired and wireless systems. When applied in a wired environment, OFDM is often referred to as discrete multi-tone (DMT). DMT has been adopted as the standard for the Asymmetric Digital Subscriber Line (ADSL), which provides digital communication at several Mbps from a telephone company central office to a subscriber. OFDM has been particularly successful in numerous wireless applications, where its superior performance in multi-path environments is desirable. OFDM is currently applied in several high rate wireless communication standards such as European digital audio broadcasting (DAB) [18], digital video broadcasting (DVB-T) [19], 802.11a wireless local areal network (WLAN) [20], 802.11g [21] and 802.16 [22]. Several DAB systems proposed in North America and Europe are also based on OFDM [23].

1.2   Multiuser OFDM Systems

The strong and compelling features of OFDM led the researchers around the globe to extend the OFDM concept to multiuser communication scenarios. OFDM itself is just a modulation technique, and it is up to system designers to choose a suitable multiple access technique which allows users to share the available resources. In wireless cellular communications, these resources may comprise of time, frequency, power and space, and therefore the choice of multiple access technique can be Time Division Multiple Access (TDMA), Frequency Division Multiple Access (FDMA), Code Division Multiple Access (CDMA), Space Division Multiple Access (SDMA) or any combination of these schemes.

The Time Division Multiple Access (TDMA) can be combined with OFDM to create the OFDM-TDMA multiple access scheme in which the data from different users is divided in distinct time slots. A time-frequency representation of OFDM-TDMA signal is shown in Figure 1.5. All the available subcarriers are allocated to a particular user for a finite duration of time to fulfill its transmission demands. In WiMAX, OFDM-TDMA is used in one of the transmission modes where the base station allocates the time slots to the users both for the downlink and uplink transmissions. A similar principle is applied in the distributed access scheme in WiFi [24]. This technique is simple but it is also less flexible due to the fact that all the subcarriers must be given to one user at any given time, even if that particular user does not require that much resource.
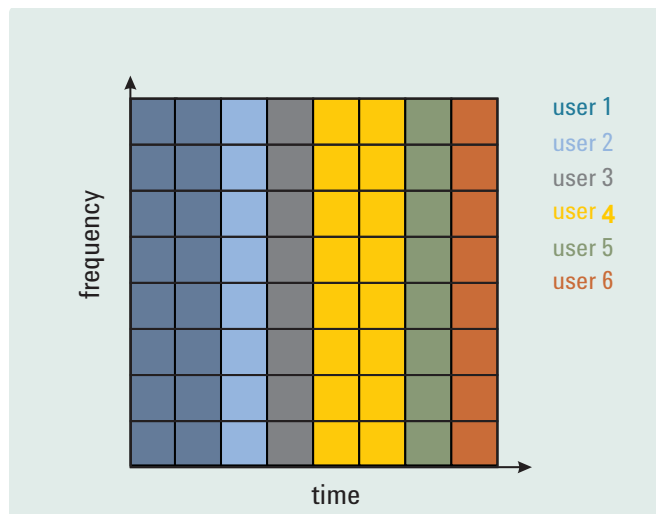
Figure 1.5: Time-frequency representation of OFDM-TDMA transmission scheme.

1.2 Multiuser OFDM Systems

The combination of Code Division Multiple Access (CDMA) and OFDM is often referred to as Multicarrier Code Division Multiple Access (MC-CDMA), where each input data bit is multiplied with a given spreading code and then modulated in the baseband by IFFT for transmission [25, 26, 27]. The spreading can be done in frequency, i.e. the spreaded bits are transmitted via parallel subcarriers, or in time, where the spreaded bits are transmitted over several OFDM symbols, or a combination of both frequency and time. MC-CDMA inherits the OFDM's sensitivity to synchronization error and PAPR issue, and in addition, it is more complex than the OFDM-TDMA scheme because of the involvement of spreading and despreading operations. SDMA employs multiple antennas to allow multiple users to transmit in the same time-frequency block. It makes use of the fact that users are seldom at exactly the same spatial location, and if we can find spatial multipath that only talk to the user being addressed but not the others, then users are said to be separable in space domain. Combination of SDMA and OFDM is attractive because OFDM effectively turns the frequency-selective fading channel into flat fading one and allows for simple SDMA algorithm to be implemented. However, the number of separable users in SDMA is restricted by the number of antennas in the system, which is often limited due to complexity and physical constrains.

Another prominent example of the extension of OFDM to a multiuser scenario is represented by the orthogonal frequency division multiple access (OFDMA) technology, which results from the combination of OFDM with a frequency division multiple access (FDMA) protocol, i.e., OFDM-FDMA. An initial performance comparison of OFDMA with other access schemes e.g. OFDM-TDMA and OFDM-CDMA was done in [28, 29] and it was shown that OFDMA outperforms other multiuser schemes. Among all other multiple access schemes, OFDMA approach permits a very high degree of adaptivity in frequency selective channels combined with a slight technical system complexity [30]. Originally this scheme was proposed by Sari and Karam for cable TV (CATV) networks [31]. In this thesis the focus of our attention is OFDMA, i.e. OFDM-FDMA. In this multiple access scheme, each user is given an independent time-frequency block, which spans one or several OFDM symbols and consists of a number of subcarriers. The main difference between the canonical OFDM and OFDMA is that in OFDMA multiple users are allowed to share the same OFDM symbol(s), but using different sets of subcarriers. The available subcarriers are divided into several mutually exclusive clusters (subchannels or subbands) that are assigned to distinct users for simultaneous transmission, as shown in Figure 1.6. For clarity, the example here uses only four subcarriers shared among four users over two OFDMA symbol periods. The orthogonality among subcarriers guarantees intrinsic protection against multiuser interference (MUI) while the adoption of a dynamic subcarrier assignment strategy provides the system with high flexibility in resource management. Furthermore, OFDMA inherits from OFDM the ability to
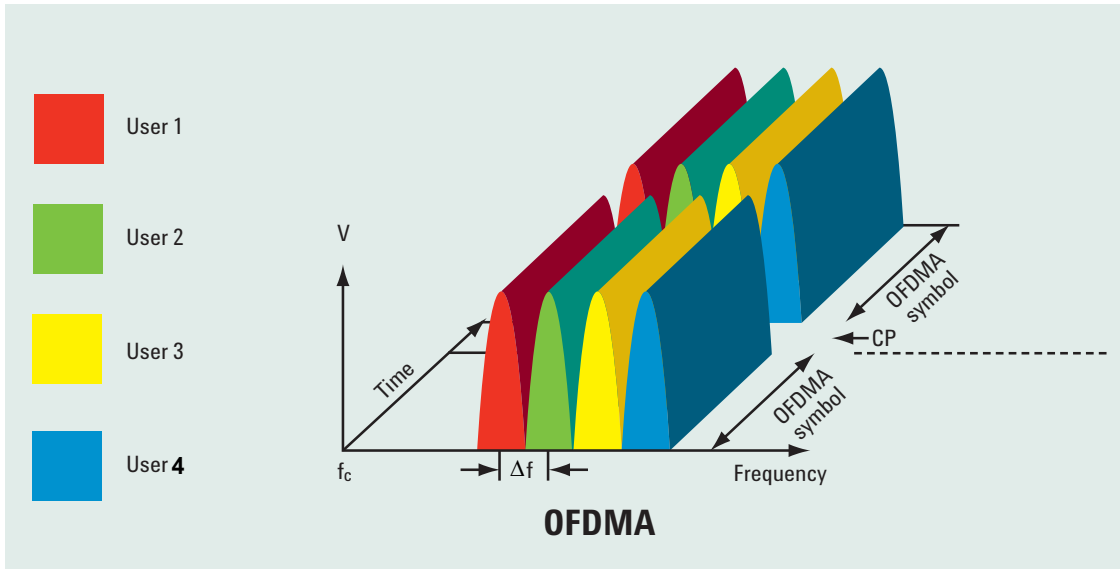
Figure 1.6: Orthogonal frequency division multiplexing with four subcarriers and four users in the system.

compensate channel distortions in the frequency domain without the need of computationally demanding time domain equalizers. One of the important advantages of OFDMA is its ability to assign system resources (i.e. subcarriers and power) to different users based on their channel state information and allows to exploit the frequency diversity and the so-called multiuser diversity [31, 32]. For these reasons OFDMA was adopted in the uplink of the Interaction Channel for Digital Terrestrial Television (DVB-RCT) [33] and more recently it has become part of the engineering IEEE 802.16 standards for wireless metropolitan area networks (WMANs), digital audio broadcasting (DAB) and terrestrial digital video broadcasting (DVB-T).

1.3   Context and Objectives

Some attractive features of OFDMA were presented in the previous section. Due to these extraordinary properties, OFDMA has come forth as the favored transmission scheme and has gained popularity. In spite of these great characteristics, the design and implementation of OFDMA systems is not a simple task and offers several challenges. A difficult engineering concerns in the RF portion of traditional OFDM modems is handling very large peak-to-average power ratios (PAPRs). A peak in the signal power will occur when all, or most, of the sub-carriers align themselves in phase. The value of the PAPR is directly proportional to the number of carriers. For example, for the 802.11a OFDM standard, a PAPR of 17 dB results if the phases of all 52 carriers line up during a symbol period. Even though this worst case peak value occurs with extremely low probability, OFDMA signals have anyway quite high PAPR. This makes the power amplifier design a challenging problem in OFDM systems [34]. One of the most prominent issues is the need for a very fine timing and frequency synchronization due to the fact that OFDMA, like OFDM, is extremely sensitive to timing errors and carrier frequency offsets [35, 36].

In this thesis we focus on the frequency synchronization errors and therefore presume that the system undergoes frequency synchronization errors and make an assumption that there exists perfect time synchronization. The task of frequency synchronization becomes more tough and challenging in the uplink of OFDMA-based systems where one OFDMA symbol is generated by the contribution of many different users with different CFOs. As a consequence, questions are still raised about the use of OFDMA in the uplink direction. We, therefore, concentrate on the uplink OFDMA transmission where the users must be perfectly aligned in frequency to maintain the orthogonality among subcarriers and prevent ICI. Our goals in this thesis include the study and analysis of problems resulting due to frequency mismatches in an uplink OFDMA system and provide solution to combat these problems.

We start by analyzing the interference resulting from CFO. Since the user terminals must be cheap, there is a high chance of CFO coming into play because of misbehavior of the low cost components installed in the user terminals. Throughout this thesis, we assume that the frequency offsets come solely from frequency mismatches of the user terminal oscillators with the base station oscillator. Cyclic prefix is an important part of an OFDMA symbol inserted to combat the interference between consecutive OFDMA symbols because of the multipath channel. Usually while analyzing the interference resulting from CFO, cyclic prefix is not taken into account. We question the effect of CFO induced interference on the cyclic prefix and study the interference behavior in an uplink OFDMA system by taking into account the cyclic prefix which is not studied previously.

In a multiuser environment, one of the resources, apart from power and modulation type, is the number of available subcarriers that need to be allocated to the users. Subcarrier allocation depends on the availability and unavailability of the channel state information (CSI). We consider an uplink OFDMA system with and without CSI and our goal is to allocate the subcarriers to the users in order to optimize system performance. But in systems with CFO, while allocating the carriers to the users, attention must be paid to the ICI resulting from frequency offsets. Therefore, for the OFDMA systems with and without CSI and undergoing CFO, we wonder for a carrier allocation scheme that can provide optimal system performance and resistance to the CFO.

As seen from previous section the nature of OFDMA transmission makes it highly sensitive to CFOs which can cause severe interference. Efficient estimation and compensation methods are required to cancel the drastic effects of CFOs. Our next goal is comprised of two tasks. The first task is to look for joint channel and CFO estimation methods which are less complex compared to existing methods and at the same time maintain the same performance level. Next based on the estimation data obtained from the joint estimation method, we aim at presenting a CFO compensation method used at the receiver with reduced complexity.

1.4   Outline of the thesis

After providing the introduction in this chapter, the remaining chapters of this dissertation are organized as follows

In chapter 2, we present the uplink OFDMA system settings under consideration. We describe the analytical signal model for considered system settings in the absence and presence of CFOs. We further explain the significance of cyclic prefix in an OFDMA symbol and the effect of CFO induced interference on the cyclic prefix is also discussed.

In chapter 3, we investigate the effect of subcarrier allocation on the CFO for uplink OFDMA systems. We discuss the idea of allocating subcarriers to the users in order to optimize throughput by making use of the channel frequency diversity. But in systems that also undergo CFO, while allocating the carriers to the users, we show that attention must be paid to the ICI resulting due to CFO. In this chapter, we look for a carrier allocation scheme that provides a good compromise between the throughput maximization and robustness to the CFO induced ICI for systems with and without CSI.

In chapter 4, we address two very important problems encountered in uplink OFDMA systems because of the CFOs, i.e. Firstly, the need of efficient joint channel impulse response (CIR) and carrier frequency offset estimation and secondly, the CFO compensation problem. We propose a joint CIR and CFO estimator based on an uplink OFDMA system model in which the CFOs resulting from the frequency mismatch of the users' oscillators with the base station oscillator appear at the output of the users' terminal rather than at the base station. For CFO estimation, we use a polynomial approximation method derived from the grid search algorithm which results in less complex CFO estimators. Then we deal with the second problem which is the CFO compensation at the receiver. Based on the CFO estimates obtained from the proposed estimation method, a self-successive interference canceler (self-SIC) algorithm is proposed to mitigate both the self intercarrier interference and multiuser interference at the base station.

At the end we conclude the manuscript and present the summary and perspectives of the work.

1.5 Contribution and Author's Publications

We summarize below the main contributions of this work:

- In chapter 2, an analysis of the effect of carrier frequency offset (CFO) in an uplink OFDMA system has been presented. We demonstrate that one must take into account the cyclic prefix while analyzing interference, i.e. both ICI and multiuser-ICI, resulting from CFO. We propose a new analytical expression of the ICI that takes into account the effect of CFO on the cyclic prefix. We also show the variations in CFO induced interference power with change in lengths of cyclic prefix.

- In chapter 3, an analysis of the trade-off between channel frequency diversity and robustness against CFO in an uplink OFDMA system has been presented. We show that in an OFDMA system with CFO, there exists a contradiction between the two. We propose a trade-off in the form of a *Threshold blocksize*, to allow a good compromise between the channel diversity and robustness for CFO for the case when no CSI is available. For system where CSI is available, we propose an optimal block carrier allocation scheme through which both robustness to CFO and channel frequency diversity can be achieved with small blocksize for small CFO. We also propose a *Critical CFO* value, above which the performance of the optimal block carrier allocation loses interest.

- In chapter 4, we propose solutions for two important issues encountered in an uplink OFDMA system. We propose an efficient method for joint estimation of channel impulse responses and carrier frequency at the receiver. The CFO estimates are obtained using polynomial approximation. These CFO estimates are then used to estimate the channel using the maximum-likelihood approach. Our proposed joint estimation method is simpler than the existing methods without any performance degradation. Next we propose a CFO compensation method based on successive interference cancellation. The proposed method reduces the implementation complexity faced in case of large DFT matrices without any significant loss in performance. Numerical results validate our CFO compensation method.

At the present date, this thesis has led to the following publications:

Journal papers

1. <u>B. Aziz</u>, I. Fijalkow and M. Ariaudo "Joint Channel and Carrier Frequency Offset Estimation based Self-Successive Interference Canceler for Uplink OFDMA," *submitted to IEEE transactions on Communications.*

2. M. Ariaudo, I. Fijalkow, J.L. Gautier, M. Brandon, <u>B. Aziz</u>, B. Milevsky "Green Radio despite "Dirty RF" front-end, " *to the special issue on "Green Radio" of the Eurasip Journal on Wireless Communications and Networking.*

International Conferences

1. <u>B. Aziz</u>, I. Fijalkow and M. Ariaudo "Trade off between Frequency Diversity and Robustness to Carrier Frequency Offset in Uplink OFDMA System," *accepted for publication in Global Telecommunications Conference, 2011. IEEE GLOBECOM '11* , Houston, USA, December 2011.

2. <u>B. Aziz</u>, M. Ariaudo and I. Fijalkow "Critical Carrier Frequency Offset for Uplink OFDMA Carrier Allocation Schemes without Channel State Information," *accepted for publication in European Microwave Conference (EuMC), 2011*, Manchester, United Kingdom, October 2011.

3. <u>B. Aziz</u>, I. Fijalkow and M. Ariaudo "Joint estimation of channel and carrier frequency offset from the emitter, in an uplink OFDMA system," *IEEE International Conference on Acoustics, Speech and Signal Processing (ICASSP), 2011*, Prague, Czech Republic, May 2011.

4. <u>B. Aziz</u>, I. Fijalkow and M. Ariaudo "Intercarrier interference in uplink OFDMA systems with carrier frequency offset," *IEEE 21st International Symposium on*

Personal Indoor and Mobile Radio Communications (PIMRC), 2010 Istanbul, Turkey, September 2010.

National Conferences

1. B. Aziz, I. Fijalkow and M. Ariaudo "Approximation polynomiale pour l'estimation conjointe du canal et le décalage en fréquence pour l'OFDMA en liaison montante," *Gretsi 2011,* Bordeaux, France, September 2011.

Chapter 2

Inter-carrier interference model for uplink OFDMA systems with carrier frequency offsets

O RTHOGONAL Frequency Division Multiple Access (OFDMA) is a very robust transmission technique in mutlipath and frequency selective radio channels. Other advantages of OFDMA include its MIMO-friendliness and ability to provide superior quality of service (QoS). Besides several advantages, OFDMA has a major drawback of being highly sensitive to the errors in carrier frequencies especially in the uplink transmission.

The goal of this chapter is to study the effect of carrier frequency offsets in an OFDMA system by analyzing the inter-carrier interference resulting from loss of orthogonality among adjacent subcarriers. Our contribution in this chapter include a new analytical model for the CFO induced inter-carrier interference that takes into account the effect of CFO on the cyclic prefix. The effect of the length of the cyclic prefix on the CFO induced ICI is also shown through simulations.

2.1 Introduction

Since an OFDMA based system divides the available bandwidth into a set of orthogonal but spectrally overlapping subcarriers, such a transmission is highly sensitive to carrier frequency offsets. The frequency synchronization problem in uplink presents a much more difficult and complicated task compared to the downlink transmission. In the uplink, every user allocates an exclusive set of subcarriers, which is superimposed with other user signals at the base station to form an overall OFDMA symbol [37]. Since every user signal in the uplink will be characterized by an in-

dividual CFO, this will result in strong interference at the base station. In the downlink transmission, there is a single transmitter (the base station) sending data towards many receivers, consequently there can only be a single CFO resulting because of the frequency mismatch at the base station. Therefore in the downlink, frequency synchronization can be achieved by counter rotating the time domain samples. Unfortunately, this is not the case for an uplink scenario because uplink signals are affected by different frequency synchronization errors and the correction of one user's CFO would misalign other initially aligned users [38]. Assume that in a particular uplink OFDMA system, there are two users which undergo CFO between $[-0.1, 0.1]$ of the subcarrier spacing. If the first user has CFO value of 0.1 and the second user has CFO value of -0.1, then by correcting the frequency mismatch with the first user could increase the CFO value of the second user to 0.2. That is why OFDMA is widely used as a universal transmission scheme for downlink direction while it has attracted less attention for use in the uplink direction since a precise synchronization of all the users to the base station is important for such a radio system.

Our aim in this chapter is to investigate the impact of inter-carrier interference (ICI) resulting from CFO in an uplink OFDMA system. CFO besides causing attenuation and rotation of each subcarrier also results in loss of mutual orthogonality among subcarriers by producing a shift of the received signal in the frequency domain. Doppler shift, due to the motion of the transmitter and receiver, is one cause of CFO in a system. Another important factor that produces CFO is the frequency mismatch of the users oscillator with the base station. The equipment installed in the user terminal, such as an oscillator, must be cheap for as they are designed for general users. As a result with the passage of time it might start to dysfunction and results in frequency mismatches. In this thesis, we only consider the case where the CFO results because of the misbehavior of the components in the user terminals and Doppler shift is not considered.

Several researchers have studied the ICI resulting due to frequency synchronization errors in OFDM/OFDMA systems and its impact on the system performance [39, 40, 41, 42, 43]. Analytical models for ICI are provided in [39, 41] but they neglect the effect of CFO on the cyclic prefix. Similarly, authors in [42, 43], while proposing solutions to combat the interference resulting from CFO have considered an interference model which does not consider the influence of frequency offsets on the cyclic prefix. Some interesting results are provided in [40] but the ICI analysis is carried out using the Fourier Transform rather than Discrete Fourier transform (DFT). Therefore, the results in [40] are suitable for the case of an infinite number of carriers which is not very realistic. When transmitting through a frequency-selective channel, the orthogonality of the subcarriers is destroyed, causing severe interference.

To combat the inter-symbol interference (ISI) and ICI, the concept of cyclic prefix was introduced which is a cyclic extension of OFDM symbols. The penalty of using a cyclic prefix is loss of signal energy proportional to the length of the cyclic prefix which in practice is between 1/4 and 1/8 of the total number of subcarriers [44, 45]. However, the benefits of using a cyclic prefix generally outweighs any loss of signal energy. Therefore, one should take into account the cyclic prefix especially while analyzing CFO. In this chapter we analyze the CFO induced ICI by taking into account the effect of the CFO on the cyclic prefix. We start by presenting the details of the OFDMA transmission system under study followed by the details of the analytical signal model and simulation results.

2.2 Uplink OFDMA system

In this section we present the details of the uplink OFDMA transmission system that will be under consideration throughout this thesis. Generally, during an uplink OFDMA transmission in a given cell, there are more than one users transmitting simultaneously towards a single base station, see Figure 2.1. The overall bandwidth is divided into several adjacent subcarriers and each user is allocated a certain number of available subcarriers in order to exclusively fulfill its transmission demands. Moreover, in order to avoid the shadowing and path loss effects, we assume that all the users in the cell are at the same distance from the base station as shown in Figure 2.1.
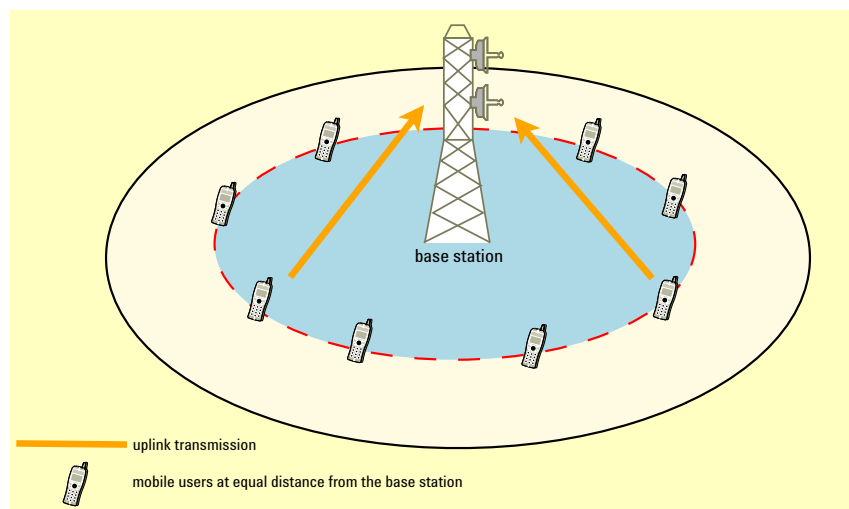
Figure 2.1: Considered uplink system model

In a classical OFDMA transmission model, the binary data stream from a user is
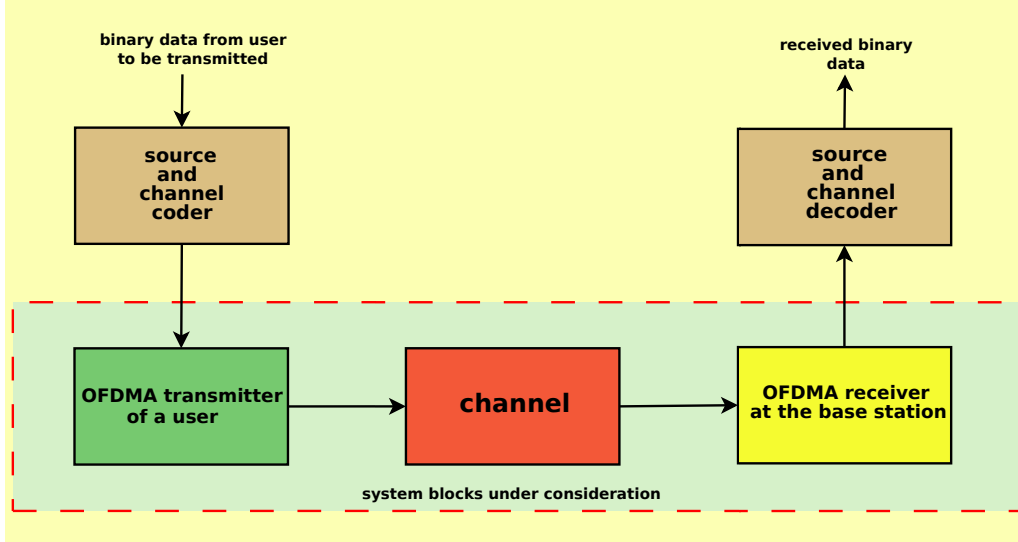
Figure 2.2: Transmission scheme showing the blocks under consideration

passed through source and channel coders before being modulated and transmitted over the physical channel to the receiver. Similarly at the receiver, the received data is demodulated and then passed through the channel and source decoders before being delivered to its final destination. However, here we are considering a non-coded uplink OFDMA transmission. Therefore, we carry out our analysis between the coders at the transmitter and decoders at the receiver as shown in Figure 2.2.

2.3 Analytical signal model

The details of OFDMA uplink transmitter and receiver structure of Figure 2.2 are succinctly presented in the block diagram of Figure 2.3 for a user u transmitting towards a base station. We use the following notation conventions throughout the paper:

N_u	the total number of users in a cell
N_p	total number of subcarriers
W	the total system bandwidth
$\mathcal{M}$	total number of subcarriers allocated to a user
L_{cp}	length of the cyclic prefix
L_h	length of the channel

As seen from the Figure 2.3, the input symbols $\left\{S_k^{(u)}\right\}_{k=0}^{N_p-1}$ denote the transmit sym-
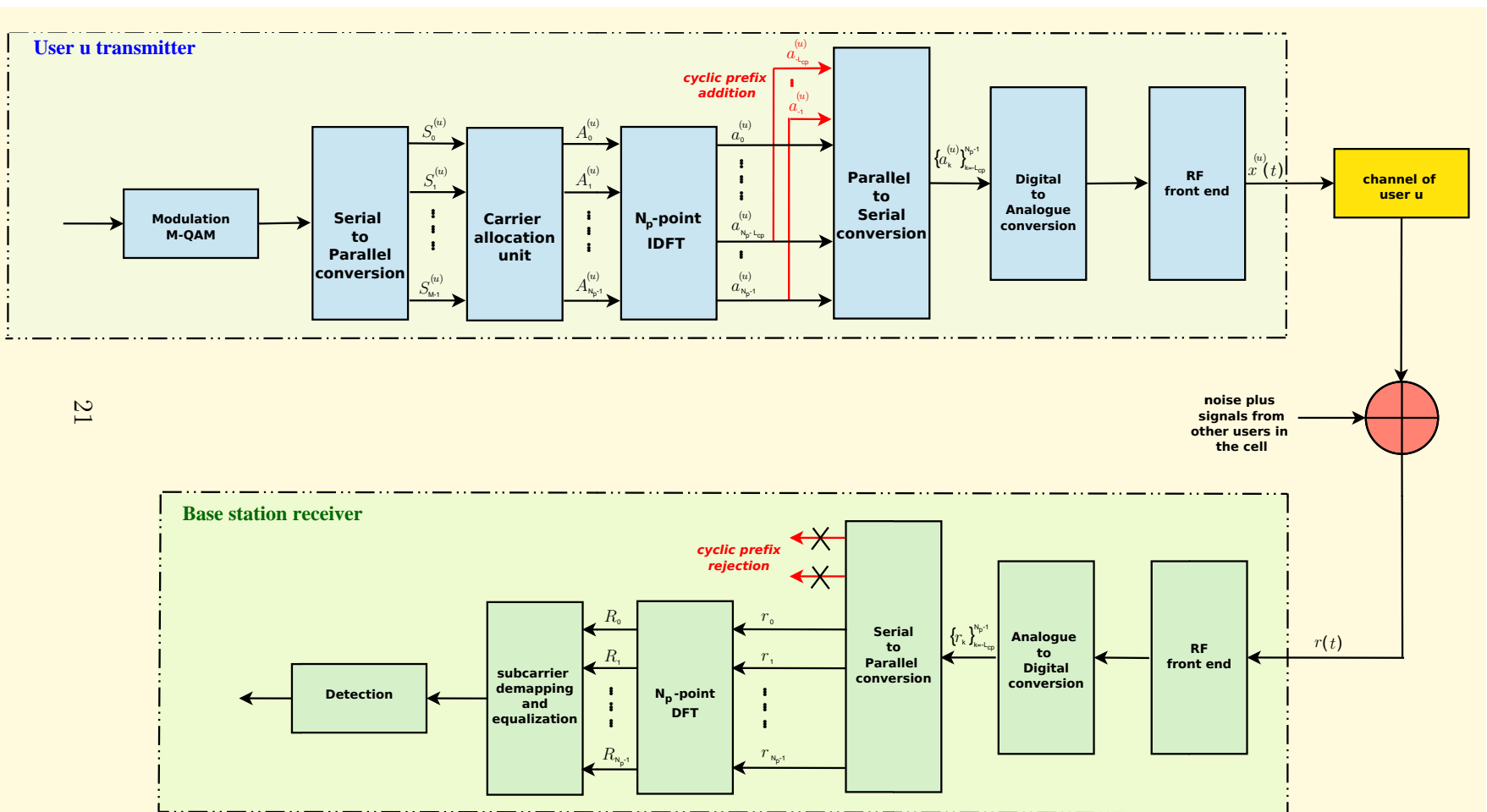
Figure 2.3: Block diagram of uplink OFDMA system

21

bols for the user u. These transmit symbols are obtained by mapping the high-rate bit stream into, for instance, say an M-QAM constellation. The symbols stream is then divided into $\mathcal{M}$ parallel sub-streams by the Serial to Parallel (S/P) conversion. Then the carrier allocation unit maps the incoming parallel symbols onto the subcarriers assigned to the corresponding users. We define $\Gamma^{(u)}$ as the subcarrier allocation set containing the indices of the subcarriers allocated to a user u. The subcarrier allocation sets of different users are independent from each other, i.e. $\Gamma^{(l)} \bigcap \Gamma^{(m)} = \emptyset$, for all $l \neq m$. The size of the set $\Gamma^{(u)}$ is denoted by $|\Gamma^{(u)}|$, which is equal to the number of the subcarriers allocated to user u. There are different methods of selecting the subcarrier allocation sets, which are referred to as carrier allocation schemes. In the generalized carrier allocation schemes, subcarriers can be assigned in different order to users, following specific resource allocation rules, to achieve a specific goal, such as maximizing the system efficiency [32, 46]. Carrier allocation schemes are discussed in detail in chapter 3. Since each user is allocated a part of the available subcarriers, mapping of the incoming data symbols on to the allocated subcarriers is achieved by inserting N_p-$\mathcal{M}$ zeros. Therefore, for a user u, the output of the carrier allocation unit is given by

$$A_k^{(u)} = \begin{cases} S_k^{(u)}, & if \ \ k \in \Gamma^{(u)} \\ 0, & otherwise \end{cases} \tag{2.1}$$

We assume that a fair carrier allocation is used, i.e. all the users get an equal share of the bandwidth. Therefore the size of the subcarrier allocation sets is equal for all the users in the system, i.e. $|\Gamma^{(u)}| = \mathcal{M}$ with $u = 1, ..., N_u$. Expression (2.1) can be written in matrix form as follows

$$\underline{A}^{(u)} = \underline{\Pi}^{(u)} \underline{S}^{(u)} \tag{2.2}$$

where $\underline{\Pi}^{(u)}$ is an $N_p \times \mathcal{M}$ subcarrier mapping matrix for user u and it models the multiple access scenario. It equals 1 for the carriers allocated to user u and zero elsewhere, e.g. for a system having $N_p = 16$ subcarriers and $N_u = 4$ users, each user will get a total of $\mathcal{M} = 4$ subcarriers for transmission. Assuming the subcarriers are allocated in the form of blocks of adjacent subcarriers with a maximum possible blocksize of 4, the subcarrier allocation matrix for user 1 will be

$$\underline{\Pi}^{(1)} = \begin{bmatrix} 1 & 0 & 0 & 0 \\ 0 & 1 & 0 & 0 \\ 0 & 0 & 1 & 0 \\ 0 & 0 & 0 & 1 \\ 0 & \cdots & \cdots & 0 \\ \vdots & \ddots & & \vdots \\ \vdots & & \ddots & \vdots \\ 0 & \cdots & \cdots & 0 \end{bmatrix} \tag{2.3}$$

The output of the carrier allocation unit is then fed to an N_p-point inverse discrete Fourier Transform (IDFT) unit. The output from the IDFT is given by

$$\underline{a}^{(u)} = \begin{bmatrix} a_0^{(u)} \\ a_1^{(u)} \\ \vdots \\ \vdots \\ a_{N_p-1}^{(u)} \end{bmatrix} = \underline{F}^{-1}\underline{A}^{(u)} = \underline{F}^{-1}\underline{\Pi}^{(u)}\underline{S}^{(u)} \tag{2.4}$$

where $\underline{F}^{-1}$ is the inverse DFT matrix given by

$$\underline{F}^{-1} = \begin{bmatrix} 1 & \cdots & \cdots & 1 \\ \vdots & W^{-1} & W^{-2} & \cdots & W^{-(N_p-1)} \\ \vdots & W^{-2} & W^{-4} & \cdots & W^{-2(N_p-1)} \\ \vdots & \vdots & \vdots & \ddots & \vdots \\ 1 & W^{-(N_p-1)} & W^{-2(N_p-1)} & \cdots & W^{-(N_p-1)^2} \end{bmatrix} \tag{2.5}$$

with $W = e^{-j\frac{2\pi}{N_p}}$. The output of the IDFT is collected into a vector and a cyclic redundancy of length (the number of cyclic prefix samples) is added as a prefix in such a way that $a_{-k}^{(u)} = a_{N_p-k}^{(u)}$ for $k = 1, 2, ..., L_{cp}$ as shown in Figure 2.3. The cyclic prefix is, therefore, typically a repetition of the last samples of the data portion of the OFDMA block which is appended to the beginning of the data payload, see Figure 2.4. The introduction of the cyclic prefix can completely eliminate the inter-symbol interference. Furthermore, the cyclic prefix makes the channel appear circular and permits low-complexity frequency domain equalization as will be shown shortly. After the D-to-A conversion and the RF-front end, the signal is sent over the communication channel to the receiver.
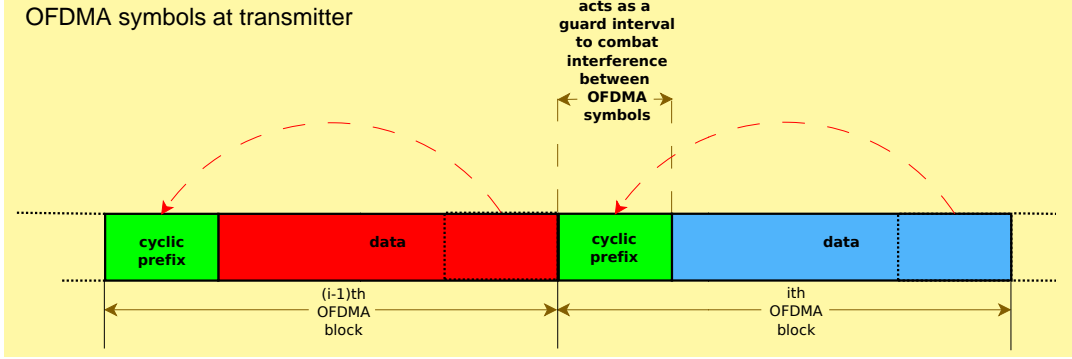
Figure 2.4: Insertion of cyclic prefix as a guard interval at the start of each OFDMA symbol at the transmitter.

2.3.1 Signal at DFT output without CFO: Significance of cyclic prefix

In order to analyze CFO induced interference, we first recall the case of an uplink OFDMA transmission where there is no CFO and assume that the base station is perfectly synchronized to all the users in the cell. The signal model for the no CFO scenario helps to see the significance of cyclic prefix. The final time domain signal present at the output of the transmitter of a user u is given by:

$$x^{(u)}(t) = Re\{e^{j2\pi f_c t} \sum_{k=0}^{N_p-1} a_k^{(u)} p^{(u)}(t - \frac{kT}{N_p})\} \tag{2.6}$$

where f_c is the carrier frequency, $p^{(u)}(t)$ is the impulse response of the low pass filter at the transmitter and T is the symbol duration of an OFDMA symbol. Signals from different users pass through individual multipath radio channels and the received signal at the base station is the sum of the signals from all users. The overall noise plus CFO free received signal is given by:

$$r(t) = Re\{\sum_{u=1}^{N_u} \sum_{k=0}^{N_p-1} a_k^{(u)} h^{(u)}(t - \frac{kT}{N_p})e^{j2\pi f_c t}\} \tag{2.7}$$

where $h^{(u)}$ represents the combined impulse response of the channel from the user u and of the transmitter and receiver filters. The baseband samples, at a symbol rate T/N_p, at the input of the receiver Discrete Fourier Transform (DFT) unit can be

24

2.3 Analytical signal model

written as

$$
\begin{bmatrix} r_{N_p-1} \\ \vdots \\ \vdots \\ \vdots \\ r_1 \\ r_0 \end{bmatrix} = \sum_{u=1}^{N_u} \begin{bmatrix} h_0^{(u)} & \dots & h_{L_{cp}}^{(u)} & \dots & h_{L_h-1}^{(u)} & 0 & \dots & \dots & \dots & 0 \\ 0 & \ddots & & \ddots & & \ddots & \ddots & & & \vdots \\ \vdots & & \ddots & & \ddots & & \ddots & \ddots & & \vdots \\ \vdots & & & \ddots & & \ddots & & \ddots & \ddots & \vdots \\ \vdots & & & & \ddots & & \ddots & & \ddots & 0 \\ 0 & \dots & \dots & \dots & \dots & h_0^{(u)} & \dots & h_{L_{cp}}^{(u)} & \dots & h_{L_h-1}^{(u)} \end{bmatrix} \begin{bmatrix} a_{N_p-1}^{(u)} \\ \vdots \\ \vdots \\ a_0^{(u)} \\ \vdots \\ a_{-L_{cp}}^{(u)} \\ a_{N_p-1}^{*(u)} \\ \vdots \\ a_{N_p-\epsilon}^{*(u)} \end{bmatrix}
$$
$$(2.8)$$

where $\epsilon = L_h - L_{cp} - 1$ is the channel length exceeding the length of cyclic prefix, L_{cp}. The entities marked in red color, i.e. $a_{N_p-1}^{*(u)} \dots a_{N_p-\epsilon}^{*(u)}$, appear only if the channel length L_h exceeds the duration of cyclic prefix, i.e. $\epsilon > 0$ and thereby contribute to what is known as inter-symbol interference (ISI).

For the simplicity of presentation, in this thesis we consider the case where the cyclic prefix length is greater than channel impulse response length, i.e. $L_{cp} > L_h$. Therefore, there will be no ISI as shown in Figure 2.5.
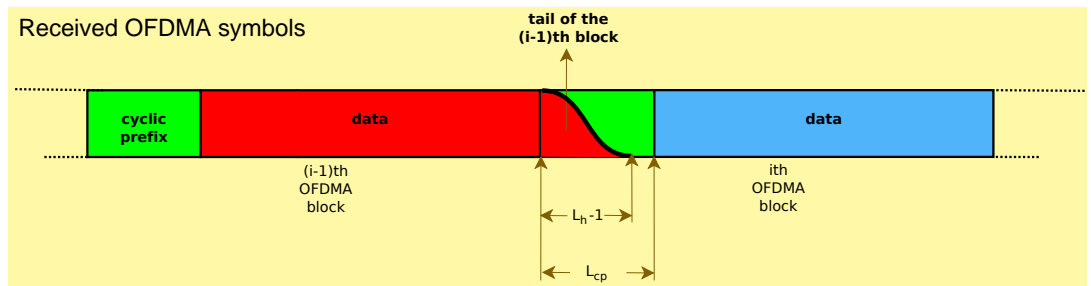
Figure 2.5: Partial overlapping between received OFDMA blocks but cyclic prefix length larger than channel delay spread ensures elimination of ISI.

The incorporation of cyclic prefix property $a_{-k}^{(u)} = a_{N_p-k}^{(u)}$ for $k = 1, 2, ..., L_{cp}$, for the case of channel impulse response being shorter than the duration of cyclic prefix

leads to the following equation,

$$
\begin{bmatrix} r_{N_p-1} \\ \vdots \\ \vdots \\ \vdots \\ r_1 \\ r_0 \end{bmatrix} = \sum_{u=1}^{N_u} \underbrace{\begin{bmatrix} h_0^{(u)} & \cdots & \cdots & h_{L_{cp}-1}^{(u)} & 0 & \cdots & 0 \\ 0 & \ddots & & & \ddots & \ddots & \vdots \\ \vdots & \ddots & \ddots & & & \ddots & 0 \\ 0 & & \ddots & \ddots & & & h_{L_{cp}-1}^{(u)} \\ h_{L_{cp}-1}^{(u)} & \ddots & & \ddots & \ddots & & \vdots \\ \vdots & \ddots & \ddots & & \ddots & \ddots & \vdots \\ h_1^{(u)} & \cdots & h_{L_{cp}-1}^{(u)} & 0 & \cdots & 0 & h_0^{(u)} \end{bmatrix}}_{\underline{h}_{circ}^{(u)}} \begin{bmatrix} a_{N_p-1}^{(u)} \\ \vdots \\ \vdots \\ \vdots \\ a_1^{(u)} \\ a_0^{(u)} \end{bmatrix}
$$

$$(2.9)$$

It is interesting to note here that the effective $N_p \times N_p$ channel matrix now becomes circulant i.e. its rows are circularly shifted versions of each other. This results in major simplifications, described below, once the receiver, as shown in Figure 2.3, takes the DFT after cyclic prefix removal. However, this circulant nature of the effective channel matrix is void if the channel is time variant, because in that case the CIR coefficients appearing in a row (corresponding to a sample of the OFDMA symbol) are potentially different than the CIR coefficients appearing in some other row. Thus, for the case of sufficient cyclic prefix (transition from equation (2.8) to (2.9)) and time-invariant channel (channel matrix in (2.9) becoming truly circulant), the under consideration system can be described by the following relationship in the subcarrier (frequency) domain,

$$
\underline{R} = \sum_{u=1}^{N_u} \underline{F} \; \underline{h}_{circ}^{(u)} \underline{F}^{-1} \underline{A}^{(u)}
\tag{2.10}
$$

The DFT matrix $\underline{F}$ is unitary in nature i.e. $\underline{F} \; \underline{F}^{-1} = \underline{I}_{N_p}$. Now because the Eigen Value Decomposition (EVD) of a circulant matrix such as $\underline{h}_{cric}^{(u)}$ can be given as [47],

$$
\underline{h}_{circ}^{(u)} = \underline{F}^{-1} \underline{\Lambda}^{(u)} \; \underline{F}
\tag{2.11}
$$

$\underline{F}$ being the unitary DFT matrix and the diagonal matrix $\underline{\Lambda}^{(u)}$ containing eigenvalues of the circulant matrix can be given in this case as

$$
\underline{\Lambda}^{(u)} = diag \left(\underline{F} \begin{bmatrix} h^{(u)} \\ 0_{N_p-L_h} \end{bmatrix} \right) \triangleq \underline{H}^{(u)}
\tag{2.12}
$$

2.3 Analytical signal model

The matrix $\underline{H}^{(u)}$ is defined to be a diagonal matrix containing the Channel Frequency Response (CFR) coefficients for user u along its main diagonal. Plugging in the substitutions from equations (2.11) and (2.12), the system model in equation (2.10) reduces to

$$\underline{R} = \sum_{u=1}^{N_u} \underline{H}^{(u)} \ \underline{A}^{(u)} \tag{2.13}$$

We note that the fading multipath channel boils down to a number of interference-free parallel subchannels whereby, each of the received subcarrier can be given as the corresponding transmitted subcarrier scaled by a scalar complex fading coefficient (CFR at that subcarrier). The detection scheme at the receiver can be as simple as just dividing the received subcarrier by the estimated channel frequency response. Presented below in Figure 2.6 is a comprehensive graphical representation of the OFDMA system model, whereby we note the existence of interference-free parallel sub-channels in the frequency domain.
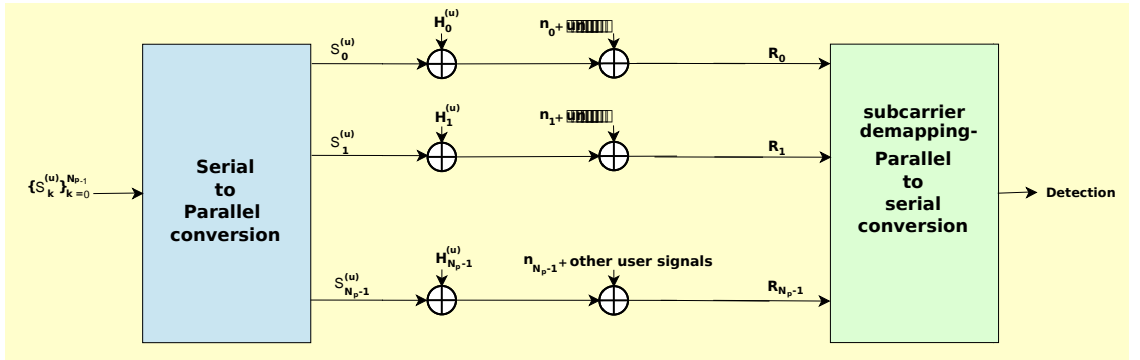
Figure 2.6: Effective OFDMA system model with a cyclic prefix exceeding the channel length and with all the users perfectly synchronized, i.e. no CFO of any kind exists in the system.

The concept of a cyclic prefix was presented by Peled and Ruiz [48] in 1980 to combat the ISI and ICI. Instead of using an empty guard space in time between OFDM symbols, they proposed to fill the guard space with a cyclic extension of OFDM symbols. This effectively simulates a channel performing circular convolution, which implies orthogonality of subcarriers when the cyclic prefix is longer than the impulse response of the channel. The drawback of using a cyclic prefix is consumption of signal energy which is proportional to the length of the cyclic prefix. However, the benefits of using a cyclic prefix overcome any loss of signal energy.

2.3.2 Signal at DFT output with CFO

Having demonstrated the no-CFO scenario in the previous section, in this section, we consider the case where the user u is not perfectly synchronized to the carrier frequency allocated to it and therefore exhibits a certain CFO. In this case the signal at the output of the transmitter of user u will become

$$x^{(u)}(t) = Re\{e^{j2\pi(f_c+\delta f_c^{(u)})t} \sum_{k=0}^{N_p-1} a_k^{(u)} p^{(u)}(t - \frac{kT}{N_p})\} \tag{2.14}$$

where $\delta f_c^{(u)}$ represents the CFO of user u with respect to f_c. CFO are mainly caused because of two factors: Doppler effects and oscillator inaccuracies in the transmitter and receiver. Frequently, these two types of CFOs are grouped together and modeled as a single frequency offset appearing at the channel output, as in [49, 50]. However, this is not sufficiently accurate since the CFO resulting from a user terminal should appear at the channel input rather than at the channel output. Since, we consider the case where the CFO solely appears because of the mismatch of a user's oscillator with the base station, therefore, the CFO appears before the channel convolution in the transmitted signal as shown by (2.14). This scenario is shown in the Figure 2.7.
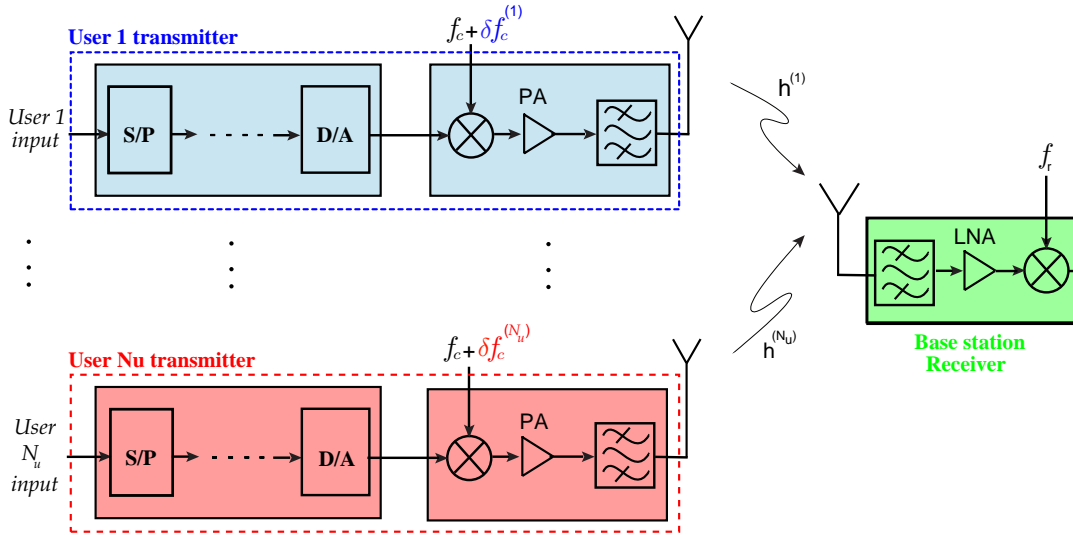
Figure 2.7: OFDMA uplink transmission where the users are not perfectly synchronized in frequency thus contributing independent and distinct CFOs. PA:Power amplifier/LNA:Low Noise Amplifier.

2.3 Analytical signal model

As a result of this CFO, the overall received signal at the base station will become

$$r(t) = Re\{\sum_{u=1}^{N_u} \sum_{k=0}^{N_p-1} a_k^{(u)} h^{(u)}(t - \frac{kT}{N_p}) e^{j2\pi(f_c+\delta f_c^{(u)})t}\} \tag{2.15}$$

and the baseband samples at the DFT input before cyclic prefix removal becomes

$$\begin{bmatrix} r_{N_p-1} \\ \vdots \\ r_0 \\ \vdots \\ r_{-L_{cp}} \end{bmatrix} = \sum_{u=1}^{N_u} \begin{bmatrix} h_0^{(u)} & \cdots & h_{L_h-1}^{(u)} & & & 0 \\ & \ddots & & \ddots & & \\ & & \ddots & & \ddots & \\ 0 & & & h_0^{(u)} & \cdots & h_{L_h-1}^{(u)} \end{bmatrix} \begin{bmatrix} \delta^{(N_p+L_{cp}-1)(u)} & & 0 \\ & \ddots & \\ 0 & & \delta^{0(u)} \end{bmatrix} \begin{bmatrix} a_{N_p-}^{(u)} \\ \vdots \\ a_0^{(u)} \\ \vdots \\ a_{-L}^{(u)} \end{bmatrix} \tag{2.16}$$

Note that $\delta^{k(u)} = e^{j2\pi k\delta f_c^{(u)}T/N_p}$ where $k = 0, ..., N_p - 1$ are the shift coefficients. The CFO of user u normalized to the subcarrier spacing Δf is given by

$$\delta f^{(u)} = \frac{\delta f_c^{(u)}}{\Delta f} = \delta f_c^{(u)} T \tag{2.17}$$

As stated earlier, $h_k^{(u)}$ is the discrete channel impulse response from user u to the base station with $k = 0, ..., L_h$. Since the channel impulse response length is smaller than L_{cp}, therefore the last terms of $h_k^{(u)}$ can be zeros. In the case of a CFO, $\delta f^{(u)}$ between a user u and the receiver base station, we show next that the channel matrix does not remain circulant. If the receiver performs the usual cyclic prefix symbols discarding and rearrangement as when there is no CFO, after some calculations, we

get,

$$
\begin{bmatrix} r_{N_p-1} \\ \vdots \\ \vdots \\ \vdots \\ r_0 \end{bmatrix} = \sum_{u=1}^{N_u} \left[\underline{h}_{circ}^{(u)} + \underbrace{(\delta^{-N_p(u)}-1)}_{x} \underbrace{\begin{bmatrix} 0 & \cdots & \cdots & \cdots & \cdots & 0 \\ \vdots & & & & & \vdots \\ 0 & & & & & \vdots \\ h_{L_{cp}-1}^{(u)} & \ddots & & & & \vdots \\ \vdots & \ddots & \ddots & & & \vdots \\ h_{L_{cp}-1}^{(u)} & \cdots & h_{L_{cp}-1}^{(u)} & 0 & \cdots & 0 \end{bmatrix}}_{\underline{h}_\Delta^{(u)}} \right] \underbrace{\begin{bmatrix} \delta^{0(u)} & 0 & \cdots & \cdots & & 0 \\ 0 & \ddots & \ddots & & & \vdots \\ \vdots & \ddots & \ddots & \ddots & & \vdots \\ \vdots & & \ddots & \ddots & 0 \\ 0 & \cdots & \cdots & 0 & \delta^{-(N_p-1)(u)} \end{bmatrix}}_{\underline{\delta}^{(u)}} \begin{bmatrix} a_{N_p-1}^{(u)} \\ \vdots \\ \vdots \\ \vdots \\ a_0^{(u)} \end{bmatrix}
\tag{2.18}
$$

From equation (2.18), we find that the channel matrix can not be written in a circulant form unless we discard the additional terms $x\underline{h}_\Delta^{(u)}$ appearing in (2.18). The received signal model presented in (2.18) is not linear in CFO. This can be illustrated through an example.

Example: A common practice, while analyzing the CFO induced ICI in uplink OFDMA systems, is to apply the CFO resulting from the oscillator misbehavior at the output of the channel. This holds true only if the received signal model is a linear function of CFOs. Through this example we show that this assumption is not true because of the cyclic prefix and finite length DFT. We show that the received signal model is not linear in CFO and that the CFO due to oscillator mismatches must be appear in the signal at the user terminal output i.e. before the channel convolution. First we consider our scenario where the CFO appears at the output of the user terminal. For illustration purposes we consider an example of uplink OFDMA system with $N_p = 4$, $L_{cp} = L_h = 2$ and $N_u = 1$. In this case the signal at

2.3 Analytical signal model

the input of the DFT block before the removal of the cyclic prefix is given by

$$
\begin{bmatrix} r_3 \\ r_2 \\ r_1 \\ r_0 \\ r_{-3} \\ r_{-2} \end{bmatrix} = \begin{bmatrix} h_0 & h_1 & 0 & \cdots & \cdots & \cdots & 0 \\ 0 & h_0 & h_1 & & & & \vdots \\ \vdots & & h_0 & h_1 & & & \vdots \\ \vdots & & & h_0 & h_1 & & \vdots \\ \vdots & & & & h_0 & h_1 & 0 \\ 0 & \cdots & \cdots & \cdots & 0 & h_0 & h_1 \end{bmatrix} \begin{bmatrix} \delta^5 a_3 \\ \delta^4 a_2 \\ \delta^3 a_1 \\ \delta^2 a_0 \\ \delta^1 a_{-3} \\ \delta^0 a_{-2} \end{bmatrix} \qquad (2.19)
$$

As the frequency error appears at the transmitter output, each transmitted symbol has a different shift coefficient as shown in Figure 2.8. The received symbols r_{-3}, r_{-2}
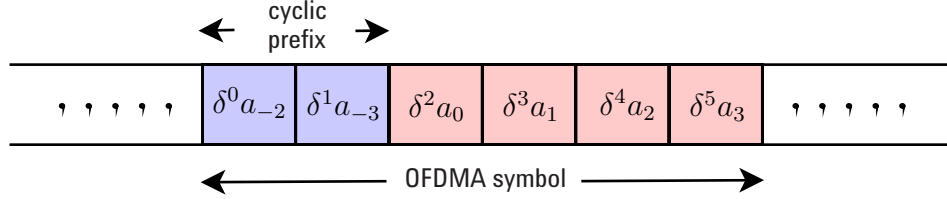
Figure 2.8: Each transmitted symbol has a different shift coefficient due to the CFO resulting from transmitter oscillator misbehavior.

correspond to the symbols transmitted in the cyclic prefix. The received symbols after the removal of the cyclic prefix are given by

$$
\begin{aligned}
r_3 &= h_0 \delta^5 a_3 + h_1 \delta^4 a_2 \\
r_2 &= h_0 \delta^4 a_2 + h_1 \delta^3 a_1 \\
r_1 &= h_0 \delta^3 a_1 + h_1 \delta^2 a_0 \\
r_0 &= h_0 \delta^2 a_0 + h_1 \delta^1 a_{-3}
\end{aligned} \qquad (2.20)
$$

We saw in section 2.3.1 that prefixing the end of the symbol to the beginning makes the linear convolution of the channel appear as though it were circular convolution. But if we look at the received symbol r_0, we have $a_{-3} = a_3$ but because of the different shift coefficient the channel matrix no longer remains circulant i.e. $a_{-3} h_1 \delta^1 \neq a_3 h_1 \delta^5$. Next we consider the received signal model presented in [41] where the authors consider that the shift because of the oscillator mismatch appears at the channel output. In this case the received symbols at the input of the

DFT block before the cyclic prefix removal are given in matrix form as

$$
\begin{bmatrix} r_3 \\ r_2 \\ r_1 \\ r_0 \\ r_{-3} \\ r_{-2} \end{bmatrix} = \begin{bmatrix} \delta^5 & 0 & 0 & 0 & 0 & 0 \\ 0 & \delta^4 & 0 & 0 & 0 & 0 \\ 0 & 0 & \delta^3 & 0 & 0 & 0 \\ 0 & 0 & 0 & \delta^2 & 0 & 0 \\ 0 & 0 & 0 & 0 & \delta^1 & 0 \\ 0 & 0 & 0 & 0 & 0 & \delta^0 \end{bmatrix} \begin{bmatrix} h_0 & h_1 & 0 & \cdots & \cdots & \cdots & 0 \\ 0 & h_0 & h_1 & & & & \vdots \\ \vdots & & h_0 & h_1 & & & \vdots \\ \vdots & & & h_0 & h_1 & & \vdots \\ \vdots & & & & h_0 & h_1 & 0 \\ 0 & \cdots & \cdots & \cdots & 0 & h_0 & h_1 \end{bmatrix} \begin{bmatrix} a_3 \\ a_2 \\ a_1 \\ a_0 \\ a_{-3} \\ a_{-2} \end{bmatrix}
$$

(2.21)

which can be written, after the removal of cyclic prefix, as

$$
\begin{aligned}
r_3 &= h_0 \delta^5 a_3 + h_1 \delta^5 a_2 \\
r_2 &= h_0 \delta^4 a_2 + h_1 \delta^4 a_1 \\
r_1 &= h_0 \delta^3 a_1 + h_1 \delta^3 a_0 \\
r_0 &= h_0 \delta^2 a_0 + h_1 \delta^2 a_{-3}
\end{aligned}
$$

(2.22)

From (2.20) and (2.22) we can see that the received signal model in (2.18) is not linear. Therefore, the CFO due to the oscillator mismatches should be considered at the channel input rather than at the output.

Going back to the model in (2.18), at the output of the DFT block, $\underline{R} = \underline{F}(r_{N_p-1}, ..., r_0)^T$ is shown [51] to be equal to

$$
\underline{R} = \sum_{u=1}^{N_u} \underline{G}^{(u)} \ \underline{A}^{(u)}
$$

(2.23)

where $\underline{A}^{(u)} = \underline{F} \ \underline{a}^{(u)}$ is the vector of transmitted modulation symbols of user u after subcarrier mapping and $\underline{F}$ is the $N_p \times N_p$ DFT matrix. The matrix $\underline{G}^{(u)}$ represents the channel and the CFO effect for a user u and is given by

$$
\underline{G}^{(u)} = \underline{H}^{(u)} \underline{F} \ \underline{\delta}^{(u)} \underline{F}^{-1} + (\delta^{-N_p(u)} - 1) \underline{F} \ \underline{h}_\Delta^{(u)} \underline{\delta}^{(u)} \underline{F}^{-1}
$$

(2.24)

where $\underline{H}^{(u)}$ is the diagonal DFT channel matrix for the user u with $\underline{H}^{(u)} = \underline{F} \ \underline{h}^{(u)}$, thanks to the channel impulse response length $L_h < L_{cp}$.

The expression (2.24) takes into account the effect of CFO on the cyclic prefix on the contrary of previous works [41]. Authors in [41], while analyzing the ICI due to CFO, have completely ignored the effect of CFO on the cyclic prefix in the received signal and the expression for the received signal at the output of the DFT block is reduced to only

$$
\underline{R} = \sum_{u=1}^{N_u} \underline{H}^{(u)} \underline{\delta}^{(u)} \underline{F}^{-1} \underline{A}^{(u)}
$$

(2.25)

The above expression does not take into account the effect of CFO on the cyclic prefix and therefore is not accurate.

2.3.3   CFO induced self and multiuser interferences

Equation (2.23) can be written in the form of the wanted signal of a user l transmitting on a subcarrier v and the CFO induced interference from all other subcarriers as follows

$$R_v = X_v^{(l)} + \zeta_v^{ici} \tag{2.26}$$

where

$$X_v^{(l)} = H_v^{(l)} A_v^{(l)} \sum_{n=0}^{N_p-1} e^{j\frac{2\pi n}{N_p}\delta f^{(l)}} \tag{2.27}$$

In (2.27), $H_v^{(l)} A_v^{(l)}$ is the desired signal while the remaining part of $X_v^{(l)}$ represents the additional loss on modulation symbol $A_v^{(l)}$ due to the individual CFO of user l transmitting on the subcarrier v. ζ_v^{ici} represents the interference coming from all the other carriers and is given by

$$\zeta_v^{ici} = \sum_{u=1}^{N_u} \sum_{\substack{k=0 \\ k \neq v}}^{N_p-1} G_{(v,k)}^{(u)} A_k^{(u)} \tag{2.28}$$

where $G_{(v,k)}^{(u)}$ is given by

$$\begin{aligned}
G_{(v,k)}^{(u)} &= \sum_{n=0}^{N_p-1} H_k^{(u)} e^{j\frac{2\pi n}{N_p}(k-v+\delta f^{(u)})} + \\
&(\delta^{-N_p(u)} - 1) \sum_{n=0}^{L-2} \sum_{m=1}^{L-1-n} h_{m+n}^{(u)} e^{j\frac{2\pi}{N_p}\left[(Np-m)(k+\delta f^{(u)})-vn\right]}
\end{aligned} \tag{2.29}$$

This interference can be further categorized into the self-ICI of user l and the multiuser-ICI (MUI) from all other users as follows

$$\zeta_v^{ici} = \underbrace{\sum_{\substack{k=\in\Gamma^{(l)} \\ k\neq v}} G_{(v,k)}^{(l)} A_k^{(l)}}_{self-ICI} + \underbrace{\sum_{\substack{u=1 \\ u\neq l}}^{N_u} \underbrace{\sum_{\substack{k\in\Gamma^{(u)} \\ k\neq v}} G_{(v,k)}^{(u)} A_k^{(u)}}_{MUI^{(u)}}}_{MUI} \tag{2.30}$$

where $\Gamma^{(u)}$ is the set of subcarriers allocated to user u. In (2.30), $self-ICI$ is the interference observed by user l, on subcarrier v, from its own allocated subcarriers other than v. $MUI^{(u)}$ and MUI represent the individual interferences of all other users present in the system and the overall interference contributed to subcarrier v

of user l, respectively.

Next we compute the quantitative impact of the CFO induce ICI by deriving its variance. The modulation symbols are assumed to be statistically independent random variables from a predefined modulation alphabet and independent from one user to another, i.e. $E\left\{A_k^{(l)} A_i^{*(j)}\right\} = 0$. Furthermore, the transmission power for the modulation symbols is normalized such that $E\left\{\left|A_k^{(l)}\right|^2\right\} = 1$. Hence according to the central limit theorem, the CFO induced ICI ζ_v^{ici} can be modeled as a zero-mean Gaussian distributed noise signal with a variance $\sigma_{v,l}^2 = E\left\{\left|\zeta_v^{ici}\right|^2\right\}$, see [52]. The analytical expression for the variance of the CFO induced interference observed by the subcarrier v, allocated to user l, is given by

$$\sigma_{v,l}^2 = \sum_{\substack{k \in \Gamma^{(l)} \\ k \neq v}}^{N_p-1} \left(\begin{array}{l} \left|H_k^{(l)}\right|^2 \frac{\sin^2\left(\pi\left(\delta f^{(l)}+k-v\right)\right)}{\pi\left(\delta f^{(l)}+k-v\right)} + \\ \left|\delta^{-N_p}(l) - 1\right|^2 \sum_{n=0}^{L-2} \sum_{d=0}^{L-2} \sum_{m=1}^{L-n-1} \sum_{c=1}^{L-d-1} \left|h_{m+n}^{(l)} h_{c+d}^{(l)+}\right|^2 e^{\frac{j2\pi}{N_p}\left[\left(k+\delta f^{(l)}\right)(c-m)+v(d-n)\right]} \end{array} \right) \tag{2.31}$$

Unlike the ICI variance expression in [41], the above expression for the CFO induced ICI takes into account the effect of the CFO on the cyclic prefix. The first term in (2.31) corresponds to the case when the influence of CFO on the cyclic prefix is ignored. The second term comes in because we take into account this effect.

As a result, the overall signal to noise plus interference (SINR) ratio for the subcarrier v is given by

$$SINR_v^{(l)} = \frac{\rho_v \left|H_v^{(l)}\right|^2}{\sum\limits_{u=1}^{N_u} \sigma_{v,u}^2 + \sigma_{v,noise}^2} \tag{2.32}$$

It is observed from (2.32) that the SINR not only depends on the CFO but also on the channel condition of user l who is allocated to the subcarrier v. It also depends on the self and multi user interferences. ρ_v represents the self-loss of user l due to frequency offset in subcarrier v and $\sigma_{v,noise}^2$ represents the additional Gaussian noise power present at the receiver.

2.4   Realistic CFO values

Before presenting the simulation results, in this section we wonder about the order of CFO values resulting due to oscillators' frequency mismatch in an uplink

2.4 Realistic CFO values

OFDMA system. A frequency offset measures the difference (misalignment) between the carrier frequency generated by the reference oscillators at the transmitter and the expected carrier frequency. At the receiver the unmodulated frequency is required for reception without errors; and is usually generated in the receiver with crystals. The transmitter is required to transmit at the nominal carrier frequency. However, due to several reasons, it is not physically possible to make the transmitter frequency exactly match with the receiver frequency which results in an unintended offset. This offset, drift, misalignment or mismatch between the transmitter and receiver frequencies is termed as carrier frequency offset.

From analytical model of the CFO induced ICI presented in previous sections, one can see that the CFO causes the following detrimental effects:

- The attenuation of received signal, since the amplitude of the periodic-sinc function, is always less than unity if $\delta f^{(u)}$ is non-zero, see Figure 2.9. This attenuation in turn reduces the effective Signal to Interference-plus-Noise Ratio (SINR), and thus degrades the system performance.

- Induces the inter-carrier interference (ICI) between subcarriers of the same user, i.e. the self-ICI, as shown in (2.30).

- Finally, CFO results in multiuser interference (MUI) from subcarriers of other active users in the OFDMA system, which is indicated in (2.30).

The frequency offset can result from the misalignment between the user terminal oscillator and the base station oscillator, and also from the Doppler shift of the wireless medium [53].

In the modern world, a vibrating quartz crystal is the heart of nearly all frequency control devices. Quartz crystal oscillators provide accurate time and are the sources of precise frequency. These are electronic circuits use the mechanical resonances of vibrating crystals of piezoelectric materials to create periodically varying electrical signals. The frequency stability, cost and size of quartz crystal oscillators has resulted in their ubiquitous usage as a frequency reference in electronic equipment. Crystal oscillators as frequency sources and frequency control components are most widely used in the time and frequency research and production fields, such as the IT industry, communications, electronic instruments, etc. As the communication world evolves, a quartz crystal oscillator is the only option for a not too expensive but reasonably precise and stable frequency source. Due to the uniqueness of the crystal structure, impurities in the crystal growth, imprecision in the cut process of the device and uneven thickness of the processed blade and a handful of other reasons, the oscillation frequency of a crystal oscillator labeled, for example, 20,0000 MHz, will never be 20,0000 MHz. This effect is known as "frequency tolerance". It is usually
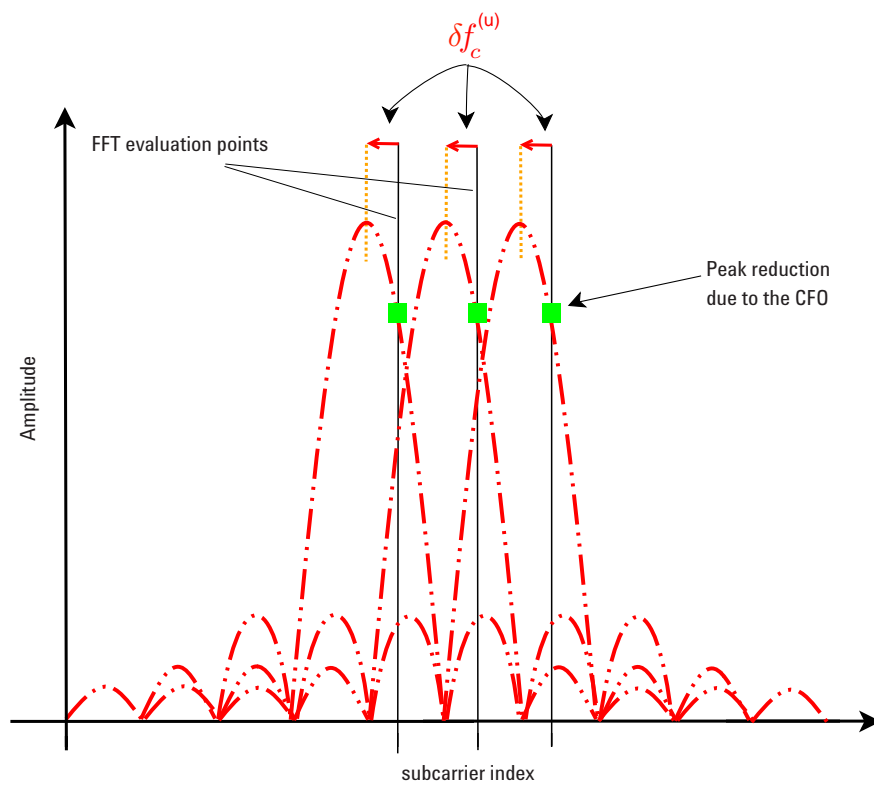
Figure 2.9: Attenuation of the received signal as seen from the peak reduction at the FFT evaluation points.

specified at ambient temperature (i.e. 25 +/- 3C). Common frequency tolerances range from +/-5 to +/-100 ppm, and this specification plays an important role in the cost of the device. PPM stands for parts per million and is used to express the frequency error of a crystal oscillator. To acquire very low frequency tolerance values, one requires an expensive and time consuming sorting process. As a result, using low tolerance crystal batches is not suitable for the user mobile terminals which must be cheap as they are intended for the general consumer and are forced to use high ppm values. Therefore, an unplanned frequency offset of oscillator from its nominal frequency is more likely to be experienced in the user terminals. This CFO in oscillator frequency can also result from changes in temperature (which alters the piezoelectric effect in a quartz crystal) aging or from the voltage regulator problem which is responsible for the bias voltage to the oscillator. Again these phenomenon are common in the user terminal oscillators because they are generally low-cost, free-running oscillators in order to reduce the user terminal cost and as a consequence are more prone to frequency errors. As mentioned earlier in section 2.3.2, we therefore focus our attention to the case where CFO results from the frequency drift of oscillators installed in user terminals, from their allocated carrier frequency.

Often the CFOs resulting from oscillators frequency misalignment and Doppler effects are studied under the same case and are modeled as a single frequency offset appearing at the channel output, see [49, 50]. The CFO from oscillators mismatch differs from Doppler shift, which is a perceived difference in frequency, because the source is moving. Furthermore, unlike the CFO from Doppler effect which appears at the channel output, the CFO resulting from a user terminal should appear at the channel input.

To investigate the range of the CFOs, we first take an example of 802.11a standard [20]. Some important parameters for 802.11a standard are presented in the Table 2.1. IEEE specifies that the transmit center frequency error shall be ± 20 ppm

Table 2.1: IEEE 802.11a Specifications

Parameter	Value
Number of Subcarriers (FFT size)	64
Subcarrier Spacing (Δf)	312.5 kHz
Carrier Frequency (f_c)	5 GHz
OFDMA symbol duration (T)	$4\ \mu sec$

maximum for the 5 GHz band and ± 25 ppm maximum for the 2.4 GHz band. For a user transmitting at $f_c = 5$ GHz towards the base station and assuming a stability

of ±20 ppm on the user terminal, this tolerance will affect the carrier frequency f_c by a maximum offset of ±100 kHz. In 802.11a specifications, the channel bandwidth of 20 MHz is sliced into 64 subcarriers having spacing of $\delta f^{(u)} = \frac{20MHz}{64} = 312.5$ kHz. Therefore, the range of normalized CFO to be expected corresponding to a frequency tolerance of ±20 ppm for this particular example is around ±0.3. Similarly, we take an example of the WiMAX where the bandwidth can be chosen from a range of 1.25 MHz to 20 MHz. Assuming a ±4 ppm crystal, a carrier frequency of 5 GHz and a 256-point FFT, a WiMAX OFDMA system operating in a 10 MHz bandwidth can experience a frequency offset of nearly ±0.5 subcarrier spacings. Here we have assumed a fairly small ppm value because typically the frequency tolerance values are well below the maximum values in IEEE specifications.

It is important to note that the CFO values we have used in the above examples are high (e.g., $|CFO| > 0.1$) compared to the CFO limits specified in some current OFDMA-based standards. For example, the IEEE 802.16e standard [54], which defines a 2048 subcarrier uplink OFDMA system with a subcarrier spacing of 9.8 KHz, specifies that the transmit carrier frequency at the user be synchronized to the base station with a maximum tolerance of 2% of the subcarrier spacing (i.e., CFO must be < 0.02), which is achieved using long preambles and closed-loop frequency correction between user transmitter and base station receiver. However, carrier frequency offset of 0.02 means that the ppm should be between ±1 for a user operating at a carrier frequency of 5 GHz, which is practically not possible. Despite the specifications in the standards, smaller as well as larger CFO values are observed and studied in uplink OFDMA systems, see [36]. In this thesis, in order to consider realistic CFO values, keeping in view the bounds mentioned in standards and also taking into account practical design limitations (very small ppm values), we therefore consider the normalized CFO values ranging between 0 and 0.5 in order to analyze the effects of both small and larger CFO values.

2.5 Numerical evaluation of CFO induced inter-carrier interference

After providing the analytical background in the previous sections, in this section we want to quantify the impact of the CFO induced ICI through simulations for an uplink OFDMA system. The results obtained from the proposed model are compared to a simulated uplink OFDMA system and to the interference model presented in [41].

For simulation purposes, it is considered that there are $N_p = 64$ subcarriers in the system. The length of the cyclic prefix is taken to be 1/4 of the total sub-

carriers, i.e. $L_{cp} = 16$. A 16-QAM modulation is used for mapping the user data streams. The channel is implemented with random impulse responses with Rayleigh fading coefficients and the length of the channel is equal to the length of the cyclic prefix $L_h = L_{cp}$. For the sake of explanation we assume that there are only two users present in the system transmitting simultaneously towards the base station, i.e. $N_u = 2$. One important factor in this context is the subcarrier allocation scheme used to allocates carriers to the users in the uplink. In order to optimize the performance of the uplink OFDMA transmission, adaptive subcarrier allocation schemes which exploit the multiuser diversity inside the system can be used [55, 56]. These adaptive subcarrier allocation schemes make use of the channel state information available at the receiver and allocate the subcarriers according to the channel states thereby increasing system's performance and throughput. However, we assume that no channel state information is available and therefore the carrier allocation is carried out in a predefined manner, which is a sub optimal way of carrier allocation. A blockwise allocation scheme is considered where each user is allocated only blocks of adjacent subcarriers. The blocksize can vary between 1 and $\mathcal{M}$ according to the system requirements. Note that a blocksize equal to 1 is a special case of the blockwise allocation and is called interleaved carrier allocation. Since here $N_u = 2$, both user will get $\mathcal{M} = 32$ subcarriers each. For the simulations we use the maximum possible blocksize, i.e. $BS = 32$, see Figure 2.10. BS stands for blocksize. This
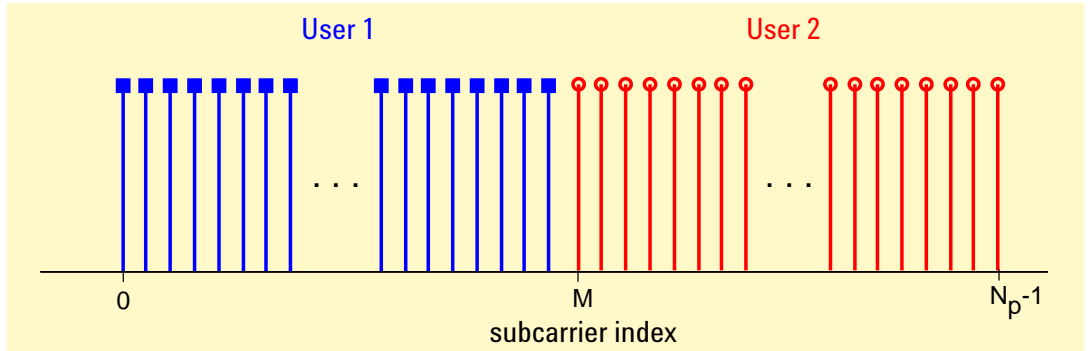
Figure 2.10: Blockwise allocation for user 1 and user 2 each getting equal share of the bandwidth

means that only two blocks are present in the OFDMA symbol, one allocated to each user. As a result, all the subcarriers of a particular user are grouped together in one block, see Figure 2.10. The subcarrier allocation matrices for the two users are given by

$$\underline{\Pi}^{(1)} = [\underline{I} \ \underline{0}]^T \tag{2.33}$$

$$\underline{\Pi}^{(2)} = [\underline{0} \ \underline{I}]^T \tag{2.34}$$

where $\underline{I}$ is an $\mathcal{M} \times \mathcal{M}$ identity matrix and $\underline{0}$ is an $\mathcal{M} \times \mathcal{M}$ matrix with all entries equal to zero.

Furthermore, at the base station a CFO for user 2 is observed $\delta f^{(2)} \neq 0$ while the base station is perfectly synchronized to user 1. Figure 2.11 gives an impression what happens when two users with distinct CFO values are received at the base station. The $\delta f^{(2)}$ leads to a loss of signal power on the sampling points of user 2 and causes energy from one subcarrier to interfere with the next, which is shown by a square. The square mark therefore represents the self loss and attenuation in subcarriers of user 2 because of its own CFO, $\delta f^{(2)} \neq 0$. The circular marks on the subcarriers of user 2 represent the self-ICI in user 2 coming from its own interfering subcarriers. Additionally, user 2 causes multiuser-ICI in the signals of user 1, which is shown with triangular marks at some points in Figure 2.11
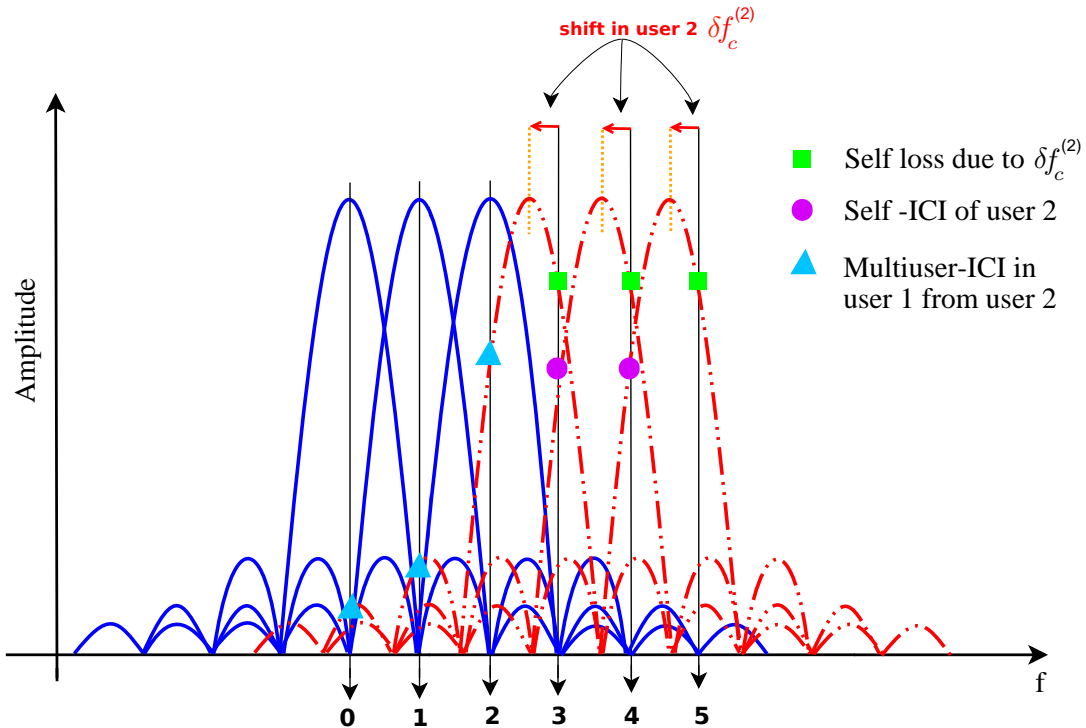
Figure 2.11: User 1 and user 2 at the base station with user 1 perfectly synchronized while user 2 has a CFO $\delta f^{(2)} \neq 0$.

2.5.1 Impact of multiuser-ICI

In this subsection, we discuss the simulation results for the two user case under consideration. Since user 1 is perfectly synchronized with $\delta f^{(1)} = 0$, so there will be no self-interference for user 1 and the interference in user 1 comes from user 2. First the effect of the multiuser-ICI in user 1 because of the frequency mismatch of user 2 is plotted against different CFO values. Figure 2.12 shows the variance of multiuser-ICI versus the normalized shift in user 2, $\delta f^{(2)}$. The variances have been averaged over all subcarriers of user 1 for each value of the normalized shift $\delta f^{(2)}$. Furthermore, the dB-values of ICI variances computed in the simulations correspond to a transmit power of $E\left\{\left|A_k^{(l)}\right|^2\right\} = 1$. The results are averaged over 500 channel realizations. The variance of interference for a particular user u in the three cases i.e. simulated OFDMA uplink transmission, our interference model and the model in [41], are denoted by $\sigma_{sim}^{2(u)}$, $\sigma_{cp}^{2(u)}$ and $\sigma_{no-cp}^{2(u)}$, respectively.

Results in Figure 2.12 show that our computed multiuser-ICI variance for user 1, $\sigma^{2(1)}$, is much closer to the simulated ICI variance of user 1, $\sigma_{sim}^{2(1)}$ than $\sigma_{no-cp}^{2(1)}$. At a shift of $\delta f^{(2)} = 0.08$, the difference between $\sigma_{sim}^{2(1)}$ and $\sigma_{no-cp}^{2(1)}$ is about 12 dB. Unlike $\sigma_{no-cp}^{2(1)}$, $\sigma_{cp}^{2(1)}$ is very close to $\sigma_{sim}^{2(1)}$ and this is because our proposed model does not ignore the effect of CFO on the cyclic prefix and takes into account the fact that the channel matrix does not remain circulant due to the presence of CFO. This result validates our proposed ICI model of multiuser interference and associated variance and shows its superiority with respect to the models in the literature.

2.5.2 Impact of self-ICI

In the previous section, we analyzed the effect of multiuser-ICI in user 1 because of the frequency mismatch in user 2. In this section, the interference seen by user 2 is studied and plotted for the three cases. The CFO induced interference in user 2 is self-ICI generated as a result of misalignment of its own subcarriers. There is no multiuser-ICI for user 2 because user 1 is perfectly synchronized and therefore contributes no CFO to the system as shown in Figure 2.11. In Figure 2.13, the curves for variance of self-ICI of user 2 are plotted against the normalized shift values $\delta f^{(2)}$. We can see that our results are much closer to the simulated variance $\sigma_{sim}^{2(1)}$ compared to the results obtained using the interference model in [41].

An important point to note in Figures 2.12 and 2.13 is the level of the interference variance in the two cases, i.e. multiuser-ICI and self-ICI. The multiuser-ICI seen by user 1 from user 2 is small compared to the self-ICI in user 2. This is because the subcarriers allocated to user 1 are far from the mismatched subcarriers
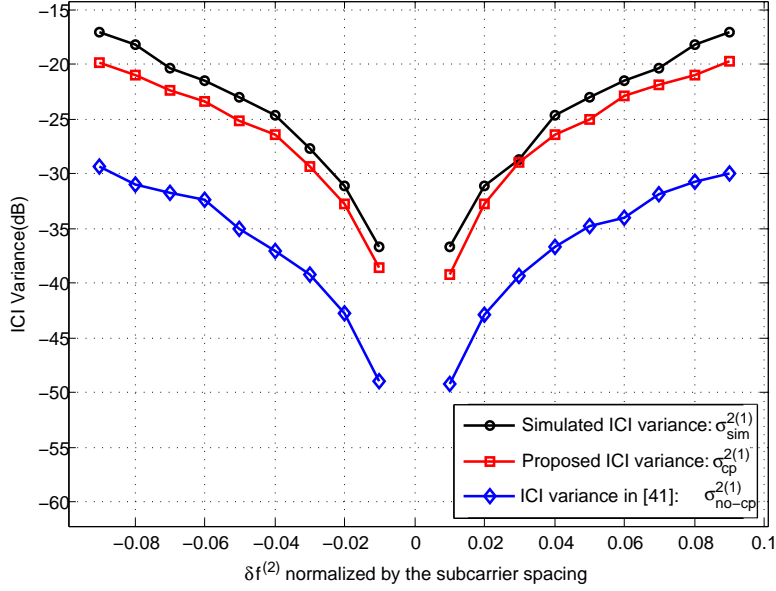
Figure 2.12: Variance of multiuser-ICI in user 1 is plotted against $\delta f^{(2)}$ for N_p=64 and $L_{cp} = 16$.
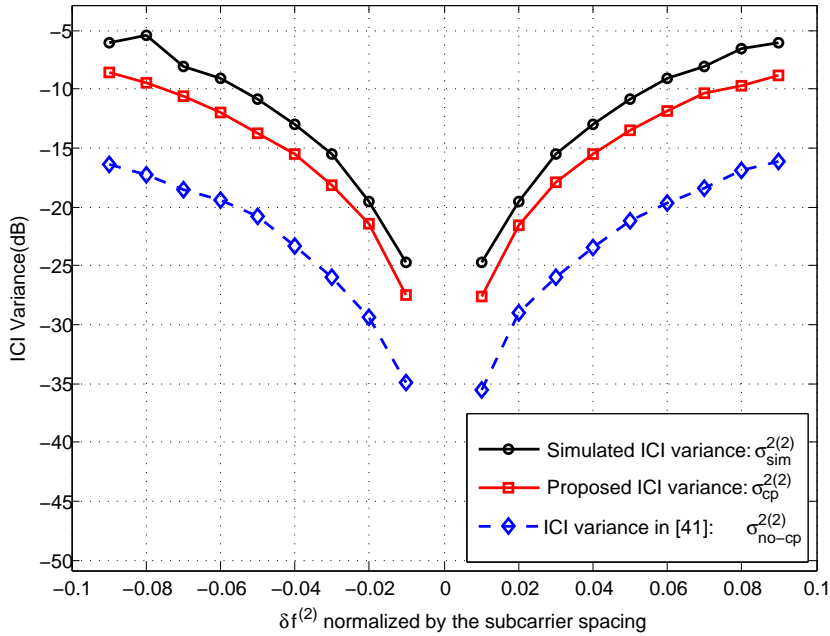
Figure 2.13: Variance of self-ICI in user 2 because of its interfering subcarriers is plotted against $\delta f^{(2)}$ for N_p=64 and $L_{cp} = 16$.

of user 2. Therefore, user 1 observes interference from user 2 only at the edges of the subcarrier blocks allocated to it. This multiuser-ICI is decreasing steadily for subcarriers which are far away from the interfering carriers. On the other hand the subcarriers of user 2 are grouped together in a single block. This results in severe self-ICI in user 2 because all the interfering subcarriers are close to each other. Thats why the level of variance of interference in user 1 is small compared to that in user 2. It is interesting to note that the power of the CFO induced interference depends on subcarrier allocation scheme used. This fact is further discussed in detail in chapter 3.

2.5.3   Effect of length of cyclic prefix on ICI

In the previous simulations we showed the effects of self-ICI and multiuser-ICI. When the cyclic prefix length is too short for the CIR, the performance of an OFDMA system is degraded due to inter-symbol interference and inter-carrier interference. As was discussed earlier, cyclic prefix is inserted to overcome the ISI and ICI. Insertion of cyclic prefix results in loss of energy which is proportional to the length of the cyclic prefix. Different lengths of cyclic prefix are used depending on system requirements, see [44, 57]. In this section, we carry out an analysis of the effect of the length of the cyclic prefix on the variance of the CFO induced interference. The
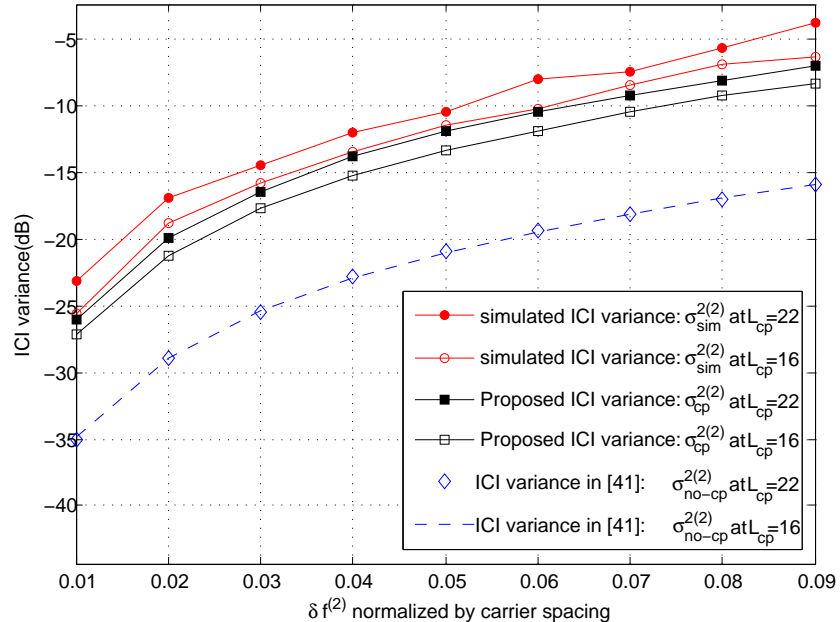
Figure 2.14: Effect of the cyclic prefix length on the CFO induced interference is shown for the three cases under consideration.

same two user scenario, presented in sections 2.5.1 and 2.5.2, is considered here. In Figure 2.14, the curves for ICI variance of user 2 are plotted against its normalized shift for different lengths of the cyclic prefix while N_p remains equal to 64. It can be seen from Figure 2.14 that as the length of the cyclic prefix increases from L_{cp} = 16 to L_{cp} = 22 (about $\frac{1}{4}th$ and $\frac{1}{3}rd$ of N_p respectively), $\sigma_{sim}^{2(2)}$ and $\sigma_{cp}^{2(2)}$ increase accordingly. Since the model in [41] does not take into account the cyclic prefix, $\sigma_{no-cp}^{2(2)}$ remains constant. This result proves that considering our proposed model of ICI in OFDMA system with CFO is more important when the cyclic prefix is long with respect to the number of subcarriers.

2.6 Conclusion

In this chapter, the influence of inter-carrier interference (ICI) resulting from carrier frequency offset (CFO) for an uplink OFDMA system is evaluated. First the uplink OFDMA system considered in this thesis is explained. Then we presented a new analytical model for the CFO induced interference that takes into account the cyclic prefix which is usually neglected. Comparison was drawn with existing interference model and it is shown that the presented model is more realistic and accurate. We also emphasized on the importance of cyclic prefix especially in the presence of CFO in uplink OFDMA transmission. We showed that while carrying out the analysis of interference resulting from frequency synchronization errors in uplink transmission, the effect of CFO on cyclic prefix should not be neglected. An important question about the subcarrier allocation scheme in relation to the self-ICI and multiuser-ICI is also raised.

This contribution has been presented in the 21st Annual IEEE International Symposium on Personal, Indoor and Mobile Radio Communications (PIMRC 2010) [51].

Chapter 3

Carrier Allocation Schemes and Robustness to CFO

PREVIOUSLY, in chapter 2, we investigated the inter-carrier interference resulting from the frequency offsets in an uplink OFDMA system. We saw that during an uplink OFDMA transmission, the modulation symbols are mapped on to the subcarriers through a carrier allocation unit at the user terminal. But the types of carrier allocation schemes used were not discussed in detail. An important question relating the subcarrier allocation and interference resulting from CFO was also put forward.

In this chapter, we start by discussing different types of carrier allocation schemes for OFDMA systems. We analyze the effect of subcarrier allocation on the performance of an uplink OFDMA transmission that is undergoing CFO. In OFDMA systems that do not suffer from frequency misalignments, the subcarriers are allocated to the users in order to optimize the performance and maximize the throughput of the system by exploiting channel frequency diversity. But when frequency offsets are likely to occur, attention must be paid to the ICI resulting from these CFOs. Therefore, our goals in this chapter involve the exploitation of the relationship between subcarrier allocation and CFO induced interference and to look for a trade-off between robustness to carrier frequency offsets and channel frequency diversity for systems with and without CSI.

3.1 Introduction

As seen from Figure 2.1, usually there are more than one users that are transmitting towards a single base station in a given cell. Therefore, the available bandwidth must be divided among the users so that the transmission demands of all the active

users can be fulfilled. Bandwidth is a shared resource among the users and needs an allocation technique to provide unique access per user. Simultaneous uplink transmission is provided through the carrier allocation unit by assigning different subcarriers to different users. The subcarriers of an OFDMA symbol are partitioned into subsets of subcarriers called subcarrier blocks. Then these blocks of adjacent subcarriers are allocated to the users. The manner in which these subcarrier blocks are assigned to the users defines the carrier allocation scheme. In this chapter we consider only the centralized carrier allocation. In centralized carrier allocation, both in the downlink and uplink, the base station is responsible for the scheduling process. Decisions are made at the base station and are communicated to the mobile users. As a first step, different carrier allocation schemes are discussed. We analyze the robustness of the carrier allocation schemes against CFO by studying their effect on the interference induced by CFO in an uplink OFDMA system.

Tremendous research has been carried out on the subject of compensating the effect of CFO on the receiver side. Different interference cancelers on the receiver side have been proposed, see for example [58]. However, some CFO always remain and it can not be eliminated completely. In this chapter, we focus on the transmitter side and we propose solutions to combat the CFO generated ICI through the use of subcarrier allocation schemes. We investigate the effect of the CFO on the throughput maximization of uplink OFDMA systems. Uplink OFDMA transmission with and without CSI are considered. In uplink OFDMA systems that do not undergo CFO and that have no CSI, channel frequency diversity is induced on average by interleaving the subcarriers allocated to different users. However, if the system experiences frequency mismatches, an interleaved carrier allocation would severely degrade the throughput because of the high level of ICI. Channel frequency diversity and robustness to CFO are therefore in contradiction. Hence, in this chapter, we look to establish a trade-off between the frequency diversity and robustness against CFO. The first goal is to efficiently allocate the subcarriers to the users, in the absence of CSI, in order to optimize the throughput and at the same time provide robustness against CFO thereby compensating the effect of ICI. On the other hand, in systems where some CSI is available, resource allocation makes use of the channel frequency diversity so that the available subcarriers are allocated to the users in a way that maximizes the sum throughput. Considering a certain point in time, the attenuation of a subcarrier is different for different users, i.e. it can be in a deep fade for one user while it may have a low attenuation for another user. Assuming that the carrier allocation unit knows the instant CSI, it can periodically assign each subcarrier to the user which can use it best to achieve the system performance target (i.e. maximum capacity or minimum transmit power). This approach is a dynamic subcarrier assignment approach since it dynamically allocates the subcarriers to optimize performance [32, 46]. For such systems we study the effect of the

carrier allocation schemes on the performance of the system in the presence of CFO.

We begin this chapter by presenting the types of carrier allocation schemes followed by their analysis in CFO affected uplink OFDMA transmission with and without CSI.

3.2 Performance Criterion

In the sequel, we will use the theoretical channel throughput as a performance criterion in order to analyze the subcarrier allocation schemes in the presence of CFO.

$$C_t = \sum_{u=1}^{N_u} C^{(u)} \tag{3.1}$$

where for a user l

$$C^{(l)} = \sum_{n=1}^{N_p/BS} \beta_n^{(l)} \sum_{k=1}^{BS} \log_2(1 + SINR_{k+nBS}^{(l)}) \tag{3.2}$$

in bits/OFDMA symbol. BS stands for blocksize and n is the block index. $\beta_n^{(l)}$ has a value 1 for blocks allocated to l and 0 elsewhere. Note that

$$SINR_k^{(l)} = \rho_k |H_k^{(l)}|^2 / (\sigma_{k(ici)}^{2(l)} + \sigma_{k,noise}^2) \tag{3.3}$$

where $\sigma_{k(ici)}^{2(l)}$ is the variance of the CFO induced ICI for a carrier k of user l, ρ_k represents the self-loss of user l due to frequency offset in subcarrier k and $\sigma_{k,noise}^2$ is the noise power. Important here is to consider the fact that using (3.1) implies that no ICI canceler is available at the receiver which behaves as if ignoring the CFO effect.

3.3 Carrier Allocation schemes

In this section, we present the subcarrier allocation schemes. Some system parameters must be explained. Let us assume that there are N_u subcarriers transmitting simultaneously towards a base station by exploiting N_p available subcarriers. The overall subcarriers are numbered from 0 to $N_p - 1$. As stated earlier the carrier allocation is fair, therefore, the total subcarriers are divided into N_u subchannels. A subchannel is the set of subcarriers allocated to a particular user and is denoted by $\Gamma^{(u)}$. Each subchannel consists of $\mathcal{M} = N_p/N_u$ subcarriers. Since the maximum number of users that a system can support simultaneously is limited to the number of subchannels which, throughout this study, are assumed to be equal to the number

of the users in the system. Moreover, to avoid that a given subcarrier is shared by different users, the sets $\left\{\Gamma^{(u)}\right\}_{u=1}^{N_u}$ must be mutually exclusive, i.e., $\Gamma^{(l)} \bigcap \Gamma^{(m)} = \emptyset$ for $l \neq m$.

In uplink OFDMA the aim is to allocate the subcarriers to the users in such a way that maximizes the system throughput by exploiting the channel frequency diversity. If the CSI is available, the subcarriers are allocated to the users depending on their channel gains which optimizes the performance. On the other hand, different allocation schemes are used to induce channel frequency diversity. Since, the CSI is one of the important factors in determining the type of carrier allocation used, for this reason, we have classified them on the basis of the availability and unavailability of the CSI.

3.3.1 Carrier Allocation without Channel State Information

In this subsection, we consider the carrier allocation schemes when there is no CSI available at the receiver. In this case, the carrier allocation is done depending on the system requirements. For example, if there is no CFO in the system the carriers can be allocated to the users to induce multiuser diversity and therefore improve system throughput. But if there is CFO, attention must also be paid to the ICI induced because of the CFO. In systems without CSI, we divide the carrier allocation schemes into two categories.

3.3.1.1 Blockwise Allocation

In a blockwise allocation scheme, the subcarriers are allocated to the users in the form of blocks of adjacent subcarriers. This type of allocation is shown in Figure 3.1. For illustration purposes, we assume $N_p = 16$ and $N_u = 2$ as system parameters. In Figure 3.1 (a) each user is allocated one block of adjacent subcarriers with each block having 8 subcarriers. This is the maximum possible blocksize for the considered system parameters. But for the blockwise carrier allocation, the blocksize BS can vary between one and $\mathcal{M}$ according to the system requirements as seen from Figure 3.1 (b) where the blocksize is 4.

From throughput optimization point of view, the main drawback of this approach is the lack of ability to exploit the frequency diversity offered by the multipath channel. This is because all the subcarriers allocated to a particular user are grouped together into a single block and a deep fade might hit a substantial number of subcarriers of a given user. This scenario is shown in Figure 3.2 for the two users. It can be seen that most of the subcarriers allocated to user 2 are in deep fade and the transmission for user 2 will be severely effected.
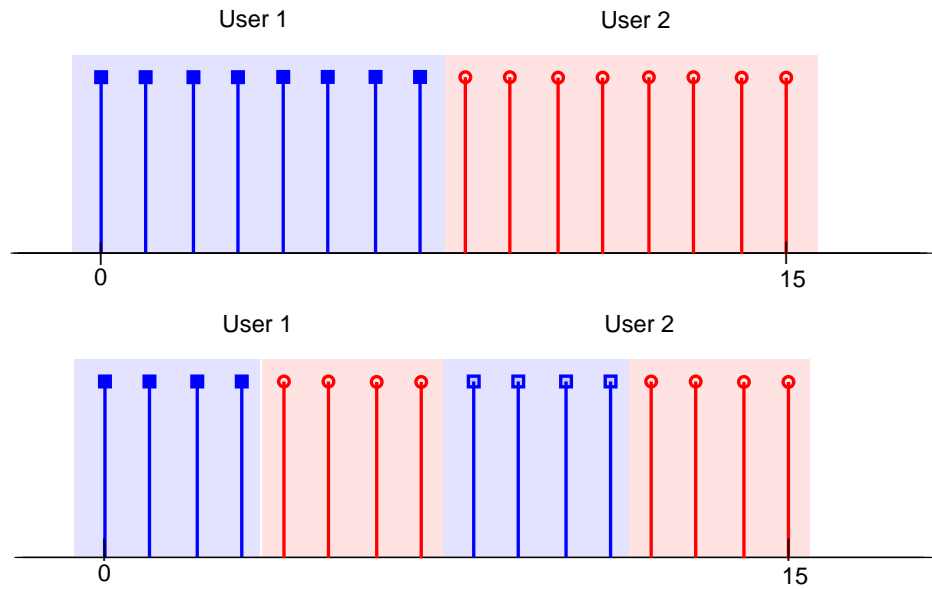
Figure 3.1: Blockwise carrier allocation scheme. (a)$N_p = 16$, $N_u = 2$ and $BS = 8$.(b)$N_p = 16$, $N_u = 2$ and $BS = 4$.
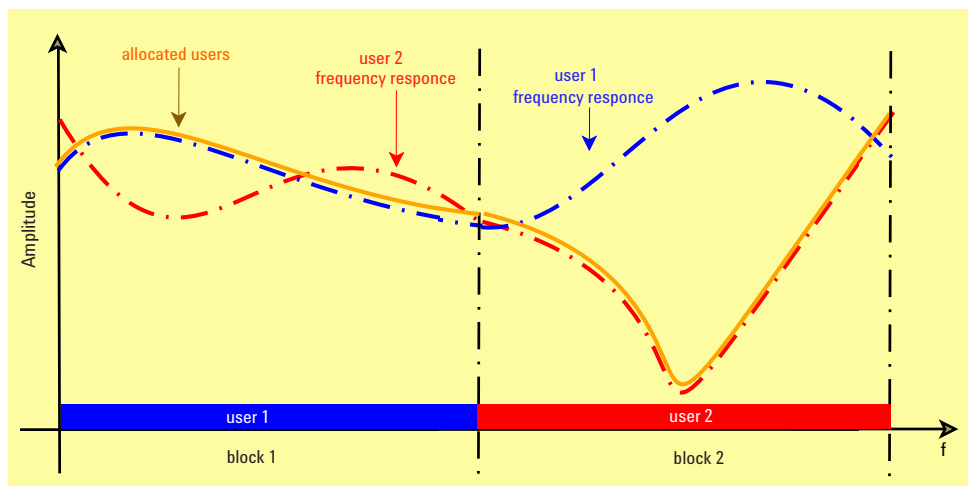
Figure 3.2: Predefined carrier allocation where block 1 is allocated to user 1 and block 2 is allocated to user 2 which experiences a deep fade because all his subcarriers are grouped into one block.
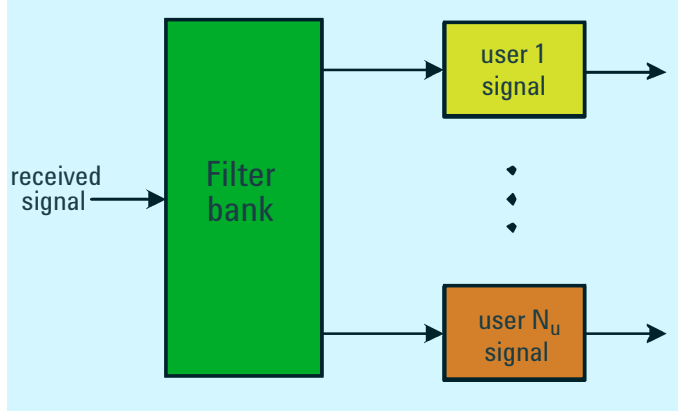
Figure 3.3: Blockwise allocation with guard intervals allows signal separation at the receiver through the use of filter bank.

Nevertheless, a significant advantage of the blockwise allocation is the simplification of the synchronization task to a large extent. If the frequency offsets are adequately smaller than the guard intervals, users signals can easily be separated at the base station by passing the received samples through a bank of digital band-pass filters, each selecting one block, as shown in Figure 3.3. Figure 3.3 assumes that each user is allocated one block. The filtering operation allows the base station to perform frequency estimation independently for each active user. Clearly, perfect users separation cannot be achieved in practice since this would require large guard intervals which will consume bandwidth and thus is not efficient.

3.3.1.2 Interleaved Allocation

Interleaved carrier allocation scheme is a special case of the blockwise allocation where the blocksize is equal to 1 subcarrier, i.e. $BS = 1$, and the subcarriers of an individual user have the maximum mutual distance. In interleaved allocation, each user modulates an exclusive set of $\mathcal{M}$ subcarriers which are uniformly spaced in the frequency domain at a distance N_u from each other. This makes users separation a challenging task as compared to blockwise transmissions. The reason is that in the presence of frequency errors, users signals partially overlap in the frequency domain and cannot be simply isolated through a filter bank. However, the interleaved carrier allocation scheme provides uplink signals with a special periodic structure that can effectively be exploited for the synchronization purpose [36]. For $N_p = 16$ and $N_u = 2$ interleaved allocation is shown in Figure 3.4. Interleaved allocation is also sometimes referred to as comb allocation. In OFDMA-based systems with perfect frequency synchronization where no CSI is available, interleaved carrier allocation
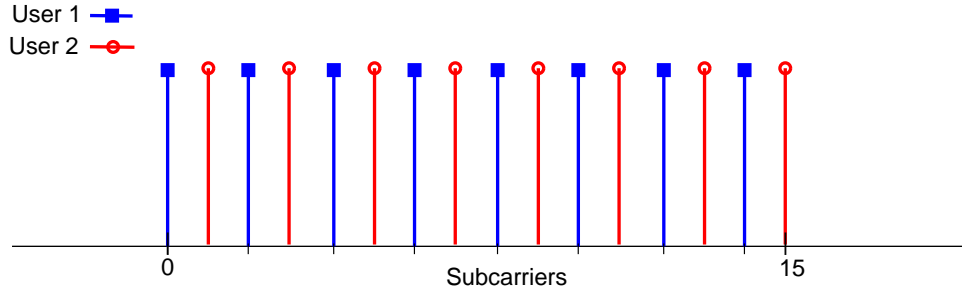
Figure 3.4: Interleaved subcarrier allocation scheme for N_p=16, N_u=2 and blocksize = 1.

can fully exploit the channel frequency diversity.

3.3.2 Carrier Allocation with Channel State Information

The subcarrier allocation schemes presented in section 3.3.1 are not flexible despite their advantages described earlier. The current trend in uplink OFDMA favors a more flexible allocation scheme where users are allocated the best subcarriers that are currently available, i.e. those with highest channel state gains. This type of carrier allocation is dynamic in nature and is referred to as an optimal carrier allocation scheme since each user gets the best available subcarriers. The optimal carrier allocation scheme assumes that an ideal feedback channel exists and perfect CSI is available. The basic concept of this optimized allocation is shown in Figure 3.5.
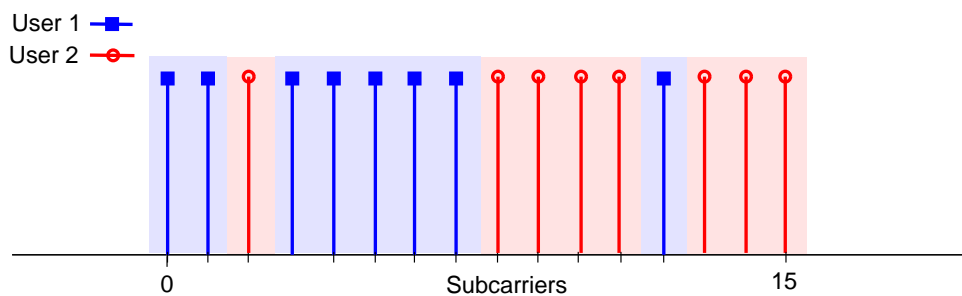
Figure 3.5: Optimized carrier allocation scheme for N_p=16, N_u=2.

We can see that there does not appear to be a fixed blocksize or allocation pattern in optimal allocation strategy. Since there is no rigid association between subcarriers and users, the optimal carrier allocation allows dynamic resource allocation. This allocation strategy is more flexible than the blockwise or interleaved carrier allocations and provides the system with some form of diversity [59] since
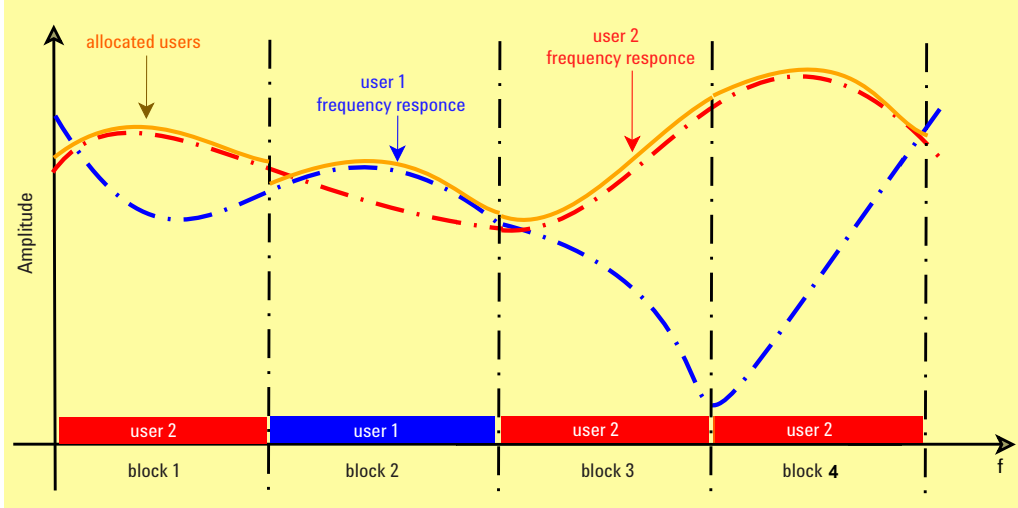
Figure 3.6: Optimal carrier allocation assigns the subcarrier blocks according to channel states of users.

a subcarrier that is in a deep fade for one user may exhibit a relatively large gain for another. For instance, consider the frequency responses of two users present at different locations in a cell. The channel frequency response for the two users will be different depending on their location. The optimal carrier allocation assigns the subcarriers by looking at the channel state gains of both the users, as seen from Figure 3.6, thus providing optimized system performance. On the other hand, the absence of any rigid structure in the allocation policy makes the synchronization task even more challenging than with interleaved carrier allocation scheme.

3.4 Blockwise allocation under CFO in a system without CSI

In the previous sections, we presented different types of carrier allocation schemes for an uplink OFDMA system assuming that there is a perfect frequency synchronization between the users and the base station. In this section, we consider that the system undergoes frequency errors and is not perfectly synchronized in frequency. We consider the blockwise allocation and start by analyzing its resistance against CFO for a system where no CSI is available.

3.4.1 Blockwise allocation and robustness to CFO

In this section, we analyze the robustness of blockwise allocation against CFO. Blockwise allocation with different blocksizes is employed. In Figure 3.7, the level

of CFO induced interference power is evaluated for a simple two user system model where the subcarriers are allocated to the user according to blockwise scheme. System parameters are $N_p = 64$ and $L_{cp} = N_p/4 = 16$. User 1 is perfectly synchronized to the carrier frequency allocated to it while user 2 experiences a certain level of CFO, $\delta f^{(2)} = 0.06$, due to component misbehavior. Since user 1 has no CFO, so,
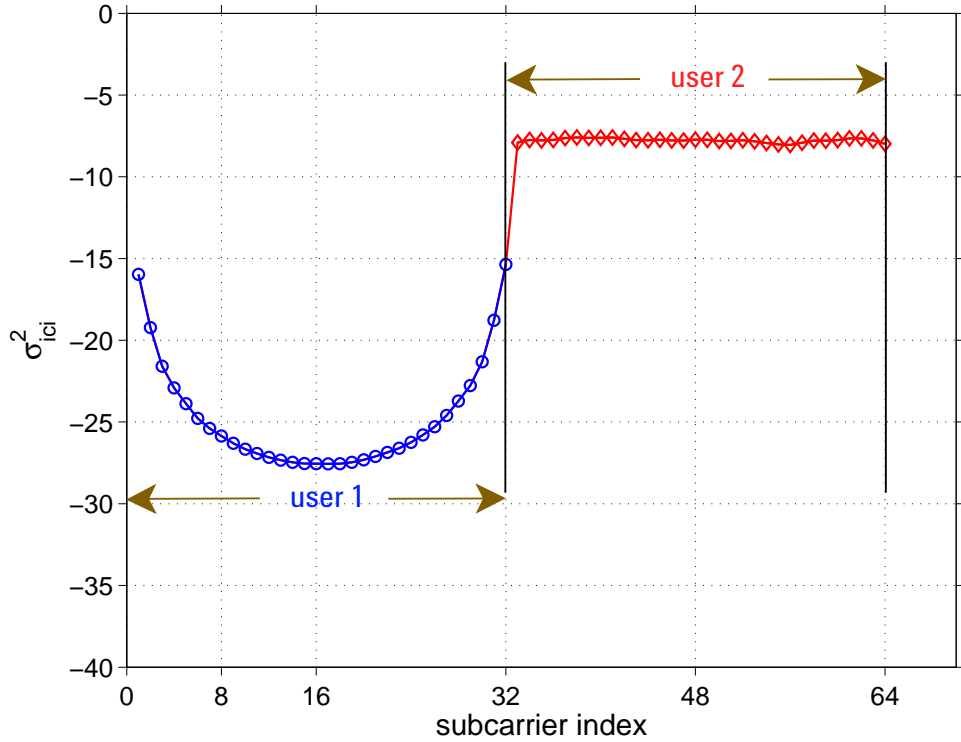
Figure 3.7: ICI for two users with blockwise allocation. Total subcarriers are $N_p = 64$, with $\mathcal{M}=32$ subcarriers for each user, $BS = 32$, user 2 with $\delta f^{(2)} = 0.06$, user 1 with $\delta f^{(1)}=0$.

it does not induce any interference while user 2 is not synchronized and contributes both self and multiuser interferences. The blocksize used is 32 which is the maximum blocksize possible. As seen from the Figure 3.7, since user 2 is not well synchronized, some ICI is observed on all his subcarriers. This ICI is constantly high for user 2, because his allocated subcarriers interfere with each other. Only at the border to user 1 the ICI decreases, because there is no interference from user 1 to user 2 due to his perfect synchronization. All ICI which will be observed by user 1 stems from user 2 and its power is steadily decreasing for subcarriers which are far away from the interfering carriers. Because of being at a far distance from the subcarriers of
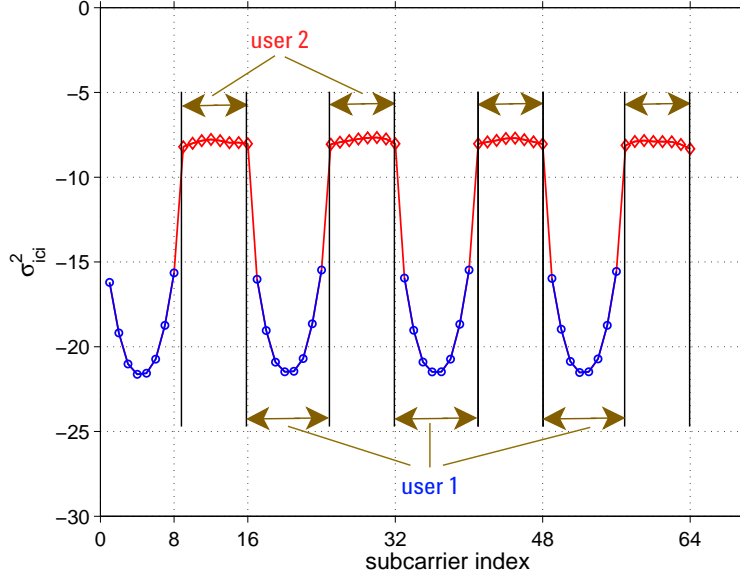
Figure 3.8: ICI for two users with blockwise allocation. Total subcarriers are N_p= 64, with $\mathcal{M}$=32 subcarriers for each user, $BS = 8$, user 2 with $\delta f^{(2)} = 0.06$, user 1 with $\delta f^{(1)}$=0.

user 2, most ICI to user 1 is well below 25 dB. In the presence of frequency errors, blocks of distinct users are differently shifted in the frequency domain from their nominal positions and, in consequence, subcarriers located at the edges of a given block may experience significant ICI. But the level of interference decreases as the distance from the misaligned user block increases. It is observed from Figure 3.7 that the blockwise allocation with large blocksize provides a good level of robustness against CFO. To further nullify the effect of the interference in blockwise allocation scheme, a specified number of unmodulated subcarriers is typically inserted among adjacent blocks to provide adequately large guard intervals.

Next the blocksize is reduced to 8 adjacent subcarriers and the allocation looks like in Figure 3.1(b) but with more subcarriers, i.e. $N_p = 64$ and more number of blocks. As the blocksize is reduced, the subcarriers assigned to the two users come closer to each other and the chances of interference due to misalignment in frequency increase. This is illustrated in Figure 3.8, where the level of the CFO induced interference is plotted against the subcarrier indexes for the two users. Unlike in the case of $BS = 32$, the performance for user 1 has worsened, (see Figure 3.7). This is because the subcarrier blocks of user 1 now face heavy interference from both sides. Furthermore, since the $BS = 8$, the number of blocks has increased which means
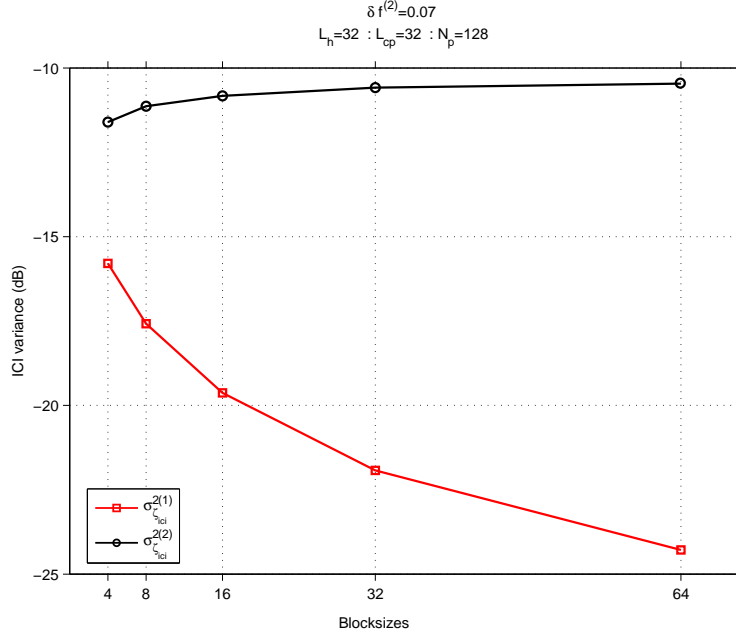
Figure 3.9: ICI variances(dB) of the two users versus blocksizes with $\delta f^{(1)} = 0$ and $\delta f^{(2)} = 0.07$.

the number of subcarriers at the borders has increased. On the other hand, the level of the interference for user 2 has somewhat decreased. The subcarriers of user 2 are neighbor to the subcarriers of user 1 which being perfectly synchronized offers no interference. Moreover, the distance among the interfering subcarriers of user 2 has also increased, as a result the overall performance of of user 2 is improved. If the blocksize is further reduced to 1 subcarrier than the situation shown in Figure 3.7 will be completely conversed, i.e., the interference in user 1 will attain highest value while the interference in user 2 will be very low. Therefore, using interleaved blocks of small sizes proves to be extremely prone to frequency offsets and offers no robustness against CFO.

In Figure 3.9, we have summarized the robustness against CFO for the blockwise allocation scheme with different blocksizes. The CFO induced interference power for user 1 and user 2, i.e. $\sigma_{ici}^{2(1)}$ and $\sigma_{ici}^{2(2)}$, respectively, is plotted against varying blocksizes. $N_p = 128$ and $\delta f^{(2)} = 0.07$ while $\delta f^{(1)} = 0$. Channel length is assumed to be equal to cyclic prefix length i.e. $L_{cp} = L_h = N_p/4 = 32$. From Figure 3.9 we can see that with increase in the blocksize the interference seen by user 1 due to user 2 reduces. Blockwise carrier allocation, with maximum blocksize of $BS = \mathcal{M}$ subcarriers, proves to be highly resistant against the frequency errors in the system.

Thus, as expected a larger blocksize provides more robustness to the CFO compared to a smaller blocksize. But using larger blocks of adjacent subcarriers does not permit us to benefit from channel frequency diversity. Therefore, in the next sections, we wonder what is the best number of adjacent subcarriers that can be allocated to a particular user in the presence of CFO in order to get benefit from channel diversity along with maintaining robustness against CFO. Different simulations are carried out where blockwise allocation with different blocksizes is employed.

3.4.2 Sum Throughput and Blocksize

As seen from the previous section, maximum robustness against CFO is achieved when a maximum blocksize of $\mathcal{M}$ is used. This resistance to CFO in blockwise allocation decreases as the blocksize is decreased. We observed that larger blocksizes provides good robustness to CFO but does not induce multiuser diversity one can get using the interleaved allocation in systems without CSI. Since channel diversity and robustness to CFO contradict each other, we look for a carrier allocation scheme that allows us to establish a compromise between the two. Since no CSI is available, the carriers are allocated to the users in a predefined manner. This type of allocation is also sometimes referred to as a static carrier allocation scheme. We assume a fair allocation where all the users in the system equally share the available subcarriers.

In Figure 3.10, the sum throughput $C_{t(no-CSI)}$ and individual user throughputs, i.e., $C_{(no-CSI)}^{(1)}$ and $C_{(no-CSI)}^{(2)}$, are plotted versus different OFDMA blocksizes. The curves in Figure 3.10 are plotted to find out the best number of adjacent subcarriers that can be allocated to a particular user in order to establish the trade off between the channel diversity and robustness to frequency errors for OFDMA transmission without CSI. Inside the system, two users share a bandwidth of 128 subcarriers with $\delta f^{(2)} = 0.07$ and $\delta f^{(1)} = 0$. Blockwise allocation with blocksizes, $BS = 2, 4, 8, 16, 32$ and 64 is used. Blocksize $BS = 64$ is the maximum blocksize possible and in this case each user will be allocated the carriers grouped into a single block. Figure 3.10(a) shows that as the blocksize is decreased from 64 adjacent subcarriers to 2 subcarriers, the sum throughput, $C_{t(no-CSI)}$, decreases. Moreover, by looking at Figure 3.10(b) we observe that with decreasing blocksize, the individual throughput for user 1, $C_{(no-CSI)}^{(1)}$, decreases but the throughput for user 2, $C_{(no-CSI)}^{(2)}$, increases with a decrease in the blocksize. At a blocksize of 64, the subcarriers of user 1 are grouped into one subcarrier block and are closed to each other. Since user 1 is perfectly synchronized it does not see any interference from its own subcarriers. The only interference user 1 experiences is at the subcarriers present at the edge of the blocks. The subcarriers at the border see heavy interference from the mismatched user 2. But majority of the subcarriers, being at a greater distance from
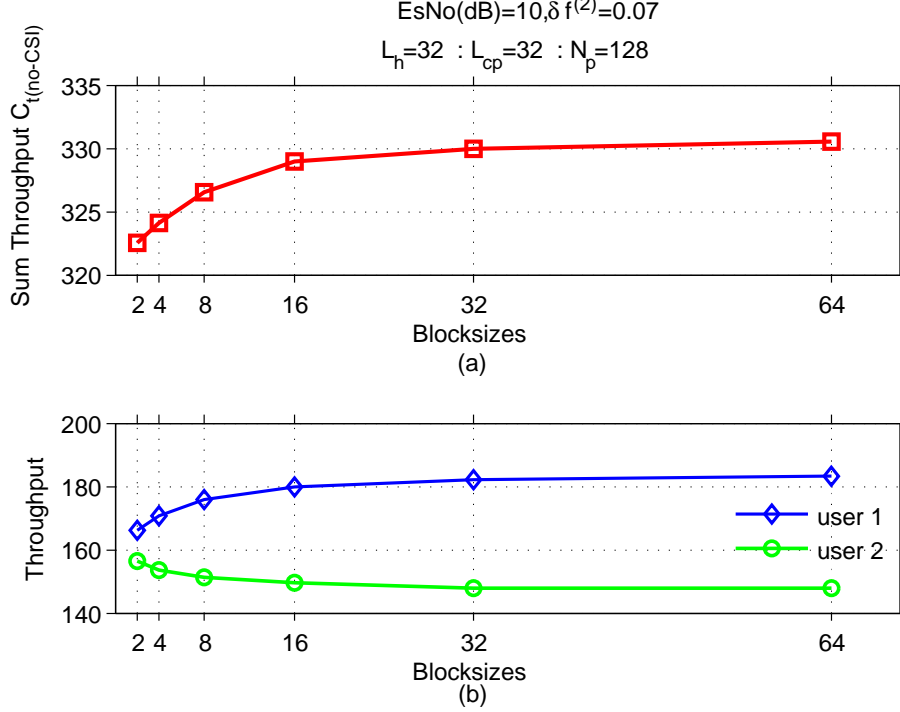
Figure 3.10: (a) Sum Throughput $C_{t(no-CSI)}$ vs. the blocksizes for $\delta f^{(2)} = 0.07$ and $\delta f^{(1)} = 0$. (b) Individual throughputs of the two users.

the interfering subcarriers of user 2, are not affected and thus the performance for user 1 is good at blocksize of $BS = 64$. As the blocksize decreases, the subcarriers of user 1 become closer and closer to the subcarriers of user 2 and as a result the multiple users interference seen by user 1 from user 2 increases. That is why we see a significant degradation in performance for user 1 at low values of blocksize. Conversely, for user 2 the performance at small blocksizes is better compared to large blocksizes because at small blocksizes the distance among the subcarriers of user 2 is large, as a consequence, the interference seen is small. At $BS = 64$, the user 2 subcarriers are grouped into one block, as a result the performance is worst because of the increased self-interference, as seen from Figure 3.10(*b*).

If we observe carefully in Figure 3.10(*a*), we can see that the overall sum throughput $C_{t(no-CSI)}$ does not change significantly as the blocksize decreases from $BS = 64$ to $BS = 16$. Besides, with a further decrease in blocksize, beyond 16 subcarriers per block, the slope of the curve exhibits a prominent increase. Important thing to note is that the blocksize $BS = 16$ is equal to the half of the length of cyclic prefix, $L_{cp} = 32$.

3.4.3 Proposed Threshold Blocksize

In the previous subsection, it was observed that the sum throughput for the OFDMA system without CSI increases with increase in the blocksize and vice versa. To further investigate this behavior, we plotted the sum throughput $C_{t(no-CSI)}$ at different values of normalized shifts of user 2 in Figure 3.11.
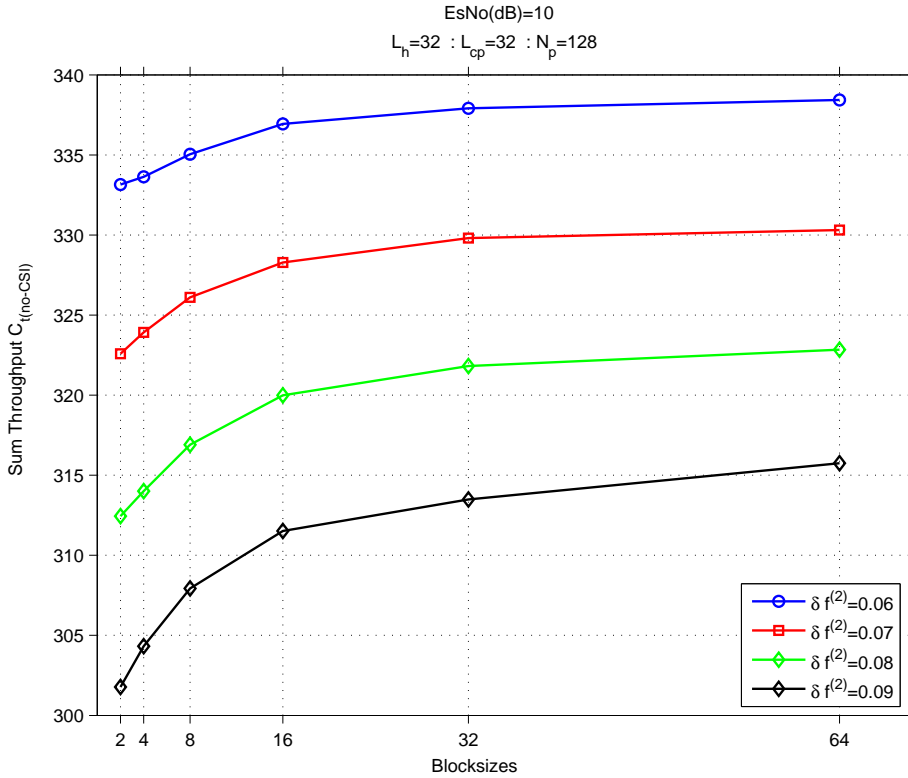
Figure 3.11: Throughput vs. the blocksizes for different values of normalized shift of user 2, $\delta f^{(2)}$ while $\delta f^{(1)} = 0$.

We can observe that the slope of the throughput curves in Figure 3.11, show a prominent increase as the blocksize further decreases beyond 16 subcarriers per block for each value of the normalized shift. We have observed similar behavior for different values of cyclic prefix. When the blocksize is reduced from $N_p/2$ to $L_{cp}/2$, the effect of ICI on the throughput does not change much and the sum throughput shows a minor decrease.

If we carefully observe the results in Figure 3.11, we observe that the slope of the sum throughput curves increases with an increasing shift beyond blocksize of 16. This is enhanced in Figure 3.12 where we have plotted the slope versus the shift

values of $\delta f^{(2)}$ for $N_p = 128, L_{cp} = L_h = 32$. Therefore, as the normalized shift increases the sum throughput decreases more rapidly beyond the blocksize $BS = 16$.
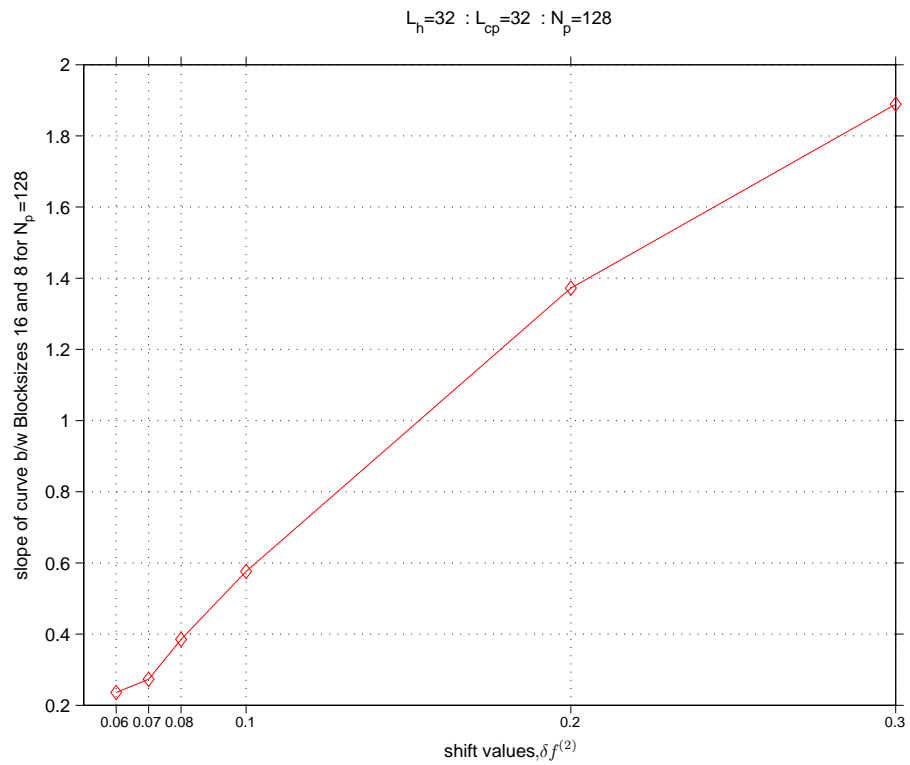
Figure 3.12: Slope of the curve versus the normalized shift values for user 2, $\delta f^{(2)}$.

Again simulations for different values of N_p, L_{cp}, L_h, yield the same behavior. For example, Figure 3.13 shows the sum throughput curve $C_{t(no-CSI)}$ for a system of two users with $N_p = 256, L_{cp} = L_h = 64, \delta f^{(1)} = 0$ and $\delta f^{(2)} \neq 0$. It is observed that as the blocksize decreases beyond $L_{cp}/2$ adjacent subcarriers, the throughput shows a significant decrease. From the results in subsection 3.4.2, it is observed that when the blocksize is reduced from $N_p/2$ to $L_{cp}/2$, the effect of ICI on the throughput does not change much and throughput shows a minor decrease. This means that as the blocksize is varied between $N_p/2$ to $L_{cp}/2$, we do not loose much in terms of throughput and still maintain the same level of robustness against CFO. With a further reduction in the blocksize beyond $L_{cp}/2$, the ICI will increase drastically and will reduce the throughput. At this point, we conclude that a subcarrier-block
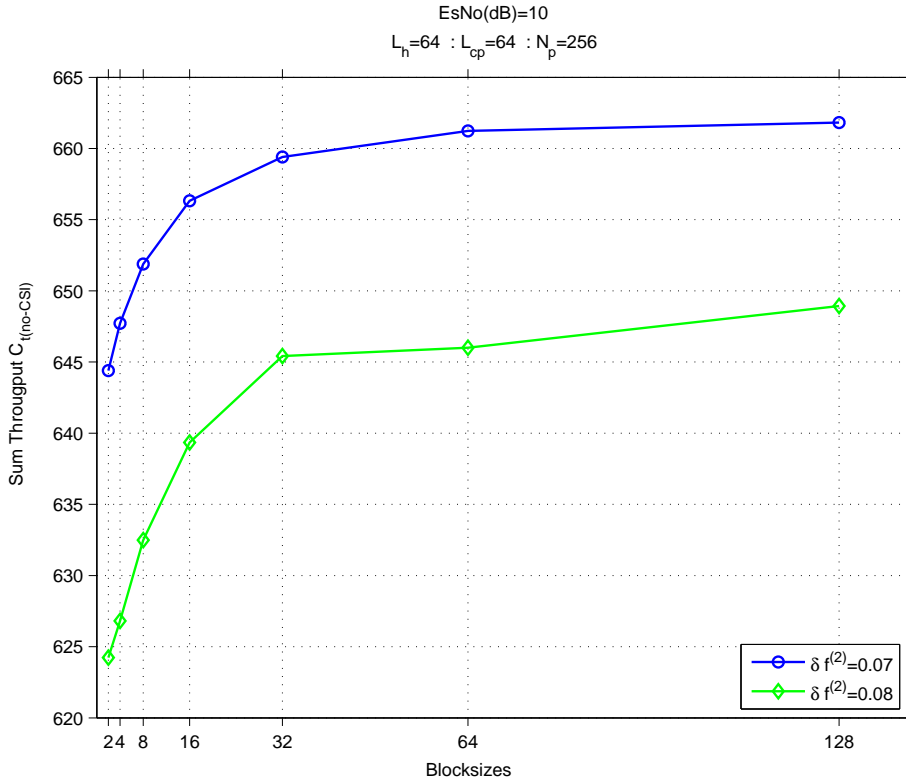
Figure 3.13: Throughput $C_{t(no-CSI)}$ vs. the blocksizes for different values of normalized shift of user 2, $\delta f^{(2)}$ while $\delta f^{(1)} = 0$.

of size equal to half of L_{cp} provides a good balance between the frequency diversity and robustness against CFO. We call this blocksize the *threshold blocksize*. Because if we further reduce the blocksize beyond this threshold value, the ICI will increase drastically and will reduce the throughput. On the other hand, if a larger blocksize is selected then we cannot benefit from channel diversity.

3.5 Blockwise Allocation under CFO in a System with CSI

In the previous section, we studied the blockwise allocation scheme for OFDMA system undergoing CFO but without any CSI available. In the presence of CFO, we analyzed the behavior of the sum throughput and we found that by maintaining a blocksize of $L_{cp}/2$, a trade off between the channel frequency diversity and robustness against CFO can be established. In this section, we consider an uplink OFDMA transmission assuming that ideal feedback channels are available to get perfect CSI.

3.5.1 Optimal Carrier Allocation Algorithm

In the presence of the CSI, the decisions to allocate the subcarriers to users are taken at the base station and then the information is conveyed to the users. Therefore, with CSI available, the subcarriers are no longer allocated to the users in a predefined manner, as was done previously in the case of no CSI, but are assigned according to the respective channel states of the users. This type of allocation is called optimal carrier allocation as each user gets the best subcarriers currently available. Optimal carrier allocation allows dynamic resource allocation and is also sometimes referred to as a dynamic carrier allocation since there is no strict association between subcarriers and users.

Optimal carrier allocation can be carried out on per carrier basis where an allocation decision is taken for each subcarrier in the available bandwidth but this procedure becomes cumbersome for large number of subcarriers and also requires an increased amount of overhead transmission in the feedback channel. For this reason we follow the strategy where the available bandwidth of N_p subcarriers is divided into $\frac{N_p}{BS}$ blocks. Then the scheduling of the blocks is done based on the channel state gains computed over these blocks. As a result we perform the allocation on per block basis rather than per carrier basis.

We consider a scheduling of the blocks based on the maximum throughput approach using each user's mean channel gain $\alpha^{(u)}$ over a particular block as follows

$$\alpha_n^{(u)} = \frac{1}{BS} \sum_{k=1}^{BS} \left| H_{k+nBS}^{(u)} \right|^2 \tag{3.4}$$

where n is the block index with $n = \{1, ..., \frac{N_p}{BS}\}$. Note that this scheduling lowers the feedback information and enhances its robustness, see [60]. A block-allocation vector for each user is generated, $\left\{ \underline{\beta}^{(u)} \right\}_{u=1}^{N_u}$, using $\alpha_n^{(u)}$ where for a particular user u

the block-allocation vector has the elements $[\beta_1^{(u)}\beta_2^{(u)}...\beta_{\frac{N_p}{BS}}^{(u)}]$.

$$\beta_n^{(l)} = \begin{cases} 1 & \alpha_n^{(l)} > \alpha_n^{(m)} \quad m \in \{[1,N_u]\setminus l\} \\ 0 & otherwise \end{cases} \tag{3.5}$$

$\beta_n^{(l)} = 1$ represents that the block n is allocated to user l. Note that the block-allocation vector is unique for each user, i.e., to avoid that a given subcarrier block is shared by different users, the block-allocation vectors $\left\{\underline{\beta}^{(u)}\right\}_{u=1}^{N_u}$ must be mutually exclusive, i.e. $\underline{\beta}^{(j)}\bigcap\underline{\beta}^{(m)} = \emptyset$ for $l \neq m$.

The algorithm we propose for the optimized carrier allocation scheme is explained in the diagram of Figure 3.14. Note that this allocation is simpler than the one based on SINR that maximizes the throughput. In practice, they are anyhow similar in most cases.
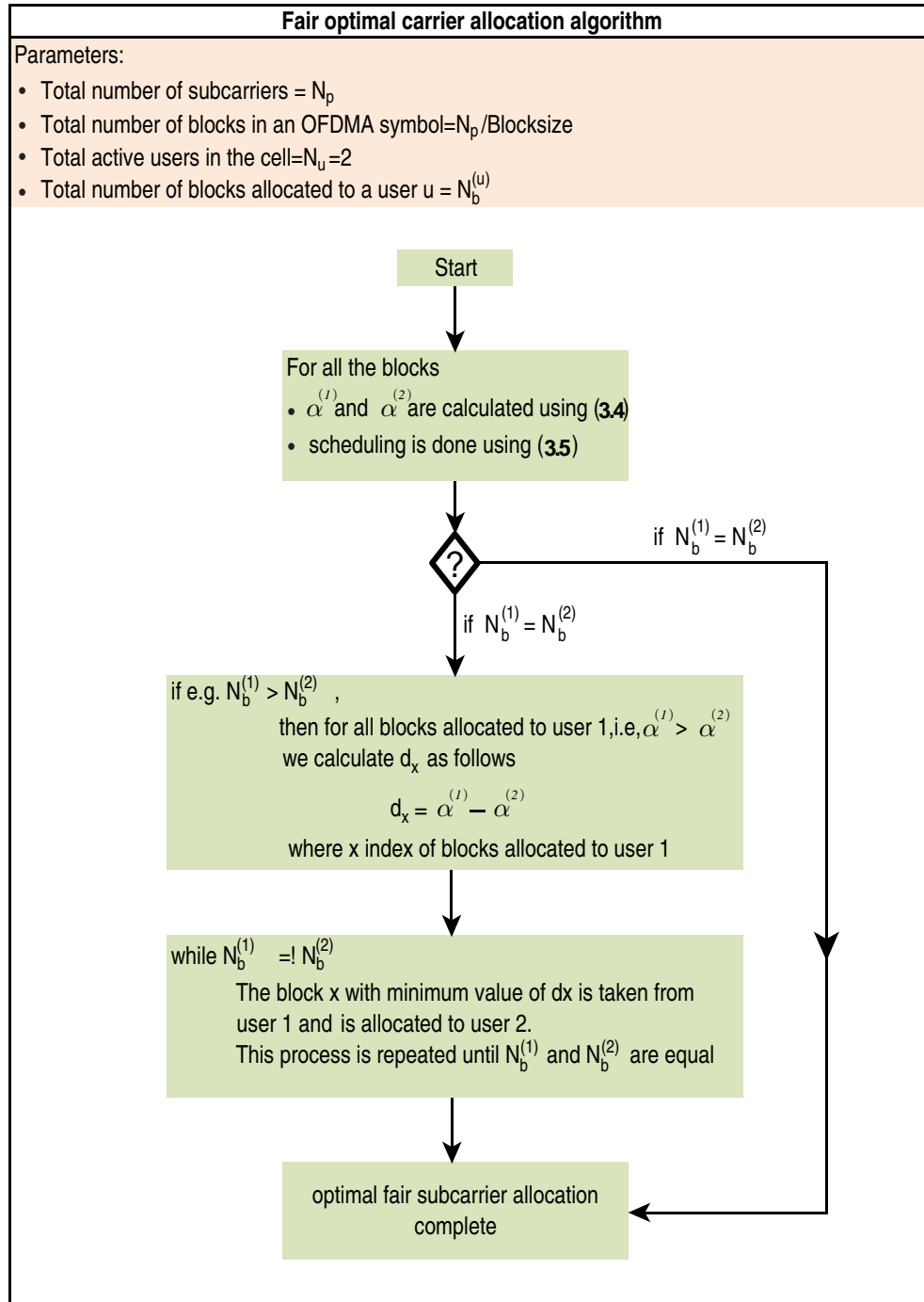
Figure 3.14: Optimal Carrier Allocation Algorithm

For a two user scenario, an optimal carrier allocation may for example look like as shown in Fig. 3.15.
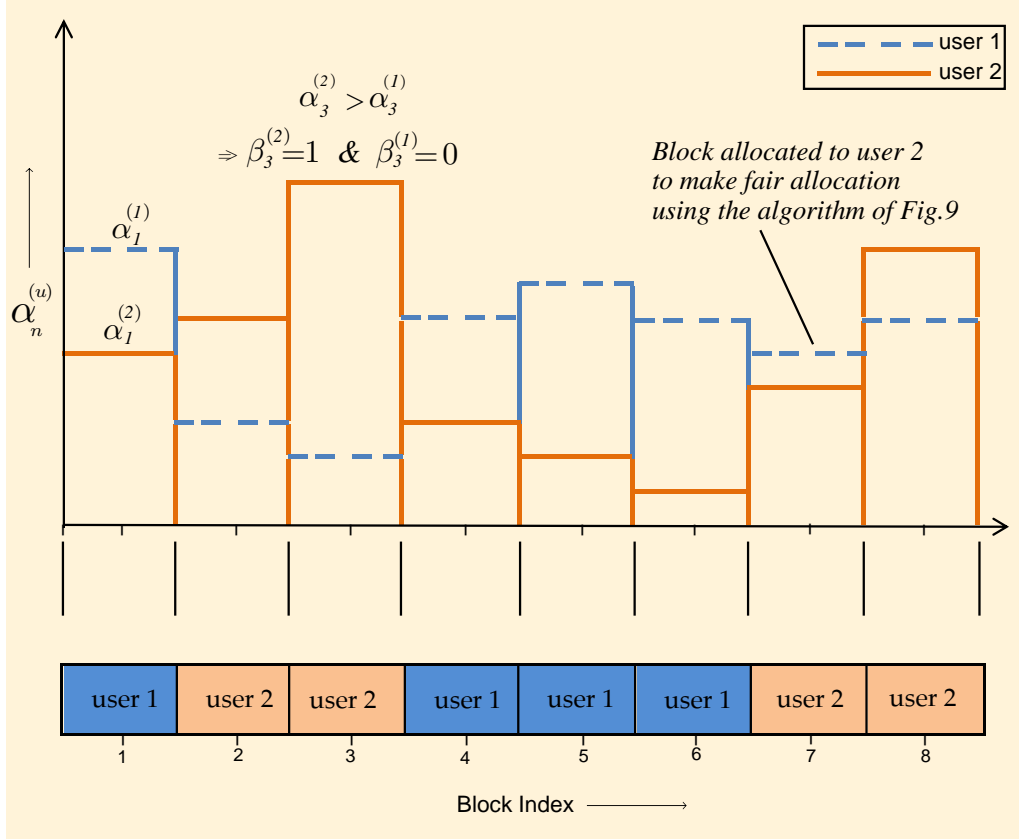
Figure 3.15: Optimal carrier allocation when channel state information is available. Two user scenario where there are total 8 blocks and each user is assigned 4 blocks according to the optimal carrier allocation algorithm.

In Figure 3.15, the mean channel state gains, computed using (3.4), for both the users are plotted against the block indexes on the x-axis. The optimized carrier allocation carries out the comparison between the two users for all the available blocks and generates the block-allocation vector for each user. Based on the channel state gains in Figure 3.15, the block-allocation vectors for the two users are as follows

$$\underline{\beta}^{(1)} = \begin{bmatrix} 1 & 0 & 0 & 1 & 1 & 1 & 0 & 0 \end{bmatrix}$$

$$\underline{\beta}^{(2)} = \begin{bmatrix} 0 & 1 & 1 & 0 & 0 & 0 & 1 & 1 \end{bmatrix}$$

(3.6)

In Figure 3.15, the resulting OFDMA symbol at the base station is also shown in

case when both the base station is perfectly synchronized to both the users, i.e. $\delta f^{(1)} = \delta f^{(2)} = 0$. Since the blocks are allocated to the users according to their channel states, two or more adjacent blocks can be allocated to the same user as shown in the Figure 3.15. Note that we consider that this carrier allocation is fair, therefore, both the users get the same share of the available bandwidth W as is obvious from Figure 3.15.

3.5.2 Robustness to CFO

In the above section we presented the optimal carrier allocation for a system without any CFO. Next we assume that there exist a certain CFO in the system and investigate the behavior of the optimal carrier allocation scheme in terms of the sum throughput $C_{t(CSI)}$. We investigate whether the trade-off relation observed for the blockwise allocation done without CSI also holds for the optimal block allocation.

To investigate the trade-off relation, the sum throughput $C_{t(CSI)}$ is plotted against different blocksizes in Figure 3.16, where $C_{t(CSI)}$ is the sum throughput for optimal carrier allocation. $N_p = 128, L_{cp} = L_h = 32$ are the system parameters. The base station is perfectly synchronized to the signal from user 1 i.e. $\delta f^{(1)} = 0$ and is not synchronized to user 2 and $\delta f^{(2)}$ is taken to be 0.07. Figure 3.16(a) shows that, unlike $C_{t(no-CSI)}$, the sum throughput $C_{t(CSI)}$ is maximum at a blocksize of 2 adjacent subcarriers and it decreases with increase in blocksize and is minimum when the blocksize is equal to 64 adjacent subcarriers. Similarly, Figure 3.16(b) shows that the individual throughputs for both user 1 and 2 have highest values for $BS = 2$ and minimum values at $BS = 64$.

The reason for this behavior is that at small blocksizes the optimal carrier allocation induces more multiuser frequency diversity hence boosting system throughput. With blocksize $BS = 2$, there are 64 blocks in the OFDMA symbol and the allocation decision is made for each smaller sized block which offers more granularity. While as the blocksize increases this granularity decreases and is minimum at $BS = 64$. For blocksize $BS = 64$, there are only two blocks in the symbol which does not allow the optimal carrier allocation to induce sufficient diversity and the system throughput reduces.

In blockwise allocation without CSI, it was observed that in the presence of the CFO, a blocksize of 64 adjacent subcarriers proved to be most resistant against the CFO induced interference. But from Figure 3.10, we see that for optimal carrier allocation this is not the case. One reason for this behavior is the better channel diversity induced at smaller blocksizes compared to the larger blocksizes which helps in improving the overall sum throughput. Another answer to this question lies in
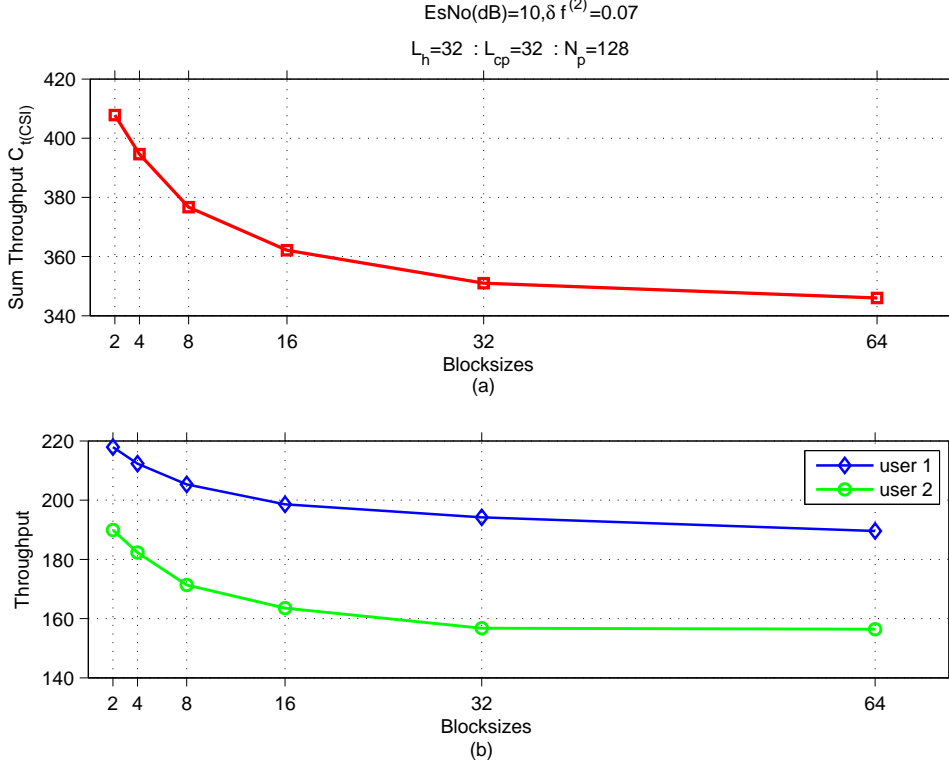
Figure 3.16: (a) Sum Throughput $C_{t(CSI)}$ vs. the blocksizes for $\delta f^{(2)} = 0.07$ and $\delta f^{(1)} = 0$. (b) Individual throughputs of the two users.

Figure 3.15(*b*). We can see that in optimal carrier allocation, for a particular user more than one blocks can be adjacent to each other. In this case, for user 1 the larger the number of adjacent blocks the farther will be the carriers of user 1 from user 2 and hence proves more robustness. The individual throughput for user 2 is less than that of user 1 because of its frequency mismatch.

Therefore, we can conclude that with CSI available and using optimal block carrier allocation, we can get channel diversity as well as robustness against the CFO even at smaller blocksizes as shown in Figure 3.16.

3.5.3   Critical CFO Value

In the previous section we found that for the optimal carrier allocation scheme, no trade-off between the channel frequency diversity and the robustness to CFO is required in terms of a blocksize. We saw small blocksizes provided both channel diversity and robustness to CFO for OFDMA systems with CSI and employing optimal block allocation scheme.

Next to further investigate this behavior of the optimal allocation, we have computed the sum throughput for the two users over different normalized CFO values. In Figure 3.17, we have plotted the sum throughput $C_{t(CSI)}$ for the two users case at different values of the normalized shift in user 2 signal. At lower values of the shift, we can see that $C_{t(CSI)}$ decreases with increase in blocksize. But at higher values of the shift $\delta f^{(2)}$ there is a dramatic change in the behavior of the sum throughput $C_{t(CSI)}$.
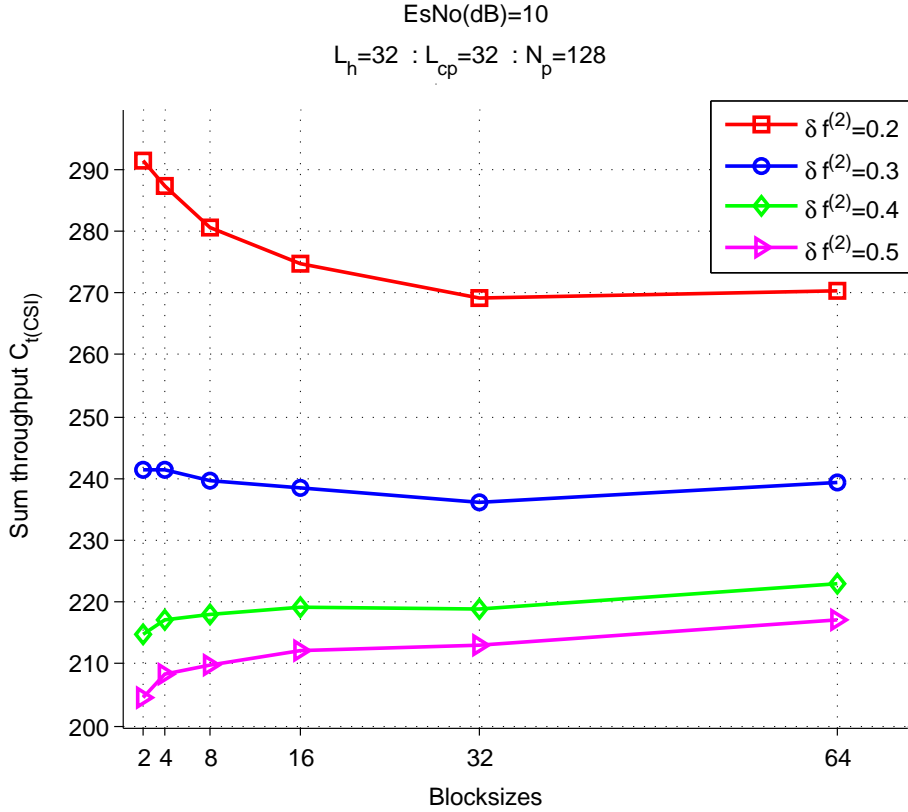
Figure 3.17: Throughput $C_{t(CSI)}$ vs. the blocksizes for different values of normalized shift $\delta f^{(2)}$ while $\delta f^{(1)} = 0$.

For $\delta f^{(2)} = 0.4$, the situation has completely conversed to that observed in Figure 3.16, i.e., the sum throughput $C_{t(CSI)}$ has a minimum value at blocksize of 2 and shows an increase with increase in blocksize with a maximum value at $BS = 64$. At high values of $\delta f^{(2)} > 0.3$, $C_{t(CSI)}$ tends to behave like $C_{t(no-CSI)}$ i.e. increasing with increase in blocksize and vice versa. This means that with increase in normalized shift, the CFO induced ICI becomes so high that it overcomes the gain achieved

due to channel diversity using small blocksizes. A sudden change in the behavior of $C_{t(CSI)}$ is observed for higher values of normalized shift. There exists a CFO value beyond which the optimal allocation behaves like the blockwise allocation without CSI.

In this section, we try to find out the value of the shift, $\delta f^{(2)}$, beyond which the behavior of $C_{t(CSI)}$ changes. We plot in Figure 3.18 the quantity $\Delta C_{t(CSI)}$ defined by

$$\Delta C_{t(CSI)} = C_{t(BS=64)} - C_{t(BS=2)} \tag{3.7}$$

for different values of the normalized shift $\delta f^{(2)}$. Figure 3.18 shows that as the
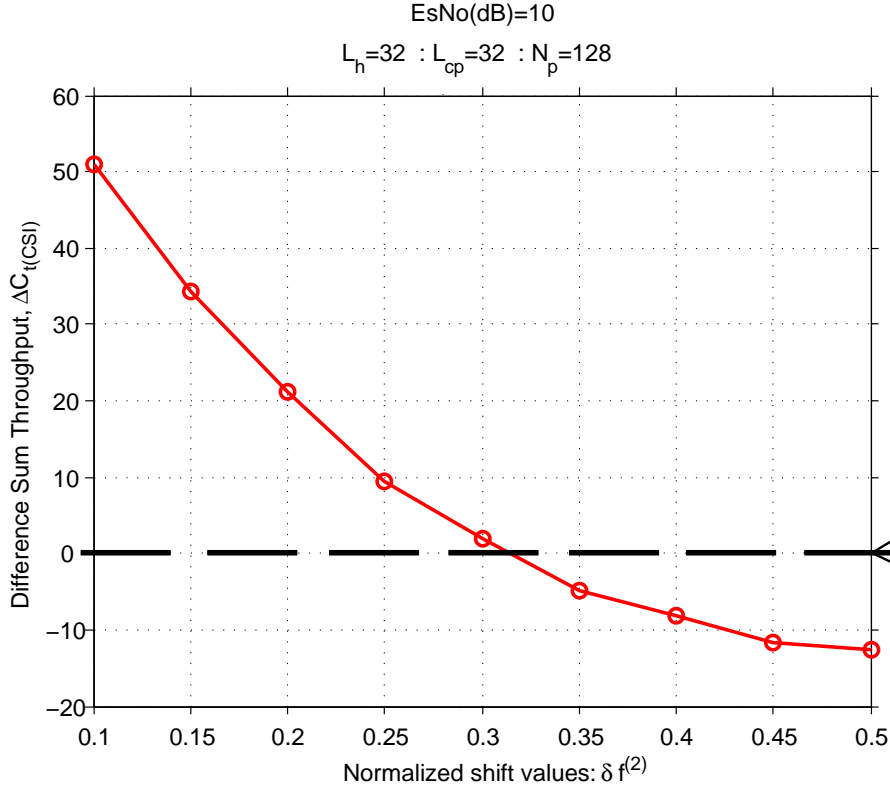
Figure 3.18: $\Delta C_{t(CSI)}$ at different values of normalized shift $\delta f^{(2)}$ while $\delta f^{(1)} = 0$.

normalized shift increases beyond 0.3, $\Delta C_{t(CSI)}$ becomes negative showing that the $C_{t(CSI)}$ no more decreases with increase in blocksize and starts behaving like $C_{t(no-CSI)}$. Therefore, with CSI available and if optimal carrier allocation is being used then the value of the CFO becomes important. In order to induce channel diversity using the CSI, it is important to pay attention to the CFO present in the system. If the CFO remains below this critical value, one can benefit from channel

diversity by using smaller blocksizes but once this value is exceeded, small blocksizes will provide no robustness against the CFO induced ICI and hence the usage of higher blocksizes becomes inevitable.

3.6 Conclusion

In this chapter we presented the carrier allocation schemes for uplink OFDMA systems with and without CSI. An analysis of the trade off between channel frequency diversity and robustness against CFO in an uplink OFDMA system has been presented. In an OFDMA system with CFO, there exists a contradiction between the two. We have studied the subcarrier allocation schemes for an OFDMA system undergoing CFO. We have proposed a trade off in the form of a *Threshold blocksize* of $L_{cp}/2$ to allow a good compromise between the channel diversity and robustness for CFO for the case when no CSI is available. With CSI available, we proposed an optimal block carrier allocation scheme through which both robustness to CFO and channel diversity can be achieved with small blocksize for small CFO. But above a *Critical CFO* value, the performance of the optimal block carrier allocation loses interest.
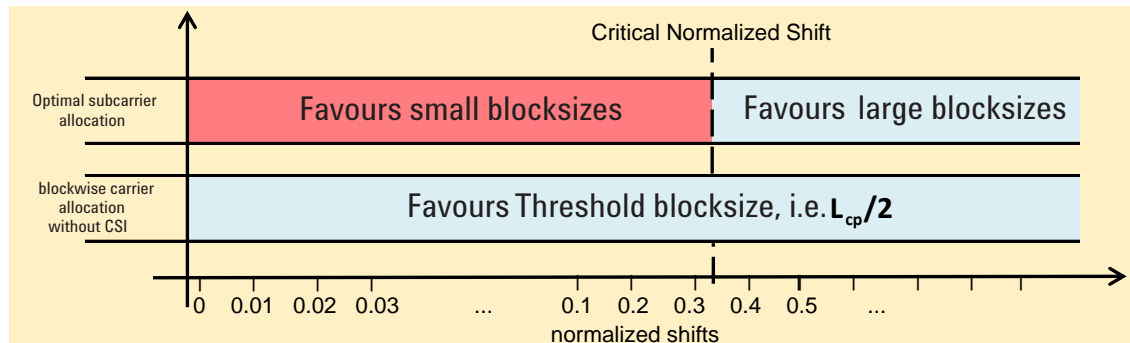
Figure 3.19: Behavior of blockwise allocation without CSI and optimal carrier allocations at various normalized shift values.

Figure 3.19 sums up the usage of blocksizes we propose at various shift values with the carrier allocation schemes i.e. blockwise allocation without CSI and optimal block carrier allocation scheme.

This contribution has been presented in the IEEE Global Communications Conference (IEEE Globecom 2011) [61].

Chapter 4

Joint Channel and Carrier Frequency Offset Estimation based Self-Successive Interference Canceler

In the previous chapters we focused our attention on studying the inter-carrier interference resulting from CFO. We also studied the different carrier allocation schemes used in an uplink OFDMA system and their robustness against the CFO induced interference. As mentioned in chapter 2, each user in the uplink of an OFDMA based system undergoes an individual and independent carrier frequency offset (CFO). These CFOs, if not corrected, destroy the orthogonality among subcarriers, causing ICI and MUI, which could degrade the system's performance severely.

In this chapter, we address two very important problems of the uplink OFDMA system, i.e. joint CFO and CIR estimation and CFO compensation at the receiver. We focus on the techniques to alleviate the negative effects of the multiple CFOs in the uplink OFDMA system. Our contributions in this chapter include:

- We propose a joint CIR and CFO estimator for an uplink OFDMA system model presented in chapter 2. A polynomial approximation method derived from the grid search algorithm is used which results in less complex CFO estimators.

- Based on the CFO estimates obtained from the proposed estimation method, a self-successive interference canceler (self-SIC) algorithm is proposed to mitigate both the self inter-carrier interference and multiuser interference at the base station.

4.1 Introduction

In contrast to the downlink OFDMA transmission, frequency synchronization in uplink OFDMA transmission represents a more challenging task since the uplink received signal at the base station is a summation of signals coming from different users. These signals come from different terminals and thus undergo distinct and independent frequency synchronization errors. As a result when an uplink OFDMA transmission is considered, an efficient joint estimation of the channel impulse responses and CFOs is required. The channel estimation and synchronization for single user OFDM systems has been widely studied, e.g. [62, 49]. However, the amount of contributions that address the synchronization problem in uplink multiuser system is thin [38, 63, 64, 65, 66, 67]. The proposed estimators are designed for particular subcarrier allocation schemes, or are blind methods that naturally require longer signal sequences than training sequence (TS) based methods to provide comparably the same performance. Most of the existing algorithms consider the estimation of the CFO alone without considering the channel estimation. Recently, a combined CFO and channel estimator with arbitrary subcarrier allocations for OFDMA systems was proposed in [68] where a joint CFO and channel estimation is done using the maximum-likelihood approach but it proves to be highly complex. The authors in [69] proposed an approximative ML estimation method of multiple CFOs and CIRs by using distinct correlation properties of the TSs. The main disadvantage of this approach is that an extensive grid search for a complex cost function must still be carried out. In [70], authors have presented a method based on a polynomial approximation for the CFO estimation which tends to reduce the complexity one faces in the grid search algorithms. However, the resulting frequency estimates are still complex. Moreover, the authors while performing the estimation assume that the CFO resulting from the frequency mismatch of the user's oscillator with the base station is applied to the transmitted signal after the channel convolution, i.e. at the receiver. This is not realistic in the uplink problem as was explained in chapter 2. Based on our transmission model for uplink OFDMA transmission where the CFO resulting from the oscillator mismatch appears in the transmitted signal present at the transmitters output of each user, we derive a new estimation algorithm that further simplify the obtained CFO estimates compared to the previous approaches provided in [70].

Using the CIRs and CFOs estimates found from the proposed joint estimation method, we next deal with the CFO induced interference in the received signal. The orthogonality among the subcarriers ensures the elimination of the self inter-carrier interference of a user as well as the multiuser interference from adjacent users. A slight disturbance in the subcarriers' orthogonality in uplink OFDMA systems results in severe interference. Once the uplink frequency offsets have been estimated,

they must be employed in some way at the base station to restore orthogonality among subcarriers. This operation is commonly referred to as CFO compensation. Various studies have been carried out to tackle the multiple CFO problems in the OFDMA uplink scenario, which can be divided into two categories, namely, Interference Avoidance (IA) and Interference Cancellation (IC) methods. One example of interference avoidance methods is the feedback-and-adjust approach. The feedback-and-adjust schemes are described in [38, 65], which suggest that the base station performs only CFO estimation, whereas adjustment of the synchronization parameters is made at the mobile station's side based on instruction transmitted on the base station's control channel. The feedback-and-adjust approach requires an established connection between base station and mobile terminal so that the users must periodically be provided with updated estimates of their synchronization parameters, which is not applicable for some scenarios. Hence the feedback approach has a major disadvantage of increasing the system overhead which reduces the system throughput. Also note that, in this approach, there is always a delay between the estimation and adjustment processes, during which the CFO estimation can be outdated (e.g. because of Doppler frequencies) [71].

For these reasons, the current trend of OFDMA favors the interference cancellation schemes in which advanced signal processing techniques are used to compensate for frequency synchronization errors directly at the base station, i.e. without the need of returning frequency estimates back to the subscriber terminals. Several authors have studied the CFO compensation at the receiver. In the compensation method presented in [72, 73], authors try to reconstruct the frequency orthogonality based on Least Square (LS) and Minimum Mean Square Error (MMSE) criteria. An interference matrix is constructed and multiplied with the transmitted symbols in order to represent the effect of CFOs. But both the LS and MMSE methods operate with high complexity matrix inversion. In [74], an iterative method is put forward to mitigate the multiuser-ICI. The presented method operates in a per-user manner and performs multiple circular convolution operations in each step which proves to be too complex. Compensation methods based on successive cancellation are presented in [75, 76]. In [75], successive interference cancellation is applied to compensate the CFO. The multiuser-ICI is removed by reconstructing and removing the interfering signals in the frequency domain. But the provided method is limited only to the interleaved (comb) carrier allocation scheme and ignores the self-interference. Similarly, a successive cancellation method is provided in [76]. However, the authors have considered an uplink OFDMA system with a carrier allocation scheme that has a blocksize of 4 adjacent subcarriers. The performance of the proposed SIC method is not discussed for blocksizes larger than 4 adjacent subcarriers. In this chapter, we propose a CFO compensation method based on a self-successive interference cancellation (self-SIC) approach. The proposed self-SIC algorithm is simple but effective

in overcoming both the self and multiuser interferences using the successive cancellation procedure.

This chapter speaks of the joint CIR/CFO estimation in the first part while the CFO compensation method is explained in the second part. The remaining chapter is organized as follows. In Section 4.2, the uplink OFDMA system model under consideration is presented. In Section 4.3, the proposed joint estimation algorithm is presented followed by its scalability analysis in Section 4.3.2. In Section 4.4 the CFO compensation problem is discussed. Section 4.4.1 presents the proposed CFO compensation method based on self-successive interference canceler algorithm followed by performance analysis of self-SIC in Section 4.4.3. Numerical results for the complete system are presented in Section 4.5. Finally, the conclusions are drawn in Section 4.6.

4.2 Received signal model for estimation

In the uplink OFDMA system, signals from N_u different users $x^{(u)}(t)$ pass through individual convolutive multipath radio channels and the received signal at the base station is the sum of the signals from all users. The received discrete-time baseband signal r_i at the base station is given by

$$r_i = \sum_{u=1}^{N_u} \left\{ a_i^{(u)} e^{\frac{j2\pi}{N_p}(L_h+i-1)\delta f^{(u)}} \right\} * h_i^{(u)} + n_i \tag{4.1}$$

where $*$ stands for convolution.

$$r_i = \sum_{u=1}^{N_u} \sum_{l=0}^{L_h-1} a_{i-l}^{(u)} e^{\frac{j2\pi}{N_p}(L_h+i-l-1)\delta f^{(u)}} h_l^{(u)} + n_i \tag{4.2}$$

where $h_l^{(u)}$ denotes the lth sample of the impulse response of the channel for user u, including the transmitter and receiver filters, n_i is the additive white Gaussian noise. L_h is the channel length which is assumed to be less than the cyclic prefix length i.e. $L_h < L_{cp}$. Note that $\delta f^{(u)}$ in (4.1) and (4.2) is the CFO of user u normalized by the subcarrier spacing $\Delta f = \frac{1}{T}$, $\delta f^{(u)} = \delta f_c^{(u)}/\Delta f = \delta f_c^{(u)}T$. Since we want to perform channel and CFO estimation, we carefully worked on (4.2) to separate the different contributions. By collecting the N_p samples corresponding to the IDFT size and removing the L_{cp}-long cyclic prefix as in [51], after some calculus we derive

the following expression for the uplink received signal:

$$
\begin{bmatrix} r_0 \\ r_1 \\ \vdots \\ \vdots \\ \vdots \\ r_{N_p-1} \end{bmatrix} = \sum_{u=1}^{Nu} \left(\begin{bmatrix} \delta^{L_{cp}-1(u)} & \cdots & \delta^{2(u)} & \delta^{1(u)} & \delta^{0(u)} \\ \delta^{L_{cp}(u)} & \cdots & \cdots & \delta^{2(u)} & \delta^{1(u)} \\ \vdots & \ddots & \ddots & & \vdots \\ \vdots & \ddots & \ddots & \ddots & \vdots \\ \vdots & & \ddots & \ddots & \vdots \\ \delta^{N_p+L_{cp}-2(u)} & \cdots & \cdots & \cdots & \delta^{N_p-1(u)} \end{bmatrix} \odot \begin{bmatrix} a_0^{(u)} & a_{-1}^{(u)} & \cdots & \cdots & a_{L_{cp}}^{(u)} \\ a_1^{(u)} & a_0^{(u)} & a_{-1}^{(u)} & \cdots & a_{L_{cp}}^{(u)} \\ a_2^{(u)} & \cdots & \cdots & \cdots & \vdots \\ \vdots & \ddots & & & \vdots \\ \vdots & & \ddots & & \vdots \\ a_0^{(u)} & \cdots & \cdots & \cdots & a_{N_p-}^{(u)} \end{bmatrix} \right)
$$

$$
\begin{bmatrix} h_0^{(u)} \\ h_1^{(u)} \\ \vdots \\ \vdots \\ \vdots \\ h_{L_{cp}-1}^{(u)} \end{bmatrix} + \begin{bmatrix} n_0 \\ n_1 \\ \vdots \\ \vdots \\ \vdots \\ n_{N_p-1} \end{bmatrix}
$$

$$(4.3)$$

or in matrix notations we have

$$
\underline{r} = \sum_{u=1}^{N_u} (\underline{\delta}^{(u)} \odot \underline{\widetilde{\mathbf{a}}}^{(u)}) \underline{h}^{(u)} + \underline{n} \tag{4.4}
$$

where $\underline{r}$ is an $N_p \times 1$ vector containing the samples of the received signal and $\underline{n}$ is the $N_p \times 1$ noise vector with noise samples. We have rewritten the equation (2.18) into (4.4) in a way that the L_{cp}-long channel impulse response $\underline{h}^{(u)}$ (completed with zeros if needed) is *pushed* to the right to allow an estimation. The $N_p \times L_{cp}$ matrix $\underline{\widetilde{\mathbf{a}}}^{(u)}$ contains the samples of the transmitted signal and the $N_p \times L_{cp}$ matrix $\underline{\delta}^{(u)}$ is the shift matrix of user u containing its shift coefficients. $\odot$ represents the Hadamard product resulting from the input data being multiplied with the CFO at the transmitter of user u. Furthermore, the $(\underline{\delta}^{(u)} \odot \underline{\widetilde{\mathbf{a}}}^{(u)})$ product takes into account the effect of CFO on the cyclic prefix. $\delta^{k(u)} = e^{j2\pi k \delta f^{(u)}/N_p}$, with $k = 0, ..., N_p + L_{cp} - 2$, are the shift coefficients of user u. Equation (4.4) can be written in a more compact form as

$$
\underline{r} = \underline{\breve{\mathbf{a}}}\,\underline{h} + \underline{n} \tag{4.5}
$$

where $\underline{\breve{\mathbf{a}}} = [(\underline{\delta}^{(1)} \odot \underline{\widetilde{\mathbf{a}}}^{(1)}), ..., (\underline{\delta}^{(N_u)} \odot \underline{\widetilde{\mathbf{a}}}^{(N_u)})]$ and $\underline{h} = [\underline{h}^{(1)T}, ..., \underline{h}^{(N_u)T}]^T$.

4.3 Joint CIR and CFO estimation

After presenting the received signal model in the previous section, in this section, we present the proposed joint CIR and CFO estimation algorithm by starting from the Maximum Likelihood (ML) approach. We show that our proposed estimation method results in estimators with reduced complexity while maintaining similar performance.

4.3.1 Proposed joint estimation algorithm

Given the received signal model in (4.5), we consider the joint maximum likelihood estimation of the channel and the CFO. Assuming the noise $\underline{n}$ is white and complex Gaussian with zero mean and variance σ_n^2, and the different users' data are independent from each other, the maximum likelihood (ML) estimate of the channel vector is given by

$$\widehat{\underline{h}} = [\underline{\breve{\mathbf{a}}}^H \underline{\breve{\mathbf{a}}}]^{-1} \underline{\breve{\mathbf{a}}}^H \underline{r} \tag{4.6}$$

where H denotes the hermitian transpose. The CFO estimate, $\widehat{\delta f}$, should be obtained by inserting $\widehat{\underline{h}}$ into the log-likelihood function as follows

$$\widehat{\delta f} = \arg \max_{\delta f}[J_{ML}(\delta f)] \tag{4.7}$$

where the cost function is given by

$$J_{ML}(\delta f) = \underline{r}^H \underline{\breve{\mathbf{a}}}[\underline{\breve{\mathbf{a}}}^H \underline{\breve{\mathbf{a}}}]^{-1} \underline{\breve{\mathbf{a}}}^H \underline{r} \tag{4.8}$$

In practice, the CFO estimates obtained from (4.7) are then used in (4.6) to find the channel estimates. The cost function in (4.8) is very complex to maximize because of the matrix inversion and the multidimensional search becomes very cumbersome to carryout. By following the approximated maximum likelihood approach presented in [70] and choosing the shift orthogonal training sequences like CHU-Codes [77], so that $\underline{\breve{\mathbf{a}}}^H \underline{\breve{\mathbf{a}}}$ can be approximated by $\underline{\breve{\mathbf{a}}}^H \underline{\breve{\mathbf{a}}} \approx \underline{I}$, the cost function in (4.8) for a CFO in user u can then be simplified as

$$J_{ML}(\delta f^{(u)}) \approx \underline{r}^H(\underline{\delta}^{(u)} \odot \widetilde{\underline{\mathbf{a}}}^{(u)})(\underline{\delta}^{(u)} \odot \widetilde{\underline{\mathbf{a}}}^{(u)})^H \underline{r} \tag{4.9}$$

After some manipulations, we further simplify (4.9) into

$$J(\delta f^{(u)}) = \underline{r}^H(\underline{\mathbf{x}}^{(u)} \odot \underline{\delta}_{her}^{(u)})\underline{r} \tag{4.10}$$

with

$$\underline{\mathbf{x}}^{(u)} = \widetilde{\underline{\mathbf{a}}}^{(u)} \widetilde{\underline{\mathbf{a}}}^{(u)H} \tag{4.11}$$

$\underline{\delta}_{her}^{(u)}$ is a hermitian matrix given by

$$
\underline{\delta}_{her}^{(u)} = \begin{bmatrix}
\delta^{0(u)} & \delta^{-1(u)} & \delta^{-2(u)} & \cdots & \cdots & \delta^{-N_p+1(u)} \\
\delta^{1(u)} & \delta^{0(u)} & \delta^{-1(u)} & \cdots & \cdots & \delta^{-N_p+2(u)} \\
\vdots & \ddots & \ddots & \ddots & & \vdots \\
\vdots & & \ddots & \ddots & \ddots & \vdots \\
& & & \ddots & \ddots & \delta^{-1(u)} \\
\delta^{N_p-1(u)} & \cdots & \cdots & \cdots & \delta^{1(u)} & \delta^{0(u)}
\end{bmatrix} \tag{4.12}
$$

By using the shift orthogonal sequences the multidimensional search of (4.8) is separated into independent search, equation (4.9). Even after these simplifications, the complexity of a grid search algorithm to minimize J_{ML} is still high. An alternative class of estimator proposed in [70, 78] uses polynomial approximations to simplify the search. For example in [78] authors have applied a polynomial approximation to the cost function. In [70] the polynomial approximation of the shift matrix is applied. We apply the polynomial approximation to the $\underline{\delta}_{her}^{(u)}$ matrix rather than the cost function or shift matrix $\underline{\delta}^{(u)}$ for user u and we show that the resulting frequency estimators are much simpler than the CFO estimates obtained using the method provided in [70]. Our approach is based on the approach that the $\underline{\delta}_{her}^{(u)}$ matrix can be approximated as follows,

$$
\underline{\delta}_{her}^{(u)} = \sum_{m=0}^{\infty} \frac{\partial^m(\underline{\delta}_{her}^{(u)})}{\partial \delta f^{(u)m}} \frac{(\delta f^{(u)} - \delta f_o^{(u)})^m}{m!} \tag{4.13}
$$

$$
= \underline{I} + \underline{D}(\delta f^{(u)} - \delta f_o^{(u)}) + \underline{D}^2 \frac{(\delta f^{(u)} - \delta f_o^{(u)})^2}{2!} \ldots \tag{4.14}
$$

$$
= \sum_{m=0}^{\infty} \underline{D}^m \frac{(\delta f^{(u)} - \delta f_o^{(u)})^m}{m!} \tag{4.15}
$$

where $\delta f_o^{(u)}$ is an initial guess of the CFO of user u and the matrix $\underline{D}^m$ is given by

$$
\underline{D}^m = \left(\frac{j2\pi}{N_p}\right)^m \left\{\underline{\Lambda}^m \odot \underline{\delta}_{her}|_{\delta f = \delta f_o}\right\} \tag{4.16}
$$

and $\underline{\Lambda}^m$ is

$$
\underline{\Lambda}^m = \begin{bmatrix}
(0)^m & (-1)^m & (-2)^m & \cdots & \cdots & (-N_p+1)^m \\
(1)^m & (0)^m & (-1)^m & \cdots & \cdots & (-N_p+2)^m \\
\vdots & \ddots & \ddots & \ddots & & \vdots \\
\vdots & & \ddots & \ddots & \ddots & \vdots \\
\vdots & & & \ddots & \ddots & (-1)^m \\
(N_p-1)^m & \cdots & \cdots & \cdots & (1)^m & (0)^m
\end{bmatrix}
\tag{4.17}
$$

Now (4.10) is approximated as

$$
J_{PE}(\delta f^{(u)}) = \underline{r}^H \left(\mathbf{\underline{x}}^{(u)} \odot \sum_{m=0}^{\infty} \underline{D}^m \frac{(\delta f^{(u)} - \delta f_o^{(u)})^m}{m!} \right) \underline{r}
\tag{4.18}
$$

$$
= \sum_{m=0}^{\infty} \frac{(\delta f^{(u)} - \delta f_o^{(u)})^m}{m!} \mathbb{R} \left\{ \underline{r}^H (\mathbf{\underline{x}}^{(u)} \odot \underline{D}^m) \underline{r} \right\}
\tag{4.19}
$$

where PE stands for Polynomial Estimator. We denote the co-efficients $d_m^{(u)}$ as

$$
d_m^{(u)} = \mathbb{R} \left\{ \underline{r}^H (\mathbf{\underline{x}}^{(u)} \odot \underline{D}^m) \underline{r} \right\}
\tag{4.20}
$$

Therefore, for a polynomial of degree M expansion, (4.19) becomes

$$
J_{PE}(\delta f^{(u)}) \approx \sum_{m=0}^{M} \frac{(\delta f^{(u)} - \delta f_o^{(u)})^m}{m!} d_m^{(u)}
\tag{4.21}
$$

To find the estimate of the frequency offsets, the first derivative of (4.21) is set equal to zero.

$$
\frac{\partial J_{PE}(\delta f^{(u)})}{\partial \delta f} = \sum_{m=0}^{M-1} \frac{(\delta f^{(u)} - \delta f_o^{(u)})^m}{m!} d_{m+1}^{(u)} = 0
\tag{4.22}
$$

The CFO estimate of a user u is then given by the real root of (4.22) with a negative second derivative, i.e. $\frac{\partial^2 J_{PE}(\delta f^{(u)})}{\partial (\delta f^{(u)2})} < 0$, which is closest to $\delta f_o^{(u)}$. For example, for a polynomial of degree $M = 2$, the CFO estimator is given by

$$
\delta \widehat{f}^{(u)} = \delta f_o^{(u)} + \frac{-\mathbb{R} \left\{ \underline{r}^H (\mathbf{\underline{x}}^{(u)} \odot \underline{D}^1) \underline{r} \right\}}{\mathbb{R} \left\{ \underline{r}^H (\mathbf{\underline{x}}^{(u)} \odot \underline{D}^2) \underline{r} \right\}}
\tag{4.23}
$$

From (4.20) and (4.22) it can be seen that the co-efficients $d_m^{(u)}$ in the cost function $J_{PE}(\delta f^{(u)})$ are much simpler and easy to calculate than those computed using the method proposed in [70]. The calculation of the coefficients $d_m^{(u)}$ involve sim-

ple Hadamard product which can be easily implemented. As a consequence, the frequency offset estimates obtained are simpler and easy to compute.

4.3.2 Degree of the Polynomial Estimator

This section presents the performance of our proposed estimation method with focus on the choice of the polynomial degree. We assume that there are two users in the system, $N_u = 2$. The main simulation parameters considered are the total number of the available subcarriers $N_p = 128$ and the length of the cyclic prefix is $L_{cp} = N_p/8$. The channel is implemented with random impulse responses with Rayleigh fading coefficients and the length of the channel is equal to the length of the cyclic prefix $L_h = L_{cp}$. The orthogonal training sequences are generated using [77].

In Figure 4.1, we have plotted the mean and the variance of the $\delta \widehat{f}^{(u)}$ estimate for 500 different channel realizations. Note that a polynomial of degree $M = 2$ is used to find the CFO estimates. The CFO experienced by both the users is taken as constant and are of low ranges i.e. $\delta f^{(1)} = 0.05$ and $\delta f^{(2)} = 0.01$. We can see that the estimated value approaches the true value with increase in SNR value. Thus, from Figure 4.1 it is seen that for small values of the normalized CFO, small values of the polynomial approximation, M, are sufficient to provide an accurate solution. But for large values of CFOs, the estimator with a polynomial degree of $M = 2$ will not converge and will fail to provide a good solution.
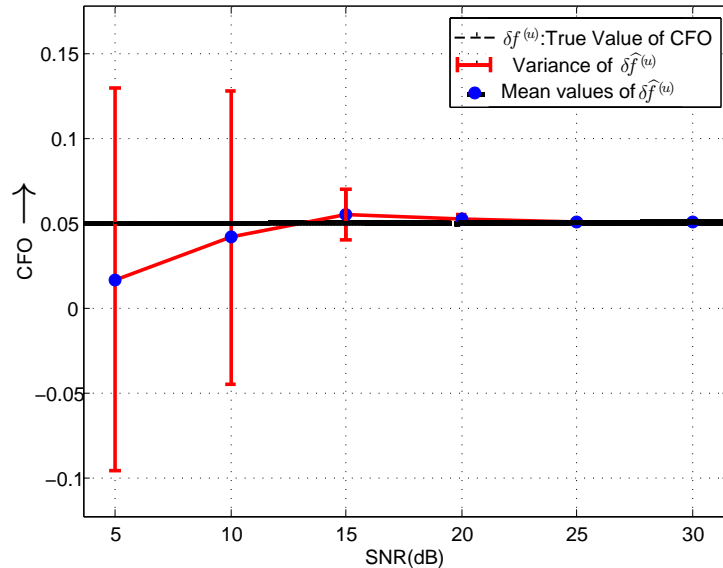
Figure 4.1: Mean and variance of the CFO, $\delta \widehat{f}^{(u)}$ vs. SNR. $\delta f^{(1)} = 0.05$, $M = 2, N_p = 128, L_{cp} = 16$ and $N_u = 2$.

This fact is shown in Figure 4.2 where we have plotted the mean square error (MSE) for the CFO estimate $\delta\hat{f}^{(u)}$ as a function of the maximum value of CFO $\delta f_{max}^{(u)}$. In order to consider a realistic and more practical scenario, the CFOs for the two users are simulated as independent random variables with a uniform distribution in $[0, \delta f_{max}^{(u)}]$. For both the users $\delta f_o^{(u)} = 0$. We can see that for $M = 2$ the MSE is of the order of 10^{-4} for very small values of CFO i.e. $\delta f_{max}^{(u)} < 0.05$. But as soon as $\delta f_{max}^{(u)}$ increases beyond 0.05 the MSE for $M = 2$ increases rapidly and becomes unbearable. Similarly, for $M = 3$, the performance of the estimator is good for $\delta f_{max}^{(u)} < 0.15$ but with a further increase in CFO the performance starts to degrade. Next the degree of the polynomial is increased to $M = 5$. The best results are obtained with $M = 5$ where the MSE is of the order of 10^{-4} for $\delta f_{max}^{(u)}$ values up to 0.3, at the cost of an increased complexity.
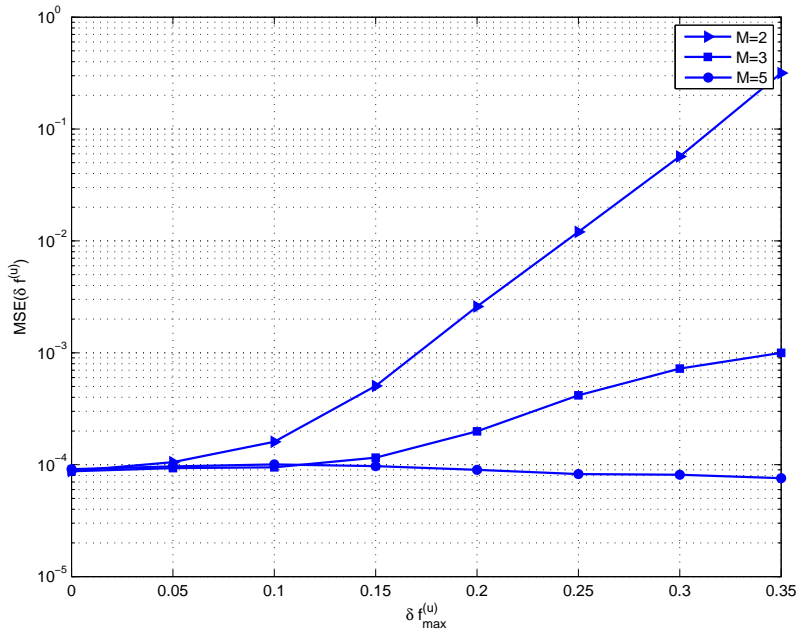
Figure 4.2: Mean square error of CFO estimates for polynomial approximation with $M = 2, 3$ and 5 as a function of $\delta f_{max}^{(u)}$. $N_p = 128, L_{cp} = 16$ and $N_u = 2$.

The estimates for the channel impulse responses can be calculated by inserting the CFO estimates in (4.6). In the sections to follow we present a CFO compensation method based on successive cancellation of interference at the base station. The carrier frequency offsets of the uplink users are estimated by the receiver by using the polynomial estimator just presented.

4.4 Self-SIC based CFO compensation

In chapter 2, we have shown that the OFDMA inherits from OFDM the sensitivity to CFO [35]. In an OFDMA system, the orthogonality among the subcarriers ensures the elimination of the self inter-carrier interference of a user as well as the multiuser interference among different users [72]. The CFOs in the system disturb this orthogonality and result in severe inter-carrier interference. While the CFO can be estimated and corrected relatively easily in the downlink, preserving orthogonality in the uplink is much more demanding. In the uplink, the received signal is the sum of multiple signals coming from different users, each of which experiences a different CFO due mainly to oscillator instability and/or Doppler shift [65]. These relative CFOs among users must be corrected, otherwise the system performance could degrade severely. Downlink CFO correction methods, which are designed for single-user scenario, are unable to correct multiple CFOs in the uplink, as correction to one users CFO would misalign the other users [38]. In the sequel, we present a CFO compensation method based on successive cancellation of CFO induced interferences at the receiver.

A CFO compensation method based on LS approach is presented in [72, 73]. In [72] the LS approach is used to remove ICI and MUI but it requires inverting the $N_p \times N_p$ interference matrix which is practically impossible for large DFT sizes. Furthermore, the nonlinearity of the model in (4.4) does not allow the LS solution of the symbols. For this reason we revert our attention to the model for the received symbols which we have already derived in chapter 2. We have shown that the signal at the DFT input in (4.2) can be written as:

$$
\begin{pmatrix} r_{N_p-1} \\ \vdots \\ \vdots \\ r_0 \end{pmatrix} = \sum_{u=1}^{N_u} \left[\underline{\tilde{h}}^{(u)} + (\underbrace{\delta^{-N_p(u)}-1}_{x}) \underbrace{\begin{pmatrix} & & 0 \\ h_{L-1}^{(u)} & & \\ \vdots & \ddots & \\ h_1^{(u)} \cdots & h_{L-1}^{(u)} & \end{pmatrix}}_{\underline{h}_\Delta^{(u)}} \right] \underbrace{\begin{pmatrix} \delta^{0(u)} & & & 0 \\ & \ddots & & \\ & & \ddots & \\ 0 & & & \delta^{-(N_p-1)(u)} \end{pmatrix}}_{\underline{\delta}^{(u)}} \begin{pmatrix} a_{N_p-1}^{(u)} \\ \vdots \\ \vdots \\ a_0^{(u)} \end{pmatrix}
$$

At the output of the DFT block, $\underline{R} = \underline{F}(r_{N_p-1}, ..., r_0)^T$ is shown to be equal to

$$
\underline{R} = \sum_{u=1}^{N_u} \underline{G}^{(u)} \ \underline{A}^{(u)} \tag{4.24}
$$

where $\underline{A}^{(u)} = \underline{F}^{-1}\underline{a}^{(u)}$ is the vector of transmitted modulation symbols of user u after

subcarrier mapping and $\underline{F}$ is the $N_p \times N_p$ DFT matrix. The matrix $\underline{G}^{(u)}$ represents the channel and the CFO effect for a user u and is given by

$$\underline{G}^{(u)} = \underline{H}^{(u)} \underline{F} \ \underline{\delta}^{(u)} \underline{F}^{-1} + (\delta^{-N_p(u)} - 1)\underline{F} \ \underline{h}_\Delta^{(u)} \underline{\delta}^{(u)} \underline{F}^{-1} \qquad (4.25)$$

where $\underline{H}^{(u)}$ is the diagonal DFT channel matrix for a user u with $\underline{H}^{(u)} = \underline{F} \ \underline{h}^{(u)}$, thanks to the channel impulse response length $L_h < L_{cp}$. The interference seen by a subcarrier v allocated to a user l coming from all the other carriers is given by

$$\zeta_v^{ici} = \underbrace{\sum_{\substack{k=\in\Gamma^{(l)}\\k\neq v}} G_{(v,k)}^{(l)} A_k^{(l)}}_{self-ICI} + \underbrace{\sum_{\substack{u=1\\u\neq l}}^{N_u} \underbrace{\sum_{\substack{k\in\Gamma^{(u)}\\k\neq v}} G_{(v,k)}^{(u)} A_k^{(u)}}_{MUI^{(u)}}}_{MUI} \qquad (4.26)$$

where $\Gamma^{(u)}$ is the set of subcarriers allocated to user u. In (4.26),

- $self - ICI$ is the interference observed by user l, on subcarrier v, from its own allocated subcarriers other than v.

- $MUI^{(u)}$ represents the individual interferences of all other users present in the system to subcarrier v.

- MUI represents the overall interference contributed by users other than l to subcarrier v, respectively, on user l.

4.4.1   Self-Successive Interference Cancellation Algorithm

In the previous section we presented the analytical expressions for the self-ICI and multiuser-ICI. In order to overcome these CFO induced interferences, we propose to use successive interference cancellation (SIC). SIC based CFO compensation is studied in [75, 76]. In [75], the proposed SIC compensation method neglects the self-interference and is limited to an interleaved carrier allocation scheme. In [76], results are proposed for a carrier allocation scheme that uses a blocksize of 4 adjacent subcarriers. For blocksize of 4, the matrix inverse involved in the self-ICI cancellation process is very simple and can be carried out efficiently. But if a carrier allocation with larger blocksize is used then it becomes difficult to implement the matrix inversion. For example, in the case of an uplink OFDMA system with 4 users and 512 subcarriers, if a blocksize of 128 adjacent subcarriers is used then the matrix inversion required to cancel the self-ICI will be very difficult to calculate and implement. In uplink OFDMA transmission where CSI is available, subcarriers are allocated to the users according to their channel gains in order to exploit multiuser

diversity [32]. In such dynamic carrier allocation schemes, the size of the subcarrier blocks allocated to users varies and the blocksize can be larger than 4 adjacent subcarriers. For such scenarios we propose a self-successive interference canceler (self-SIC) that avoids matrix inversion of large matrices.

The block diagram of the self-SIC algorithm is shown in Figure 4.3. Subcarriers are allocated to the users using a fair blockwise allocation and all the users equally share the available bandwidth, i.e. $|\Gamma^{(u)}| = \mathcal{M} = N_p/N_u \; \forall \; u$. N_B is the total number of blocks in an OFDMA symbol and the size of each block is equal to K adjacent subcarriers. As a first step, the received subcarrier blocks are ranked in descending order based on their respective signal to interference plus noise ratio (SINR) values as in [79]. Note that most of the authors do the ordering with respect to SNR only, see [75, 76], which is not as accurate. The self-SIC compensation method employs the successive cancellation procedure to remove the interference coming from the subcarriers within a particular block.
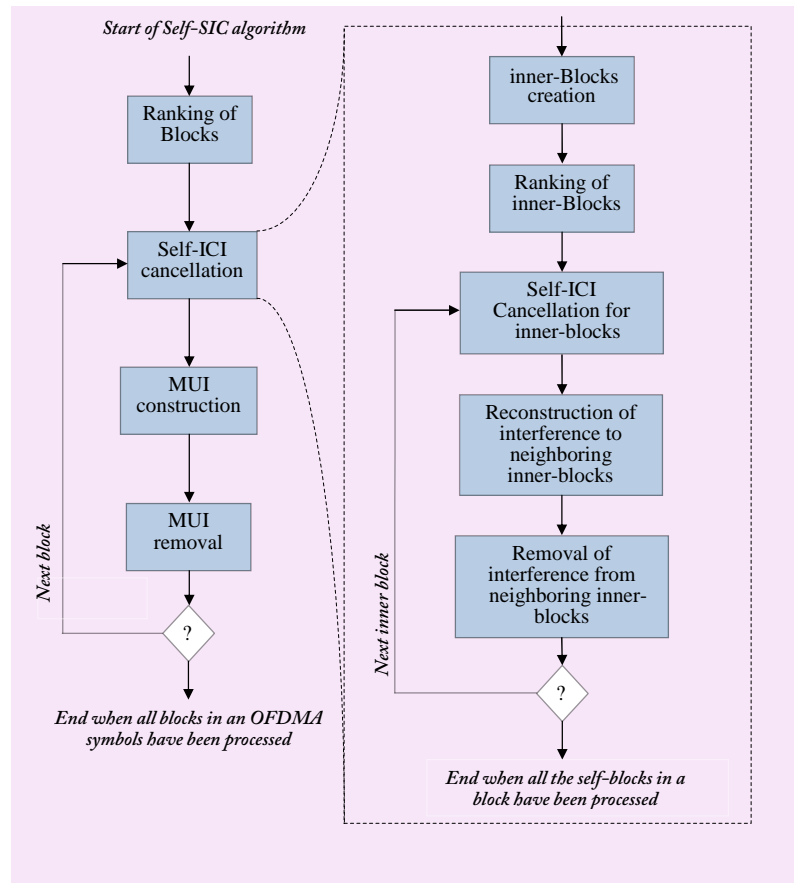
Figure 4.3: Block diagram of the proposed successive CFO compensation algorithm.

4.4.1.1   Inner-blocks creation

Assuming that a particular block, say block B, in an OFDMA symbol has the highest SINR value, the self-SIC process starts by further breaking down block B into smaller blocks, as shown in Figure 4.4. These smaller blocks, each of size S adjacent subcarriers, are called the inner-blocks of block B. N_s is the total number of inner-blocks in block B.
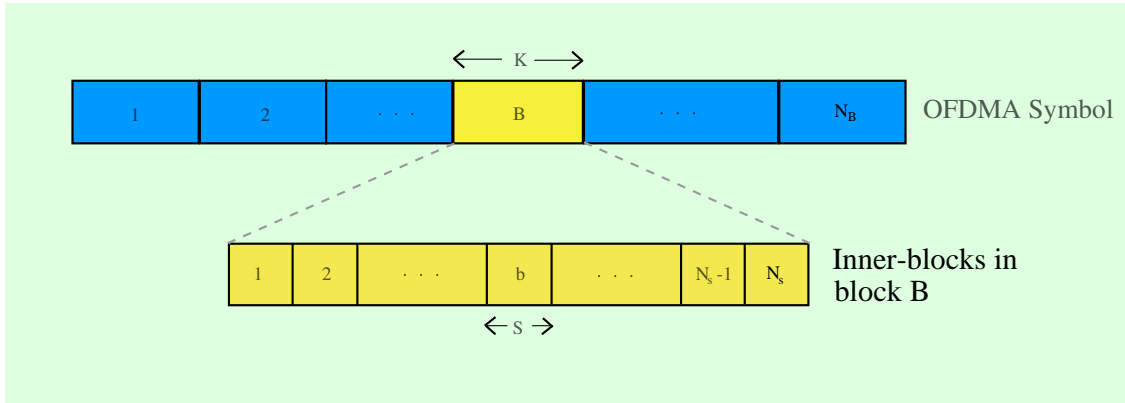
Figure 4.4: Division of block B into a total of N_s inner-blocks each of size S during the self-SIC algorithm.

4.4.1.2   Ranking of Inner-Blocks

The resulting inner-blocks are ranked according to their SINR values. The SINR value for a particular inner-block b is calculated as follows

$$SINR_b = \frac{|H_b|^2}{\sigma_n^2 + \sum_{s=1,s\neq b}^{N_S} \sigma_{(s,b)}^2} \tag{4.27}$$

where H_b is the channel frequency response over the self-block b, σ_n^2 is the noise power and $\sum_{s=1,s\neq b}^{N_S} \sigma_{(s,b)}^2$ is the variance of the total interference seen by the inner-block b from its neighboring inner-blocks present within the block B and can be calculated from (2.29).

4.4.1.3   Decorrelation

From (4.24), the DFT output for the bth inner-block, belonging to the block B, is given by:

$$\underline{R}_b = \underline{G}_b\underline{A}_b + \underline{n}_b \tag{4.28}$$

where $\underline{R}_b = [R_v...R_{v+S}]^T$ is the received signal vector for the inner-block b, $\underline{G}_b$ is the $S \times S$ matrix containing the contributions of both the channel and the CFO induced interference terms, $\underline{A}_b$ is the vector of transmitted symbols and $\underline{n}_b$ represents the noise contributions. Note that for simplicity the user indexes are removed. In this step the decorrelator $\underline{G}_b^{-1}$ is applied, as in [76], to the highest ranked inner-block in order to remove the ICI within the inner-block. Now the decorrelator output can be calculated using (4.28) as follows, assuming perfect channel and CFO knowledge

$$\widehat{\underline{A}}_b = \underline{G}_b^{-1} \underline{R}_b \tag{4.29}$$
$$= \underline{A}_b + \underline{G}_b^{-1} \underline{n}_b \tag{4.30}$$

The receiver can then make decisions on the detected symbols, $\widehat{\underline{A}}_b$.

4.4.1.4   Interference Cancellation

In this step, the decoded signal of the top ranked inner-block is used to reconstruct and remove the interference to the other neighboring inner-blocks present in the block B. The interference of the bth inner-block on a subcarrier v within the block B can be calculated using (2.28) as follows

$$\zeta_{(b,v)} = \sum_{k \in \Gamma_b} G^{(u)}_{(v,k)} \widehat{A}^{(u)}_k \tag{4.31}$$

Note that $v \in \Gamma_B$ but $v \notin \Gamma_b$ where Γ_B and Γ_b represent the subcarriers in block B and inner-block b respectively. In this way the multiuser-ICI from the inner-block b to all neighboring inner-blocks is calculated and then subtracted from the received signals of other inner-blocks as follows

$$\begin{aligned} \underline{R}'_1 &= \underline{R}_1 - \underline{\zeta}_{(b,1)} \\ \underline{R}'_2 &= \underline{R}_2 - \underline{\zeta}_{(b,2)} \\ \vdots \quad &\vdots \quad \vdots \\ \vdots \quad &\vdots \quad \vdots \\ \underline{R}_{N_s}' &= \underline{R}_{N_s} - \underline{\zeta}_{(b,N_s)} \end{aligned} \tag{4.32}$$

The variance of interference contributed by inner-block b to different neighboring inner-blocks will be different mainly depending upon the respective distances of other inner-blocks from b as shown in Figure 4.5, i.e., $\sigma^2_{\zeta(b,1)} < \sigma^2_{\zeta(b,b-1)}$. Accordingly, the second highest ranked inner-block is decoded, its interference is calculated and removed from the remaining inner-blocks in the block B. This procedure is continued until all the inner-blocks in the block B are processed. At the end of the self-SIC step all the self interference in the block B has been removed without any
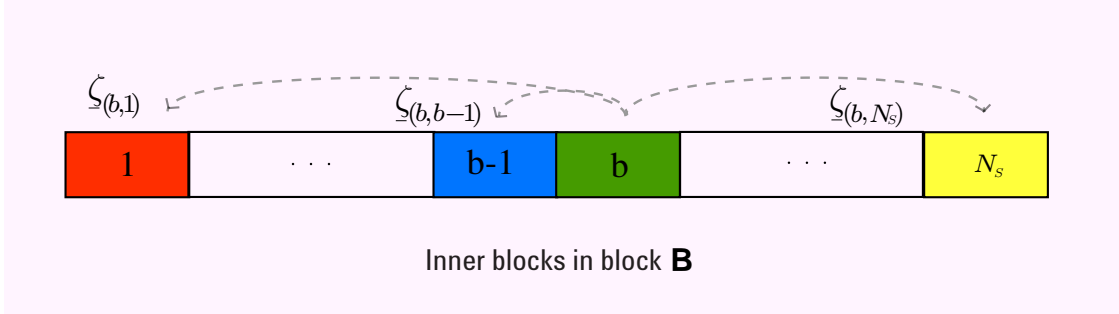
Figure 4.5: Multiuser-ICI contributed from the inner-block b to neighboring blocks within the block B.

large matrix inversion when there is no error propagation. This self-SIC procedure can be performed for larger blocksizes using any suitable inner-blocksize.

The overall decoded signal for block B obtained from the self-ICI cancellation step is then used to reconstruct the multiuser-ICI of the current block from other adjacent blocks present in the OFDMA symbol. The procedure is the same as described in subsection 4.4.1.4. Next the second ranked block is decoded using the self-SIC CFO compensation method and its interference is removed from the remaining blocks. This successive procedure is repeated until all the blocks are processed.

4.4.2 Computation Complexity of Self-SIC algorithm

In this section, the computation complexity of our proposed self-SIC algorithm is compared to the SIC algorithm in [76], so-called the conventional SIC method. The conventional SIC method involves an inversion of a matrix of size K in the self-ICI cancellation process where K is the size of the blocks in OFDMA symbol. For subcarrier allocations with larger blocksizes the implementation of matrix inverse will become cumbersome. On the other hand, the self-ICI cancellation stage in the proposed self-SIC algorithm requires N_s inversions of a small matrix of size S, i.e. the size of inner-block. Note that S is the size of inner-blocks and $S<<K$. Since the matrix $\underline{G}^{(u)}$ is an arbitrary matrix, the complexity of inverting is of the power 3 of its size. Table 4.1 shows the complexity of the conventional and the proposed self-SIC algorithm. The second line of Table 4.1 shows the complexity of the two algorithms for the system settings where $N_p = 512, N_u = 4, K = 64$ and $S = 4$. It is clear that our proposed self-SIC overcomes the hardships of large matrix inversion especially where the blocksize is large.

Self-SIC algorithm	conventional SIC
$N_s O(S^3)$	$O(K^3)$
	with $K = N_s S$
$16 O(64)$	$O(262144)$

Table 4.1: Algorithm complexity

4.4.3   Performance Analysis of the Self-SIC algorithm

In this section, we analyze the performance of the proposed self-SIC algorithm in comparison to the conventional SIC algorithm. We quantize the degradation that is observed in the self-SIC algorithm while avoiding the full matrix inversion which is used in conventional SIC method to cancel all the ICI within a block. The comparison is done in terms of the mean square error of the detected symbols. In order to validate the proposed self-SIC, it is assumed that perfect channel knowledge is available at the receiver and the CFOs are also known.

4.4.3.1   Conventional SIC algorithm

For a block of interest, lets say block B allocated to a user l as shown in Figure 4.4, the received signal is given by

$$\underline{R}_B^{(l)} = \underline{G}_B^{(l)} \underline{A}_B^{(l)} + \underline{n}_B^{(l)} \tag{4.33}$$

where $\underline{R}_B^{(l)}$ is $K \times 1$ vector of the received signals over the block B, $\underline{G}_B^{(l)}$ is the $K \times K$ channel and CFO induced interference matrix, $\underline{A}_B^{(l)}$ is $K \times 1$ vector containing the transmitted symbols and $\underline{n}_B^{(l)}$ is the $K \times 1$ noise vector for block B. In the conventional SIC process, the decoded symbols for block B are obtained through decorrelation which involves inversion of a $K \times K$ matrix as follows

$$\underline{\hat{A}}_B^{(l)} = \underline{G}^{-1}{}_B^{(l)} \underline{R}_B^{(l)} \tag{4.34}$$

The mean square error for the detected symbols $\underline{\hat{A}}_B^{(l)}$ is given by

$$E\left[\left\|\underline{\hat{A}}_B^{(l)} - \underline{A}_B^{(l)}\right\|^2\right] = E\left[\left\|\underline{G}^{-1}{}_B^{(l)} \underline{R}_B^{(l)} - \underline{A}_B^{(l)}\right\|^2\right] \tag{4.35}$$

$$MSE_{csic} = \sigma_n^2 tr\left[\left(\underline{G}^{-1}{}_B^{(l)}\right)^H \underline{G}^{-1}{}_B^{(l)}\right] \tag{4.36}$$

where $tr[x]$ stands for *trace of x* and σ_n^2 is the noise power.

4.4.3.2 Self-SIC algorithm

Next we calculate the mean square error of the detected symbols for the self-SIC algorithm. We assume an optimistic case and consider that there is no error propagation while performing self-SIC approach, hence the results obtained will represent an upper bound. The self-SIC scheme breaks the block B into smaller inner-blocks. We further assume that these inner-blocks of B are ranked in ascending order i.e. inner-block 1 has the highest SINR and inner-block N_s has the least SINR value. To get a better insight of the self-SIC operation, we can write (4.33) in matrix form as follows

$$\underline{R}_B^{(l)} = \begin{bmatrix} \underline{R}_{(1)} \\ \underline{R}_{(2)} \\ \vdots \\ \vdots \\ \underline{R}_{(N_s)} \end{bmatrix} = \begin{bmatrix} \underline{G}_B^{(l)} \end{bmatrix} \begin{bmatrix} \underline{A}_{(1)} \\ \underline{A}_{(2)} \\ \vdots \\ \vdots \\ \underline{A}_{(N_s)} \end{bmatrix} + \begin{bmatrix} \underline{n}_{(1)} \\ \underline{n}_{(2)} \\ \vdots \\ \vdots \\ \underline{n}_{(N_s)} \end{bmatrix} \tag{4.37}$$

where the $K \times K$ matrix $\underline{G}_B^{(l)}$ is shown in Figure 4.6. Since the self-SIC algorithm
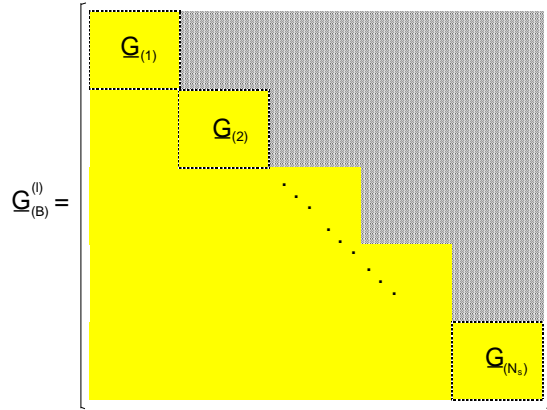
Figure 4.6: The $K \times K$ matrix $\mathrm{G}_B^{(l)}$ for block B allocated to user l. K is the size of block B.

divides the block B into N_s inner-blocks of size S, $\underline{R}_{(1)}$ represents the received symbols on the inner-block 1 and is given by

$$\underline{R}_{(1)} \approx \underline{G}_{(1)}\underline{A}_{(1)} + \underline{n}_{(1)} \tag{4.38}$$

The approximation sign $\approx$ appears because the self-SIC ignores the interference contribution to the inner-block 1 from other inner-blocks present in B. The symbols $\widehat{\underline{A}}_{(1)}$ are detected using the decorrelation process and the inter-carrier interference from inner-block 1 is subtracted from all the remaining blocks. For inner-block 2,

4.4 Self-SIC based CFO compensation

the expression for detected symbols $\widehat{\underline{A}}_{(2)}$ is given by

$$\widehat{\underline{A}}_{(2)} = \underline{G}_{(2)}^{-1} \left[\underline{R}_{(2)} - \underline{G}_{(1,2)} \widehat{\underline{A}}_{(1)} \right] \tag{4.39}$$

From above expression it is observed that the total interference taken into consideration while computing $\widehat{\underline{A}}_{(2)}$ is that from the inner-block 1 and the remaining interference seen by inner-block 2 from all other inner-blocks is neglected. The total neglected interference by the self-SIC procedure for all the inner-blocks is shown by the shaded portion in the matrix $\underline{G}_B^{(l)}$ in Figure 4.6. The remaining portion represents the effective $\underline{G}_{ssic}^{(l)}$ for the self-SIC algorithm. Neglecting a portion of the interference within a block results in degradation in the performance of self-SIC compensation method which makes it a sub-optimal approach but we will show through numerical results that this degradation is very small and can be neglected practically. In order to see this degradation in self-SIC, we calculate the mean square error MSE_{ssic} of the detected symbols for the block B as was done in section 4.4.3.1.

$$MSE_{ssic} = E\left[\left\| \widehat{\underline{A}}_B^{(l)} - \underline{A}_B^{(l)} \right\|^2 \right] \tag{4.40}$$

where

$$\widehat{\underline{A}}_B^{(l)} = \begin{bmatrix} \underline{G}_{(1)}^{-1} \underline{R}_{(1)} \\ \underline{G}_{(2)}^{-1} \left[\underline{R}_{(2)} - \underline{G}_{(1,2)} \widehat{\underline{A}}_{(1)} \right] \\ \vdots \\ \vdots \\ \underline{G}_{(N_s)}^{-1} \left[\underline{R}_{(N_s)} - \sum\limits_{s=1}^{N_s-1} \underline{G}_{(s,N_s)} \widehat{\underline{A}}_{(s)} \right] \end{bmatrix} \tag{4.41}$$

After some calculation we get the following result

$$MSE_{ssic} = \sigma_n^2 \sum\limits_{s=1}^{N_s} tr\left[\left(\underline{G}_{(s)}^{-1} \right)^H \underline{G}_{(s)}^{-1} \right] + \\ \sum\limits_{s=1}^{N_s} \sum\limits_{k=1}^{s-1} tr\left[\underline{G}_{(k,s)}^H \left(\underline{G}_s^{-1} \right)^H \underline{G}_s^{-1} \underline{G}_{(k,s)} \right] \tag{4.42}$$

where N_s is the total number of inner-blocks in block B. For simplicity the user indexes are removed in above equation. From (4.42) we can see that the first term on the right hand side is equal to the MSE calculated for full matrix inversion in (4.36). The second term in (4.42) represents the additional degradation that is observed in the case of self-SIC algorithm. This additional term in the MSE_{ssic} represents the additional loss in self-SIC algorithm.

4.4.4 Simulation results with perfect channel and CFO knowledge

We have seen in the previous section that the degradation in self-SIC is due to the neglected interference coming from shaded portion of the matrix $\underline{G}$ (in Figure 4.6). In this subsection, we will show through simulations the practical significance of this additional loss in performance observed in case of the self-SIC. Figure 4.7 shows the plot of the bit error rate of the four users as a function of the blocksize K. The total subcarriers are $N_p = 256$ and $L_{cp} = N_p/4$. The CFOs of the all the users are modeled as random variables with uniformly distribution in $[0, \delta f_{max}^{(u)}]$ and $f_{max}^{(u)} \leq 0.3$. The size of the blocks in an OFDMA symbol is $K = 64$ subcarriers for both conventional SIC and self-SIC methods while the size of the inner-blocks for the self-SIC method is varied, i.e. $S = 4, 8, 16, 32$ and 64, along x-axis. In order to validate the self-SIC algorithm, we consider that a perfect knowledge of channel and CFO is available at the receiver.
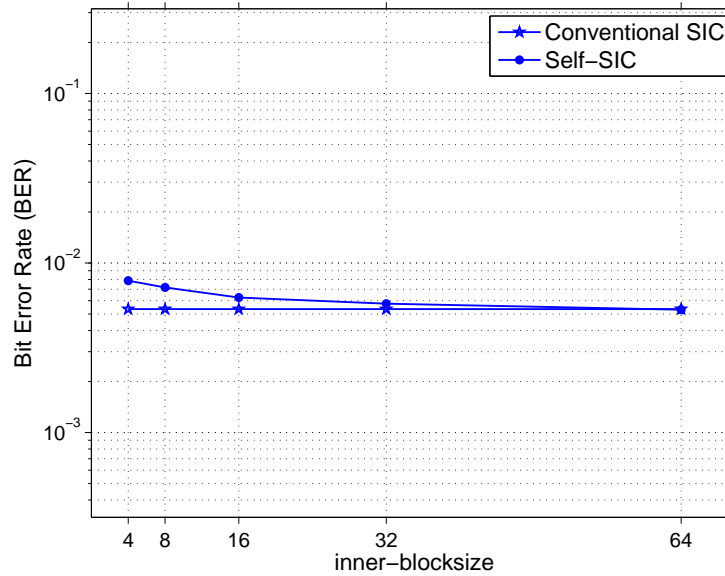
Figure 4.7: Bit error rate (BER) as a function of blocksize in an OFDMA symbol at an SNR of 15dB, $\delta f_{max}^{(u)} = 0.3$.

The curve for the conventional SIC algorithm represents the BER at a blocksize $K = 64$. Figure 4.7 shows that there is a small difference in the performance of the two algorithms in terms of BER for small values of S, i.e. inner-blocksize. As the inner-blocksize increases this slight difference vanishes. This is because with

an inner-blocksize of $S = 4$, the neglected portion of the matrix $\underline{G}$ is large and so as the difference between the performance of the self-SIC and the conventional-SIC methods. As the inner-blocksize is increased the shaded portion in $\underline{G}$ matrix decreases and performance improves. For an inner-blocksize equal to K, the self-SIC becomes conventional SIC method that is why there is no difference in performances but this is achieved at more computational complexity. Therefore, Figure 4.7 shows that by using small inner-blocksizes, the self-SIC algorithm not only avoids large matrix inversions but also remains performant.

4.5 Performance of the complete system: Self-SIC with estimated channel and CFOs

In this section, we analyze the performance of the complete proposed system, i.e. joint CIR and CFO estimation method and self-SIC algorithm. For simulation purposes we consider an uplink OFDMA system with four users and a total of $N_p = 256$ subcarriers. The channel is simulated as random impulse responses with Rayleigh distributed coefficients. Note that the length of the channel is assumed to be equal to that of the cyclic prefix. The CFOs of different users are generated as independent random variables with uniform distribution having a maximum value of δf_{max}.

First the performance of the polynomial estimator, proposed in Section 4.3, is tested in application to the self-SIC algorithm. Figure 4.8 shows the bit error rate of all the users for the proposed self-SIC algorithm as a function of the SNR (dB). Note that for the polynomial estimator, the degree of polynomial is $M = 5$ and no initial knowledge of CFOs is considered to be available i.e. $\delta f_o^{(u)} = 0$. Figure 4.8 shows that the results obtained for the self-SIC algorithm with polynomial estimation are accurate enough. So for small values of the CFOs a polynomial of degree $M = 5$ is sufficient to obtain satisfactory results. Next in Figure 4.9 we compare the bit error rates (BER) for the four users versus the SNR (dB) for the proposed self-SIC algorithm, the conventional SIC method and for the no CFO compensation case. The channel and CFOs are estimated using the joint channel and CFO estimator proposed earlier. Therefore, Figure 4.9 shows the performance of our complete proposed system, i.e. the joint CIR/CFO estimator and the self-SIC algorithm. The blocksize in OFDMA symbol is assumed to be $K = 64$ adjacent subcarriers, since the total number of subcarriers is $N_p = 256$, each user will be allocated one block each. We have chosen the maximum blocksize in order to analyze the self-SIC performance in the worst case. For the self-SIC algorithm, the size of the self-blocks is equal to $S = 4$ adjacent subcarriers. We can observe that there is only a slight degradation in the performance of the self-SIC method in comparison to the conventional SIC. For lower SNR values the results for the conventional and the self-SIC algorithm are

Figure 4.8: Bit error rate (BER) as a function of average SNR. The normalized frequency offset has a uniform distribution with a maximum value of $\delta f_{max}^{(u)} = 0.3$.
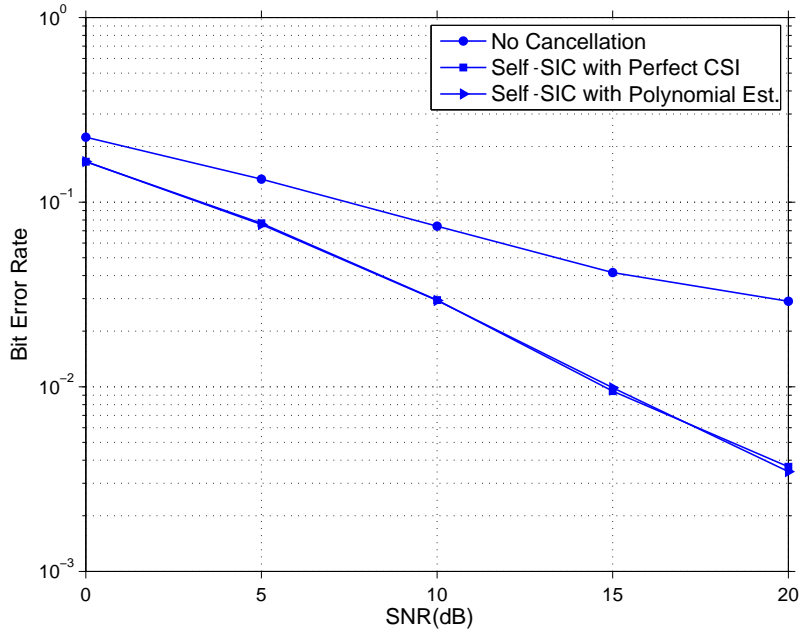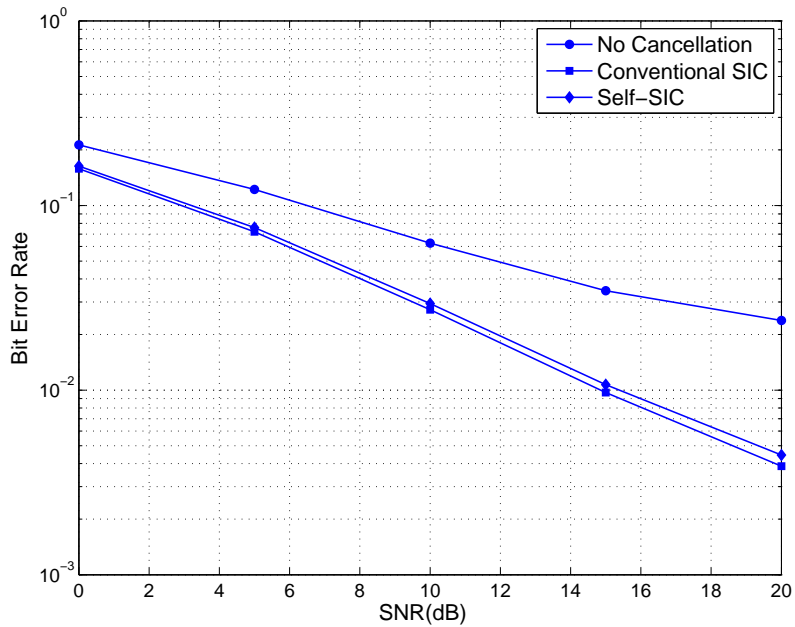

Figure 4.9: Bit error rate (BER) as a function of average SNR. The normalized frequency offset has a uniform distribution with a maximum value of $\delta f_{max}^{(u)} = 0.3$.

very close even with estimated CFO values, as shown by the Figure 4.9. The slight difference appears because of the increased error propagation in case of self-SIC but it remains minute. The conventional SIC provides slightly better results but at a cost of large matrix inversions. However, the performance loss observed in case of the self-SIC is very small and practically negligible.

To further investigate this degradation of performance as a function of the maximum CFO, Figure 4.10 presents curves of the BER versus maximum normalized frequency offset $\delta f_{max}^{(u)}$ at 15dB SNR value. It can be seen that for smaller CFO values the difference in terms of the BER between the two algorithms is very small. The BER for the self-SIC increases slightly more with δf_{max} above 0.3 compared to the conventional SIC method. As frequency offset becomes larger, the effectivity of the self-SIC algorithm decreases slowly because of the increased amount of error propagation but it remains negligible and can be ignored practically.
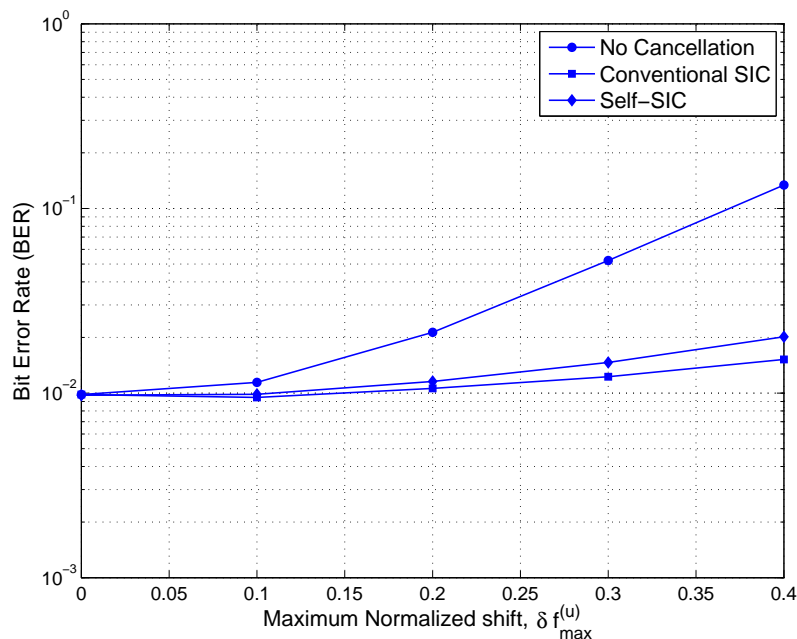

Figure 4.10: Bit error rate (BER) as a function of maximum normalized frequency offset for average SNR of 15 dB.

4.6 Conclusion

In this chapter, we have proposed solutions for two important problems encountered in an uplink OFDMA system due to carrier frequency offsets. The problem

of channel and CFO estimation is addressed first. We have proposed an efficient method for joint estimation of channel impulse responses and carrier frequency at the receiver. Based on a received signal model that takes into account the effect of CFO on the cyclic prefix, the CFO estimates are obtained using polynomial approximation. For CFO estimation, a polynomial approximation method derived from the grid search algorithm is used which results in less complex CFO estimators. These CFO estimates are then used to estimate the channel using the maximum-likelihood approach. We have shown that our joint estimation method is simpler than the existing methods without any performance degradation. The CFO estimates obtained are then used by the proposed self-successive interference canceler (self-SIC) compensation method to cancel out the interferences at the base station. The proposed self-SIC canceler reduces the implementation complexity faced in case of large DFT matrices without any significant loss in performance. Numerical results validate our CFO compensation method and show that proposed cancellation scheme is very effective against the effects of multiple CFOs scenario in the uplink of the OFDMA-based system

Work presented in this chapter has been presented in the proceedings of the IEEE International Conference on Acoustics, Speech, and Signal Processing, ICASSP 2011 [80] and submitted to IEEE Transaction on Communications.

Conclusions and perspectives

Technology advancements have changed the way we communicate, cooperate and entertain ourselves. The goal of the next generation wireless systems is to provide high-quality information and services to people ubiquitously, i.e. having reliable and high-speed connections *on anytime and anywhere basis.* Orthogonal Frequency Division Multiplexing (OFDM) has proven to be the key modulation technique for realizing the broadband wireless communications. It is capable of simplifying the equalization task at the receiver in a frequency-selective fading environment, increases the robustness to narrowband interference and offers high spectral efficiency. A multiuser version of the OFDM technique is Orthogonal Frequency Division Multiple Access (OFDMA), which combines the advantages of Frequency Division Multiple Access (FDMA) technique with those of OFDM.

Among other problems faced in the design of an OFDMA system, one major trouble encountered is its sensitivity to Carrier Frequency Offset (CFO). OFDMA inherits this drawback from OFDM and this sensibility becomes more prominent in the uplink transmission where each user experiences an independent frequency offset and the received signal is the sum of multiple signals coming from different users. Any frequency misalignment present in an OFDMA-based system destroys the orthogonality among subcarriers, which causes Inter-Carrier Interference (ICI) and consequently produces Multi-User Interference (MUI) among users. The two main sources of frequency misalignments are the Doppler effect coming from the channel and the misbehavior of oscillators installed in user terminals. Authors while analyzing the interference in uplink OFDMA transmission assume that the CFO resulting from oscillator mismatch and Doppler shift is one and the same. This is not practical for uplink OFDMA which is more sensitive to carrier frequency misalignments than the downlink OFDMA transmission. In this thesis, we consider the case where the CFO comes from the mismatch of a local oscillator in a user terminal with the carrier frequency allocated to it. For this scenario, we have proposed in chapter 2, a new analytical model for the received signal and intercarrier interference. Our

proposed model takes into account the effect of CFO on the cyclic prefix which is usually rejected at the receiver assuming that the channel matrix is circulant. We show that this assumption is not true in the presence of CFOs and numerical evaluations validate our results. Therefore, while carrying out analysis of uplink OFDMA system undergoing frequency offset, the effect of CFO on the cyclic prefix must be taken into account.

One of the many advantages of OFDMA is its ability to allocate system resources (i.e. subcarriers and power) to different users based on their channel state information. This allows to exploit the frequency diversity and the so-called multiuser diversity. In chapter 3, we have studied different subcarrier allocation schemes by examining their robustness against the CFO induced interference. By letting users share available subcarriers simultaneously, OFDMA offers an increment in the level of bit-granularity and also the possibility to achieve multiuser diversity by applying dynamic subcarrier allocation scheme. But at the same time attention must be paid to the CFO present in the system since using interleaved carrier allocation can provide frequency diversity but at the same time gravely increase the ICI. As a consequence the robustness to CFO induced interference and multiuser diversity are in contradiction. We have proposed a trade off in the form of a *Threshold blocksize* of $L_{cp}/2$, to allow a good compromise between the channel diversity and robustness against CFO in the case when no CSI is available. With CSI available, we have proposed an optimal block carrier allocation scheme through which both robustness to CFO and channel diversity can be achieved using small blocksize for small values of CFO. We further show that above a *critical CFO* value, the performance of the optimal block carrier allocation loses interest.

While the CFO can be estimated and corrected relatively easily in the downlink using traditional methods designed for OFDM technique, these tasks become more challenging in the uplink. During the uplink transmission, each user undergoes distinct frequency error and as a result it becomes very difficult to achieve frequency synchronization at the base station. These multiple CFOs must be corrected, otherwise the system performance degrades severely. Due to the fact that the correction of one user's CFO might cause even larger misalignments with other users, new techniques must be introduced to alleviate this problem. In chapter 4, our main contributions include the joint channel impulse response (CIR) and CFO estimation method followed by the CFO compensation method based on a self-successive interference cancellation. For CFO estimation, a polynomial approximation method derived from the grid search algorithm is used resulting in less complex CFO estimators. We show that our proposed joint estimation method proves to be simpler compared to the existing methods, yet as performant. Once the CFO is estimated, we address the CFO compensation at the receiver. Based on the CFO estimates ob-

tained from the proposed estimation method, a self-successive interference canceler (self-SIC) algorithm is proposed to mitigate both the self-intercarrier interference and multiuser interference at the base station. We show that for a carrier allocation with large blocksizes, the proposed compensation algorithm significantly reduces the implementation complexity without performance degradation.

Throughout the thesis, we assume equal transmit powers from all active users in the system. Furthermore, in order to avoid the shadowing and path loss effects, we assumed that all the users in the cell are at similar shadowed distance from the base station. In the future, it could be an interesting topic to relax this assumption, and consider the impact of near-far effect on CFO estimation and ICI compensation algorithms. Investigating the problem of received power measurement and channel estimation in the OFDMA uplink in the presence of excessive multiple CFOs is also an attractive direction for the future works.

Bibliography

[1] M. Shafi, A. Hashimoto, M. Umehira, S. Ogose, and T. Murase, "Wireless communications in the twenty-first century: A perspective," *Proceedings of the IEEE*, vol. 85, no. 10, pp. 1622 – 38, 1997.

[2] J. Mikkonen, C. Corrado, C. Evci, and M. Progler, "Emerging wireless broadband networks," *IEEE Communications Magazine*, vol. 36, no. 2, pp. 112 – 17, 1998.

[3] M. Frodigh, S. Parkvall, C. Roobol, P. Johansson, and P. Larsson, "Future-generation wireless networks," *IEEE Personal Communications*, vol. 8, no. 5, pp. 10 – 17, 2001.

[4] T. Zahariadis, "Trends in the path to 4G," *Communications Engineer*, vol. 1, no. 1, pp. 12 – 15, 2003.

[5] W. C. Jakes and D. C. Cox, Eds., *Microwave Mobile Communications*. Wiley-IEEE Press, 1994.

[6] G. L. Stuber, *Principles of Mobile Communication*, 1st ed. Norwell, MA, USA: Kluwer Academic Publishers, 1996.

[7] T. Rappaport, *Wireless Communications: Principles and Practice*, 2nd ed. Upper Saddle River, NJ, USA: Prentice Hall PTR, 2001.

[8] J. G. Proakis, *Digital Communications*. McGraw-Hill, New York, 1995.

[9] J. D. Parsons, *The Mobile Radio Propagation Channel, 2nd Edition*, 2nd ed. Wiley, Nov. 2000.

[10] R. van Nee and R. Prasad, *OFDM for Wireless Multimedia Communications*. Artech House, Inc., 2000.

[11] J. Cimini, L., "Analysis and simulation of a digital mobile channel using orthogonal frequency division multiplexing," *Communications, IEEE Transactions on*, vol. 33, no. 7, pp. 665 – 675, jul 1985.

[12] R. v. Nee and R. Prasad, *OFDM for Wireless Multimedia Communications*, 1st ed. Norwood, MA, USA: Artech House, Inc., 2000.

[13] T. Keller and L. Hanzo, "Adaptive multicarrier modulation: a convenient framework for time-frequency processing in wireless communications," *Proceedings of the IEEE*, vol. 88, no. 5, pp. 611 –640, may 2000.

[14] R. W. Chang, "Synthesis of Band-Limited Orthogonal Signals for Multichannel Data Transmission," *Bell Systems Technical Journal*, vol. 45, pp. 1775–1796, Dec. 1966.

[15] B. Saltzberg, "Performance of an efficient parallel data transmission system," *Communication Technology, IEEE Transactions on*, vol. 15, no. 6, pp. 805 –811, december 1967.

[16] R. Mosier and R. Clabaugh, "Kineplex, a bandwidth-efficient binary transmission system," *AIEE Transaction*, vol. 76, pp. 738 – 728, january 1958.

[17] S. Weinstein and P. Ebert, "Data transmission by frequency-division multiplexing using the discrete fourier transform," *Communication Technology, IEEE Transactions on*, vol. 19, no. 5, pp. 628 –634, october 1971.

[18] "Radio broadcasting systems: Digital audio broadcasting to mobile, portable and fixed receivers," *ETS 300 401, Eur. Telecommun. Standard*, 1995, ETSI.

[19] *Digital Video Broadcasting (DVB-T); Frame Structure, Channel Coding, Modulation for Digital Terrestrial Television,*, ETS 300 744, Eur. Telecommun. Standard, 1997, ETSI. Std., 1997.

[20] *Part 11: Wireless LAN Medium Access Control (MAC) and Physical Layer (PHY) specification: High-speed Physical Layer in the 5 GHz Band*, IEEE Std 802.11a-1999 Std., 1999.

[21] *Wireless LAN medium access control (MAC) and physical layer (PHY) specifications*, IEEE Std 802.11g Std., 2003.

[22] *IEEE Standard for Local and Metropolitan Area Networks Part 16: Air Interface for Fixed Broadband Wireless Access Systems*, IEEE Standard 802.16-2004 Std., 2004.

[23] T. K. et al., *Report on digital audio radio laboratory tests.* Technical Report, Electronic Industries Assocition, May, 1995.

[24] M. S. Gast, *802.11 Wireless Networks*, 2nd ed. O'Reilly Publications, April, 2005.

[25] R. Prasad and S. Hara, "An overview of multi-carrier CDMA," vol. vol.1, New York, NY, USA, 1996//, pp. 107 – 14.

[26] A. McCormick and E. Al-Susa, "Multicarrier CDMA for future generation mobile communication," *Electronics amp; Communication Engineering Journal*, vol. 14, no. 2, pp. 52 – 60, 2002.

[27] V. Chakravarthy, A. Nunez, J. Stephens, A. Shaw, and M. Temple, "Tdcs, ofdm, and mc-cdma: a brief tutorial," *IEEE Communications Magazine*, vol. 43, no. 9, pp. 11 – 16, Sept. 2005.

[28] H. Rohling and R. Gruneid, "Performance comparison of different multiple access schemes for the downlink of an ofdm communication system," in *Vehicular Technology Conference, 1997 IEEE 47th*, vol. 3, may 1997, pp. 1365 –1369 vol.3.

[29] H. Sari, Y. Levy, and G. Karam, "An analysis of orthogonal frequency-division multiple access," in *Global Telecommunications Conference, 1997. GLOBECOM '97., IEEE*, vol. 3, nov 1997, pp. 1635 –1639 vol.3.

[30] H. Rohling, D. Galda, and R. Grunheid, "Ofdm: A flexible and adaptive air interface for a 4g mobile communication system," vol. vol.2, Beijing, China, 2002, pp. 396 – 400.

[31] H. Sari and G. Karam, "Orthogonal frequency-division multiple access and its application to catv networks," *European Transactions on Telecommunications*, vol. 9, no. 6, pp. 507 – 16, 1998/11/.

[32] C. Y. Wong, R. Cheng, K. Lataief, and R. Murch, "Multiuser ofdm with adaptive subcarrier, bit, and power allocation," *Selected Areas in Communications, IEEE Journal on*, vol. 17, no. 10, pp. 1747 –1758, oct 1999.

[33] *Interaction Channel for Digital Terrestrial Television (RCT) Incorporating Multiple Access OFDM*, ETSI DVB RCT, Mar. Std., 2001.

[34] M. Ariaudo, "Dirty RF pour les Systèmes de Communication," HDR, Université de Cergy Pontoise, Nov. 2010.

[35] T. Pollet, M. Van Bladel, and M. Moeneclaey, "Ber sensitivity of ofdm systems to carrier frequency offset and wiener phase noise," *Communications, IEEE Transactions on*, vol. 43, no. 234, pp. 191 –193, feb/mar/apr 1995.

[36] M. Morelli, C.-C. Kuo, and M.-O. Pun, "Synchronization techniques for orthogonal frequency division multiple access (ofdma): A tutorial review," *Proceedings of the IEEE*, vol. 95, no. 7, pp. 1394 –1427, july 2007.

[37] M. A. F., *Wideband wireless digital communication.* Upper Saddle River: Prentice Hall, 2001.

[38] J.-J. van de Beek, P. Borjesson, M.-L. Boucheret, D. Landstrom, J. Arenas, P. Odling, C. Ostberg, M. Wahlqvist, and S. Wilson, "A time and frequency synchronization scheme for multiuser ofdm," *Selected Areas in Communications, IEEE Journal on*, vol. 17, no. 11, pp. 1900 –1914, nov 1999.

[39] P. Robertson and S. Kaiser, "Analysis of doppler spread perturbations in ofdm(a) systems," *European Transactions on Telecommunications*, vol. 11, no. 6, pp. 585 – 592, 2000.

[40] Y. Li and J. Cimini, L.J., "Bounds on the interchannel interference of ofdm in time-varying impairments," *Communications, IEEE Transactions on*, vol. 49, no. 3, pp. 401 –404, mar 2001.

[41] M. Stemick and H. Rohling, "Effect of carrier frequency offset on the channel capacity in multiuser ofdm-fdma systems," *Wireless Personal Communications*, vol. 47, no. 1, pp. 5 – 14, 2008.

[42] J. Armstrong, "Analysis of new and existing methods of reducing intercarrier interference due to carrier frequency offset in ofdm," *Communications, IEEE Transactions on*, vol. 47, no. 3, pp. 365 –369, mar 1999.

[43] Y. Zhao and S.-G. Haggman, "Intercarrier interference self-cancellation scheme for ofdm mobile communication systems," *Communications, IEEE Transactions on*, vol. 49, no. 7, pp. 1185 –1191, jul 2001.

[44] Collaboration, "Part 11: wireless lan medium access control (mac) and physical layer (phy) specifications: high-speed physical layer in the 5 ghz band," vol. IEEE Std 802.11a-1999, 1999.

[45] J. Gonzalez-Bayon, C. Carreras, and A. Fernandez-Herrero, "A comparison of frequency offset synchronization algorithms for wimax ofdm systems," in *EUROCON, 2007. The International Conference on 34;Computer as a Tool 34;*, sept. 2007, pp. 997 –1004.

[46] W. Rhee and J. Cioffi, "Increase in capacity of multiuser ofdm system using dynamic subchannel allocation," in *Vehicular Technology Conference Proceedings, 2000. VTC 2000-Spring Tokyo. 2000 IEEE 51st*, vol. 2, 2000, pp. 1085 –1089 vol.2.

Bibliography

[47] R. M. Gray, "Toeplitz and circulant matrices: A review," *Deptartment of Electrical Engineering, Stanford University*, 1971.

[48] A. Peled and A. Ruiz, "Frequency domain data transmission using reduced computational complexity algorithms." *Record - IEEE International Conference on Acoustics, Speech amp; Signal Processing*, vol. 3, pp. 964 – 967, 1980.

[49] P. Moose, "A technique for orthogonal frequency division multiplexing frequency offset correction," *IEEE Transactions on Communications*, vol. 42, no. 10, pp. 2908 – 14, 1994.

[50] T. Roman, M. Enescu, and V. Koivunen, "Joint time-domain tracking of channel and frequency offsets for mimo ofdm systems," *Wireless Personal Communications*, vol. 31, no. 3-4, pp. 181 – 200, 2004.

[51] B. Aziz, I. Fijalkow, and M. Ariaudo, "Intercarrier interference in uplink ofdma systems with carrier frequency offset," in *IEEE PIMRC*, September 2010.

[52] K. Sathananthan and C. Tellambura, "Probability of error calculation of ofdm systems with frequency offset," *Communications, IEEE Transactions on*, vol. 49, no. 11, pp. 1884 –1888, nov 2001.

[53] J. Heiskala and J. Terry, Ph.D., *OFDM Wireless LANs: A Theoretical and Practical Guide.* Indianapolis, IN, USA: Sams, 2001.

[54] *IEEE Standard for Local and Metropolitan Area Networks. Part 16: Air Interface for Fixed Broadband Wireless Access Systems. Amendment 2: Physical and Medium Access Control Layers for Combined Fixed and Mobile Operation in Licensed Bands*, IEEE Standard 802.16-2005 Std., 2005.

[55] J. Gross, H. Karl, F. Fitzek, and A. Wolisz, "Comparison of heuristic and optimal subcarrier assignment algorithms," Las Vegas, NV, United states, 2003, pp. 249 – 255.

[56] M. Stemick, S. Olonbayar, and H. Rohling, "Phy-mode selection and multiuser diversity in ofdm based transmission systems," 2006.

[57] M. Batariere, K. Baum, and T. Krauss, "Cyclic prefix length analysis for 4g ofdm systems," in *Vehicular Technology Conference, 2004. VTC2004-Fall. 2004 IEEE 60th*, vol. 1, sept. 2004, pp. 543 – 547 Vol. 1.

[58] T. Ycek and H. Arslan, "Carrier frequency offset compensation with successive cancellation in uplink ofdma systems," *IEEE Transactions on Communications*, vol. 6, no. 10, pp. 2908–2914, Oct. 2007.

[59] J. Li, H. Kim, Y. Lee, and Y. Kim, "A novel broadband wireless ofdma scheme for downlink in cellular communications," in *Wireless Communications and Networking, 2003. WCNC 2003. 2003 IEEE*, vol. 3, march 2003, pp. 1907 – 1911 vol.3.

[60] A. Alsawah and I. Fijalkow, "Base-station and subcarrier assignment in two-cell ofdma downlink under qos fairness," in *PIMRC*, 2008, pp. 1–6.

[61] B. Aziz, I. Fijalkow, and M. Ariaudo, "Trade off between frequency diversity and robustness to carrier frequency offset in uplink ofdma system," in *Global Telecommunications Conference, 2011. GLOBECOM '11. IEEE*, dec. 2011.

[62] J. jaap Van De Beek, O. Edfors, M. S, S. K. Wilson, and P. O. Brjesson, "On channel estimation in ofdm systems," in *in Proc. of the IEEE Vehicular Technology Conference, VTC ?5*, 1995, pp. 815–819.

[63] S. Barbarossa, M. Pompili, and G. Giannakis, "Channel-independent synchronization of orthogonal frequency division multiple access systems," *Selected Areas in Communications, IEEE Journal on*, vol. 20, no. 2, pp. 474 –486, feb 2002.

[64] Z. Cao, U. Tureli, and Y.-D. Yao, "Deterministic multiuser carrier-frequency offset estimation for interleaved ofdma uplink," *Communications, IEEE Transactions on*, vol. 52, no. 9, pp. 1585 – 1594, sept. 2004.

[65] M. Morelli, "Timing and frequency synchronization for the uplink of an ofdma system," *Communications, IEEE Transactions on*, vol. 52, no. 2, pp. 296 – 306, feb. 2004.

[66] H. Bolcskei, "Blind high-resolution uplink synchronization of ofdm-based multiple access schemes," in *Signal Processing Advances in Wireless Communications, 1999. SPAWC '99. 1999 2nd IEEE Workshop on*, 1999, pp. 166 –169.

[67] Y. Yao and G. Giannakis, "Blind carrier frequency offset estimation in siso, mimo, and multiuser ofdm systems," *Communications, IEEE Transactions on*, vol. 53, no. 1, pp. 173 – 183, jan. 2005.

[68] M.-O. Pun, M. Morelli, and C.-C. Kuo, "Maximum-likelihood synchronization and channel estimation for ofdma uplink transmissions," *Communications, IEEE Transactions on*, vol. 54, no. 4, pp. 726 – 736, apr. 2006.

[69] S. Ahmed, S. Lambotharan, A. Jakobsson, and J. Chambers, "Mimo frequency-selective channels with multiple-frequency offsets: estimation and detection techniques," *Communications, IEE Proceedings-*, vol. 152, no. 4, pp. 489 – 494, aug 2005.

Bibliography

[70] L. Haring, S. Bieder, A. Czylwik, and T. Kaiser, "Estimation algorithms of multiple channels and carrier frequency offsets in application to multiuser ofdm systems," *Wireless Communications, IEEE Transactions on*, vol. 9, no. 3, pp. 865 –870, mar. 2010.

[71] D. Huang and K. Letaief, "An interference-cancellation scheme for carrier frequency offsets correction in ofdma systems," *Communications, IEEE Transactions on*, vol. 53, no. 7, pp. 1155 – 1165, july 2005.

[72] Z. Cao, U. Tureli, Y.-D. Yao, and P. Honan, "Frequency synchronization for generalized ofdma uplink," in *Global Telecommunications Conference, 2004. GLOBECOM '04. IEEE*, vol. 2, nov.-3 dec. 2004, pp. 1071 – 1075 Vol.2.

[73] Z. Cao, U. Tureli, and Y.-D. Yao, "Analysis of two receiver schemes for interleaved ofdma uplink," in *Signals, Systems and Computers, 2002. Conference Record of the Thirty-Sixth Asilomar Conference on*, vol. 2, nov. 2002, pp. 1818 – 1821 vol.2.

[74] D. Huang and K. Letaief, "Carrier frequency offsets mitigation for broadband ofdm in a multiuser environment," in *Personal, Indoor and Mobile Radio Communications, 2003. PIMRC 2003. 14th IEEE Proceedings on*, vol. 2, sept. 2003, pp. 1149 – 1153 vol.2.

[75] R. Fantacci, D. Marabissi, and S. Papini, "Multiuser interference cancellation receivers for ofdma uplink communications with carrier frequency offset," in *Global Telecommunications Conference, 2004. GLOBECOM '04. IEEE*, vol. 5, nov.-3 dec. 2004, pp. 2808 – 2812 Vol.5.

[76] T. Yucek and H. Arslan, "Carrier frequency offset compensation with successive cancellation in uplink ofdma systems," *Wireless Communications, IEEE Transactions on*, vol. 6, no. 10, pp. 3546 –3551, october 2007.

[77] D. Chu, "Polyphase codes with good periodic correlation properties (corresp.)," *Information Theory, IEEE Transactions on*, vol. 18, no. 4, pp. 531 – 532, jul. 1972.

[78] A. Abdel-Samad, "Fine frequency offset estimation for frequency-selective channels," in *Vehicular Technology Conference, 2006. VTC 2006-Spring. IEEE 63rd*, vol. 4, may 2006, pp. 1879 –1883.

[79] A. Roumy, I. Fijalkow, D. Pirez, and P. Duvaut, "Iterative multi-user algorithm for convolutionally coded asynchronous ds-cdma systems: turbo-cdma," in *Acoustics, Speech, and Signal Processing, 2000. ICASSP '00. Proceedings. 2000 IEEE International Conference on*, vol. 5, 2000, pp. 2893 –2896 vol.5.

[80] B. Aziz, I. Fijalkow, and M. Ariaudo, "Joint estimation of channel and carrier frequency offset from the emitter, in an uplink ofdma system," in *ICASSP*, 2011, pp. 3492–3495.